People's Democratic Republic of Algeria

University M'hamed Bougara, Boumerdes

Institute of Electrical and Electronic Engineering

Department of Electronics

Thesis submitted for partial fulfillment of the degree of

Ph.D. in Computer Engineering

Title:
Automatic methods for the analysis and recognition of the Electrocardiogram

Presented by

BELKADI Mohamed Amine

In front of the jury:

DAHIMENE Abdelhakim	President,	Professor, UMBB
DAAMOUCHE Abdelhamid	Supervisor,	Professor, UMBB
SOUISSI Boularbah	Examiner,	MCA, USTHB
ADNANE Mourad	Examiner	Professor, ENP

Aug. 2020

Abstract

Cardiac diseases rank first in the cases of death all over the world; Electrocardiogram (ECG) bears valuable information about the person health state. Therefore, ECG became a standard tool for heart disease exploration. Beats segmentation is a necessary step before disease type identification. The segmentation is based on the QRS detection. In this thesis, we proposed three different methods for ECG segmentation. First, an optimized Pan-Tompkins algorithm is developed, in which the parameters of the benchmark algorithm are optimized using the particle swarm optimization (PSO). Second, the QRS is detected in the time-scale domain; the stationary wavelet transform is applied to the filtered ECG signal to enhance the QRS wave, and then thresholding is carried out to extract the wanted signal. Finally, a machine learning technique is used to identify the QRS. In particular, a deep learning autoencoder is trained by standard datasets for the purpose of QRS detection.

Keywords: Electrocardiogram (ECG), Pan-Tompkins algorithm, Stationary Wavelet Transform, Autoencoders, QRS, Deep learning.

List of Publications

1. **Conferences**

[1] An improved QRS detection method using Hidden Markov Models," presented at the *6th Int. Conf. Systems and Control*, Batna, Algeria, May. 7-9, 2017.

[2] Stationary Wavelet Transform with High Order Wavelet Mother with Robustness to Noise For QRS Detection, presented at the *5th International Conference On Electrical Engineering*, October 29-31 2017, BOUMERDES, ALGERIA.

[3] Fast Wavelet Approach PSO-Based QRS Detector, presented at the *1st International Conference On Networking Telecommunications, Biomedical Engineering and Applications*, November 4-5 2019, BOUMERDES, ALGERIA.

2. **Articles**

[1] Swarm Intelligent Approach to QRS Detection, *The International Arab Journal of Information Technology (IAJIT)*, vol. 17, no. 4, July 2020. Impact Factor: 0.708

[2] A Robust QRS Detection Approach Using Stationary Wavelet Transform, *Multimedia Tools and Applications*, vol. 1130T, Apr 2021. Impact Factor: 2.6

[3] An Approach to QRS Complex Detection using Deep Neural Networks Autoencoder, *Expert Systems With Applications*, *Under review*.

Dedications

In Memory of my sister Moufida, and father. ´

The present work is dedicated To my loving parents, I owe them

all from my young age, especially because they spent all their time an their entire life

for my education and to make me a men, also this work is dedicated to

my brother, Mounir.

Acknowledgements

This dissertation would not have been possible without the help of my supervisor, professor DAAMOUCHE Abdelhamid. I would like to take this opportunity to express my deep appreciation to all those who helped me during the last five years, the period along which I was preparing this humble work. First and foremost, I would like to thank my supervisor, Professor DAAMOUCHE Abdelhamid, for his constant support, comments and guidance throughout my research. He gave me the freedom to pursue my ideas and constantly encouraged me by refining my research direction through his evaluations and feedback. I am thankful to the pedagogical staff (Institute of Eletrical and Eletronic of BOUMERDES), whose constant guidance has helped me to shape my research work, especially, Dr NAAMANE, Pr BENTERZI, Pr KOUADRI Abdelmalek, Dr BELAIDI, Pr CHAALLAL, Pr DAHIMENE and Pr KHALDOUN. I am deeply grateful to my parents, for their invaluable support. They have stood by me every step of the way and have always supported me through their guidance and encouragement. And to my beautiful brother, Mounir, for his unwavering support. I could always rely on them for friendship and advice or for a joke or both when needed. I am thankful to Pr. MELGANI Farid for his knowledge and support during my intership at the University Trento, in Italy. His support and theorical basis, his support is invaluable. I would also like to thank Pr KOUADRI Abdelmalek for his technical support during my interactions with him at the office. I am thankful to Dr ZEGGADA Abdellah and Dr MALEK Selim for their precious technical help and support.

Mr. BELKADI Mohamed Amine

All my gratitudes

Table of Contents

List of Figures

List of Tables

List of Terms and Abbreviations

Symbols

1-D variant: 1 Dimentional variant.

µs: Micro seconds.

#: Number.

A

AAMII: Association for the Advancement of Medical Instrumentation I.

Acc: Accuracy.

ANN: Artificial Neural Network.

ANSI: American National Standards Institute.

Apnea DB: Apnea database.

C

Challenge 2014 DB: Challenge 2014 database.

CPU: Centeral processing unit.

CNN: Convolutional Neural Networks.

CSE database: CiPA ECG Validation Study database.

CUDA: Compute Unified Device Architecture.

CWT: Contious Wavelet Transform.

D

db4: Daubechies Wavelet mother at the fourth order.

DER: Detection error rate.

DL: Deep Learning.

DS1: Dataset 1.

DS2: Dataset 2.

DWT: Discrete Wavelet Transform.

E

ECG: Eletrocardiogram.

EDB: European ST-T Database.

ePatch: Extended Holter Monitor.

F

Fantasia DB: Fantasia database.

FIR: Finite Impulse Response.

FN: False negatives.

FP: False positives.

FPGA: Field Programmable Gate Arrays.

FSM: Finite State Machine.

G

GB: Giga bytes.

GHZ: Giga heurtz.

GPU: Graphical processing unit.

GUI: graphical user interface.

H

HMM: Hidden Markov Models.

HR: Heart rate.

Hz: Hertz.

I

IIR: Infinite Impulse Response.

INCART DB: In Cardiology Database (St Petersburg INCART 12-lead Arrhythmia Database).

ISO: Isolation.

K

KNN: K Nearest Neighbor.

L

LM optimization: Levenberg-Marquardt optimization.

LSTM: Long Short Term Memory.

LTSTDB: Long Term ST Database.

M

MAC: Macintosh.

MaMeMi filter: maximum mean minimum filter.

MIT: Massachusset Institute of Technology.

MIT/BIH: Massachusset Institute of Technology / Boston's Beth Israel Hospital.

MITDB: Massachusset Institute of Technology Database.

MLP: Multi Layer Perceptron.

ms: Milliseconds.

N

Nb: Number.

NSTDB: Noise Stress Test Database.

NSTMIT: Noise Stress Test MIT Database.

NSRDB: Normal Sinus Rhythm Database.

O

OA: Overall accuracy.

P

PC: Personal computer.

PDF: Portable document format.

Ph. D: Philosophiae Doctor or Pilled Higher and Deeper.

PPV: Positive productivity value.

PSO: Particle Swarm Optimization.

Q

QRS: QRS complex wave regrouping Q, R and S waves parts from the ECG signal.

QTDB: QT database.

R

rbio2.2: Reverse biorthogonal 2.2 wavelet.

RR intervals: R peak to R peak intervals.

S

s : Seconds.

SA: Stacked Autoencoder.

SD: Secure Digital.

Se: Sensitivity.

SNR: Signal to noise ratio.

STC: Sequence to be Threshold Compared.

STFT: Short Time Fourier Transform.

ST-T: S wave to T wave.

SVDB: Supra Ventricular Database.

SWT: Stationary Wavelet Transform.

T

TP: True positives.

U

USB: Universal Serial Bus.

V

VLSI: Very large scale integration.

W

WT: Wavelet Transform.

CHAPTER I

INTRODUCTION

I. Introduction

Human is constantly working toward commodities and modeling features for easier adaptation. Human can think, and his intelligence is very developed in comparison with other mammals, it seems that this intelligence is his principal adaptation tool, and over thousands of years, it gave him a clear dominance advantage over all other species on this planet. Moreover, since human existence, he elaborated many tools and instruments at the aim of simplifying his daily life. Hence, from fire discovery to silicon-based technology, long time duration, many efforts and crucial resources have been exploited to make this progress possible.

Computer engineering society incidence is very important regarding the influence of its algorithms on daily life and the large usage of electronics devices embedding software used in different fields. Indeed, computers are present on all administrations, universities, and many other offices, also embedded devices find their integration in special fields, e.g., avionics, cars, telecommunications, factories, oil extraction, hydraulic instruments, etc. Thus, silicon-based instruments are now part of human life, and are indispensable for human, each time a computer or an electronic instrument is introduced, tasks will be rapidly executed, efforts become considerably reduced and human intervention will be restricted or completely not required, especially, with the emerging revolutionary filed of artificial intelligence, which completely changes the human perception of machines on its environment, from biometric recognition to person speech identification, passing by autopilot and self-driving cars, artificial intelligence begin to impose itself and will invade many unexplored fields in the near future. In particular, we mention the emerging field of electronics or medical instruments based on computers. These instruments make clinicians confidant, faster in their decisions, and anticipate emergency situations. For instance, while automatic cancer detection from scanner imaging systems can identify cancer regions, the majority of medical staff misses them.

The computer speed and the memory size are increasing since decades; this allowed the design of more accurate intelligent techniques, also emerging systems with high precision offered opportunity to better physical phenomena monitoring and anticipation.

Signal processing techniques offer a precious decision maker by the hidden information extraction and the features fed to the classifier. In deep learning, huge training set size provides robust and more accurate prediction, opening large horizons for semi-perfect systems and instruments redefining completely the field of the artificial intelligence, and the human vision about machines. Furthermore, the automatic features extraction on that way reduces engineer's intervention, decreases the algorithmic complexity for possible implementation on embedded devices and decreases in many cases the execution time to a reasonable duration.

I. 1. Motivations

The Electrocardiogram is by far the most used tool for the purpose of diagnosis. Therefore, a large number of scientists have attempted to develop automatic algorithms to help the medical staff in obtaining fast and accurate decisions. The two major fields regarding the ECG analysis are the QRS waveform detection and arrhythmia classification. The reported results on common databases are very promising for the future of automatic ECG signal exploitation. However, the challenge remains, and the problem of perfect ECG analyzer is still open. Indeed, ECG signal variability is the main challenge. Although, it seems that the ECG signal is periodic, it is in fact varying from one person to another (inter variability), and varies from one beat to another for the same person (intra variability). Factors such as stress, respiration and instruments imperfections generate additive noise at different frequencies, which increase automatic processing failures probability. Hence, necessity of investigation of automatic ECG processing field is indispensable. Moreover, heart diseases are the first human mortality cause. In addition, reaction time for certain cardiac pathologies, like tachycardia, is crucial and each second is important, hence elaboration of an accurate and fast automatic analysis tool is necessary.

I. 2. Approach

The content of this thesis focuses on our developed techniques. It is an attempt to constructing an automatic analysis tool for arbitrary ECG signals. We will give more details of the proposed QRS algorithms and their comparison with the state-of-the-art algorithms.

The developed algorithms throughout this thesis preparation are parts to be integrated on a global system. We project to design and implement a fully automated arrhythmia classification software and hardware suitable for implementation on different environments and machine architectures, all interconnected with possibility of data exchange under availability of a network interface or external storage memories. It is worth noting that the main challenge of the developed system is the accuracy of detection, either for QRS waveform or arrhythmia classification. Initially, our main concern was the design and development of new algorithms for beat separation commonly called QRS detection. Beat separation is very important as it has a big impact on the final result of any automatic arrhythmia classification.

The work realized throughout the present thesis could be inserted in an automatic diagnosis system as shown in Fig. 1. The developed software can be implemented on computers and Android devices. It can acquire the ECG signal from any kind of recording devices such as USB storage or SD Card storage, in addition, database is included on the software for patient history retracing, permitting future stored statistics processing. Also, devices and machines under the same router can exchange data, detection and classification results for database saving in addition to possibility of data visualization either on smartphone or computers. Moreover, mobility offered by this software when installed on Smartphone or tablets can be very useful especially for ambulatory recordings. Our major contribution on Fig. 1 is an artificial intelligence block, which consists in developing an automatic system for ECG signal processing that involves a QRS detector and arrhythmia identification.

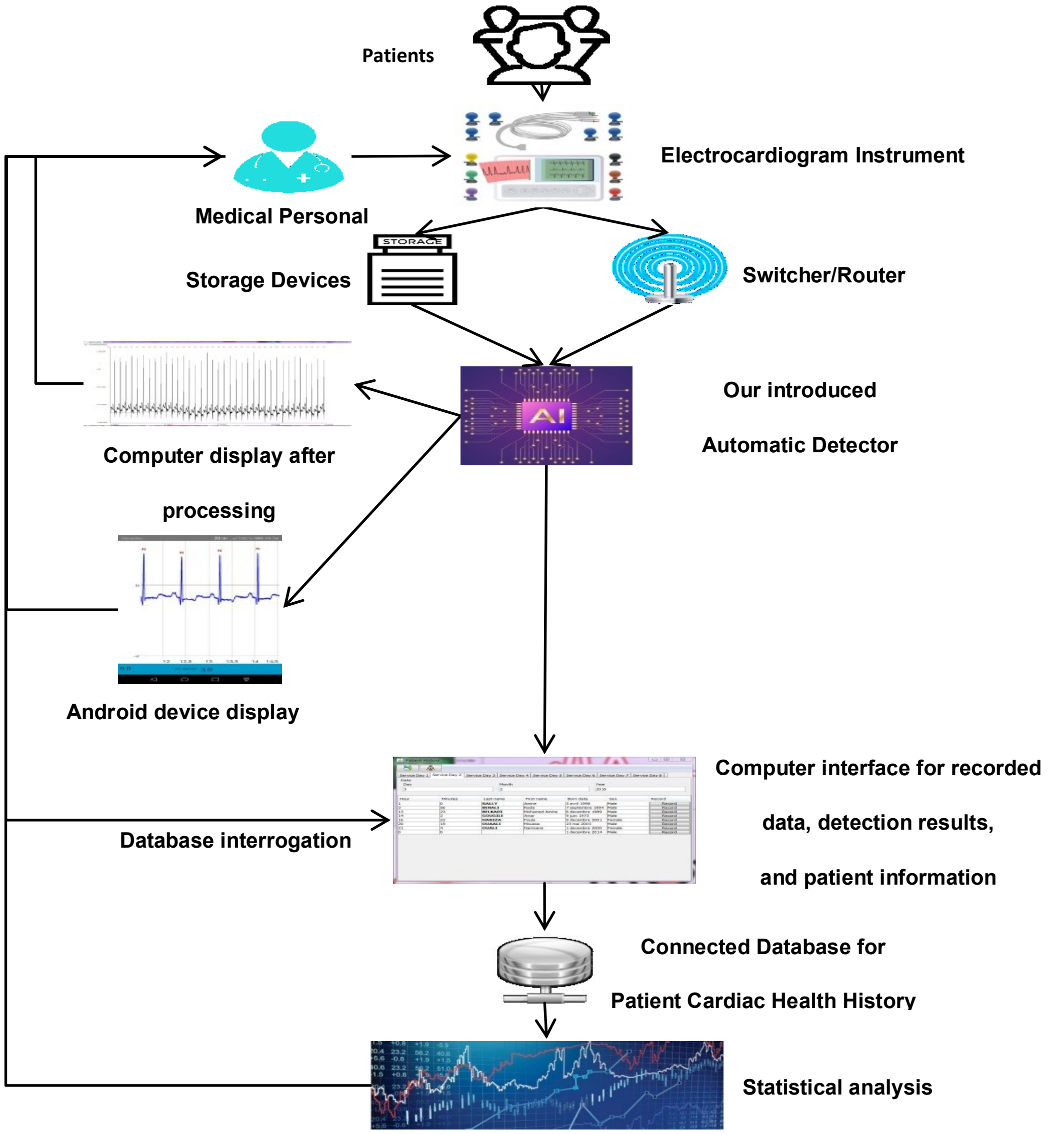

Fig. 1 : Ambitious automatic heart health decision diagram

I. 3. Major Contributions

The main works that have been done in the frame of this Ph. D. dissertation could be summarized in the following:

- Introduction of the Particle Swarm Optimization (PSO) algorithm to the Pan and Tompkins algorithm for an optimal QRS detection. Regarding the simplicity and low complexity of the well-known Pan-Tompkins algorithm, we started from the fact that a number of parameters are not optimal; hence the improvement of the detection is still possible. After the optimization by the PSO algorithm, the detection error decreased from 0.675% to 0.169% on the MIT benchmark database, confirming the validity of our hypothesis.
- A robust QRS detector using the Stationary Wavelet Transform (SWT) is proposed. The developed scheme uses solely the first decomposition level SWT coefficients. It turns out that the scheme is suitable for noise-free signals and noisy

environments. A very promising QRS detection error rate of 0.228% was obtained using the benchmark MITDB. Furthermore, the performance on noisy environments surpasses all existing methods evaluated on NSTDB, with 10.12% of detection error, confirming superiority of this method.

- A deep learning neural network to QRS detection algorithm containing Stacked Autoencoder (SA) and MLP classifier was developed. Levenberg-Marquardt has been used for the training of the Stacked Autoencoder in the aim of better results than gradient descent. AAMII recommendation training and testing samples have been enlarged with samples from SVDB, INCART DB and EDB for a more general and efficient learning scheme. The proposed architecture was tested on a huge number of samples collected from many widely used datasets. RR intervals and initial estimation features are inputted to second and third stages MLP estimation for final QRS positions identification. The obtained detection error rate is 0.82% using more than 1400000 beats from five different databases demonstrating the good learning of our proposed architecture for the real features present on training set, guaranteed by the potentially global convergent LM optimization algorithm and enlargement of training dataset.
- Implementation of a complete software tool operating under Android environment or computers for patient health monitoring: The developed methods, especially for QRS detection, have been embedded in medical software; realized in the purpose to aid the medical staff, especially cardiologists in their daily tasks.

I. 4. Dissertation Organization

This thesis has been organized into six chapters, the first one helps the reader to understand the interest by the elaboration of this document, and the second presents a historical description of the chronological appearance and evolution of the sensing instrument. The electrocardiogram, classification delimitation, QRS detection, and proposed schemes are described on chapter three. Chapter four explains the proposed solutions to identify the arrhythmia. The last chapter presents the achievements of the present dissertation and the remaining challenges to surmount.

CHAPTER II

STATE OF THE ART OVERVIEW

II. State of The Art Overview

II. 1. Introduction

Early on the 80s, field leader engineers have investigated automatic analogue and digital ECG signal processing [1-2]. They addressed field challenges exploiting an important number of mathematical and algorithmic tools [1-2]. Throughout this chapter, we will review the proposed methods for QRS detection, alternatively called signal delineation or segmentation. During this investigation, we revealed that some published papers were distinguished by quality, importance of the introduced contributions, originality of the research and the obtained results. We divided the published methods into four categories corresponding to the nature of the processing to extract QRS positions, and the domain in which the detection is done. The categories are: time-domain, frequency domain, scale-domain, and learning-based approach.

II. 2. Time Domain Methods

A number of time-domain QRS detection methods have been proposed in the literature. This type of methods was introduced first before any other type. Consequently, this kind of methods has attracted the attention of researchers for a long period of time. Perhaps this is due to their high accuracy, low complexity and simplicity of implementation. Furthermore, the parameters of time-domain methods are obtained analytically from global knowledge of target characteristics of the processed signal, and conditions of signal recording. Whereas, other methods like learning approaches are data dependent.

In the following, we describe several works for the identification of the different QRS complexes present on the input signal. Hamilton and Tompkins [3] proposed a scheme shown in Fig. 2 determining the influence of varying QRS detection rules on the final detection error. The proposed detection rules were optimized for an optimal detection.

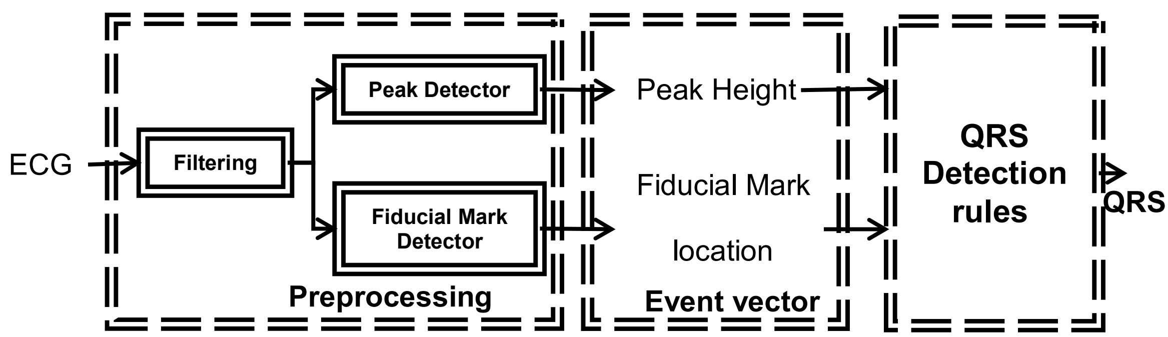

Fig. 2 : Hamilton and Tompkins's Block diagram QRS detector algorithm. The preprocessor does linear and nonlinear digital filtering and peak analysis to produce event vectors. The vectors are processed by decision rules to locate QRS complexes [3]

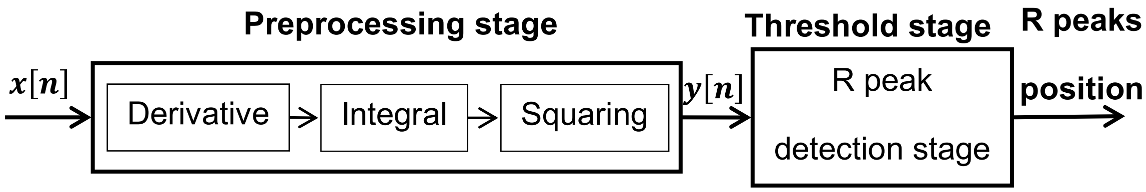

Fig. 3 : Gutiérrez-Rivas's *et al* block diagram of the proposed detector [5]

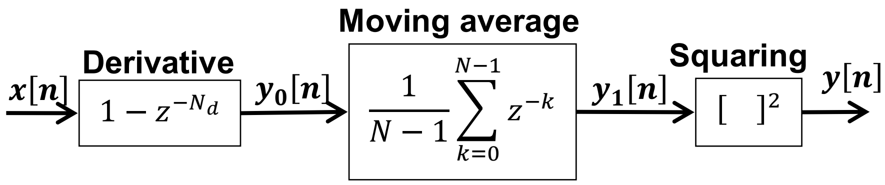

Fig. 4 : Block diagram of the preprocessing stage for the Gutiérrez-Rivas method [5]

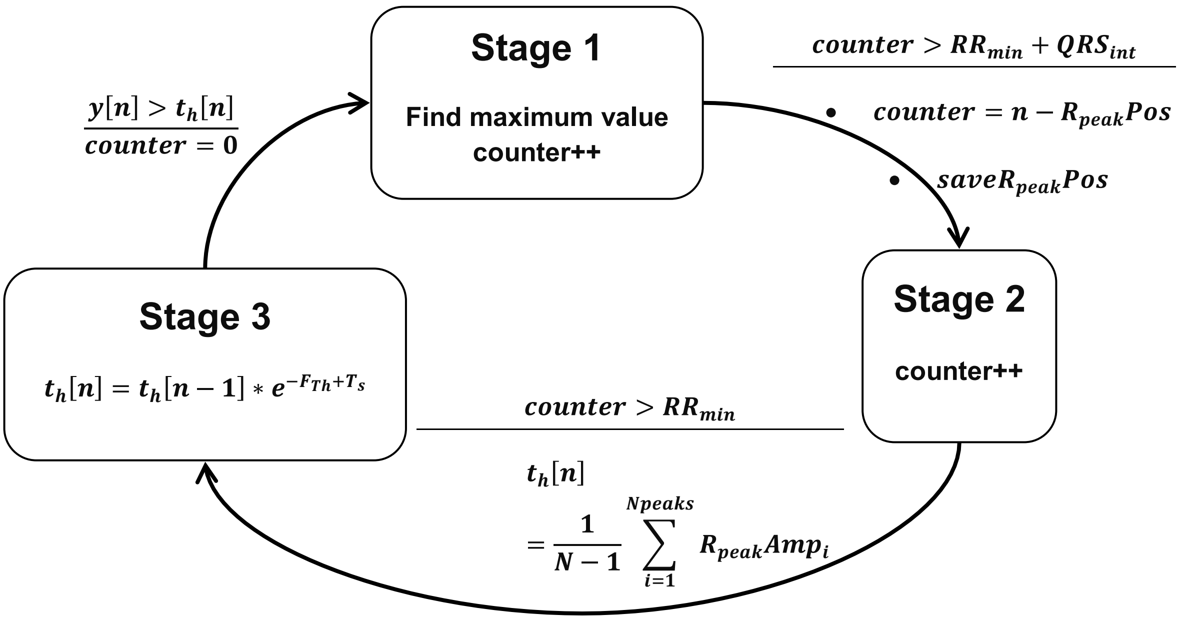

Fig. 5 : Block diagram of the proposed FSM (Finite State Machine) for the Gutiérrez-Rivas method [5]

The noise on their developed chain is attenuated using a baseline removal comprising low-pass and high-pass filters, and in parallel, peak detection with fiducial mark location is done. Simultaneously, the peak detection process extracts peaks positions, when fiducial mark examine and estimate the acceptable temporal occurrences of the QRSs. Then, from peaks positions and height and fiducial marks, an optimized version of the algorithm presented on [4] to determine the most probable QRS positions. Gutiérrez-Rivas et al [5] elaborated a simple processing scheme, with only a derivative, integrator and squarer, slightly different from the Pan-Tompkins algorithm [4] (see Fig. 3, 4), with a state machine of three states for thresholding as shown in Fig. 5, with low complexity, low resources consumption and better accuracy. Benmalek et al [6] utilized the same filtering steps like Pan-Tompkins [4], the chain illustrated in Fig. 6 is based on the fractional-order operators to determine the QRS positions. The elementary processing for this method are differentiation, squaring and smoothing. Two fractional order differentiators were used to decide about the appropriate positions of QRSs.

In particular, the input ECG signal is filtered for noise attenuation using the steps illustrated in Fig. 7. This filtering scheme is based on triangular filtering and the fractional order differentiation. Concerning the QRS positions identification strategy, fusion of two parallel fractional order differentiation are employed (see Fig. 8), one of order comprised between 0.5, and 1, and the second in the interval $1 < 2\alpha < 2$; the QRS positions are then the maximum detected peaks. Ruha et al. [7] utilized amplitude gain amplification, a set of filters, and a noise suppressor filter. They also proposed a new strategy for decision on QRS positions. Ravanshad et al. [8] exploited an analogue to digital converter for noise suppression, and a level-crossing for QRS positions identification. In addition, two adaptive thresholds determine the real QRS positions. In [9], the detection of the QRS complexes from the input signal is done by MaMeMi filter developed by Castells-Rufas et al. This algorithm utilizes morphological filters to detect the present QRS complexes, and an adaptive thresholding extracts QRS positions. Saadi et al [10] introduced an interesting method, their optimized scheme shown in Fig. 9 for QRS detection has been validated on a very large set of data to guarantee reliability and efficiency. The proposed chain has been embedded on e-Patch system for real use. Indeed, the design and optimization of the proposed method is assessed over the MIT/BIH Arrhythmia and eTDB databases for the consistency of them, and its validation is done over the European ST-T database for its long duration to overcome the challenge of the variability of the ST-T segments. The different processing steps used to

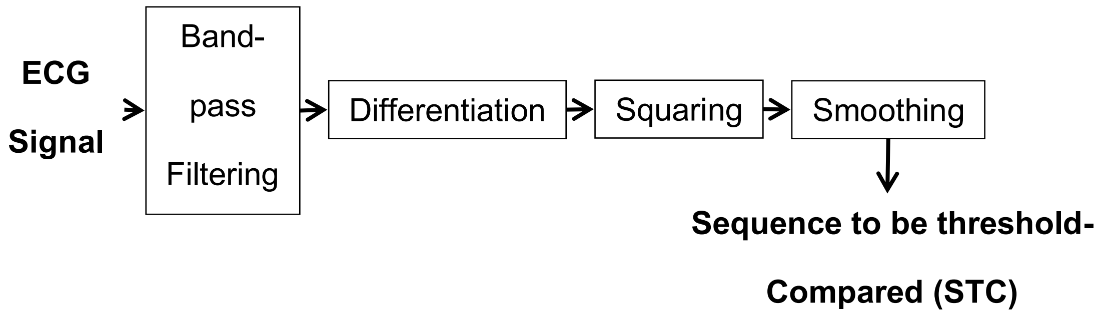

Fig. 6 : Benmalek's preprocessing scheme [6]

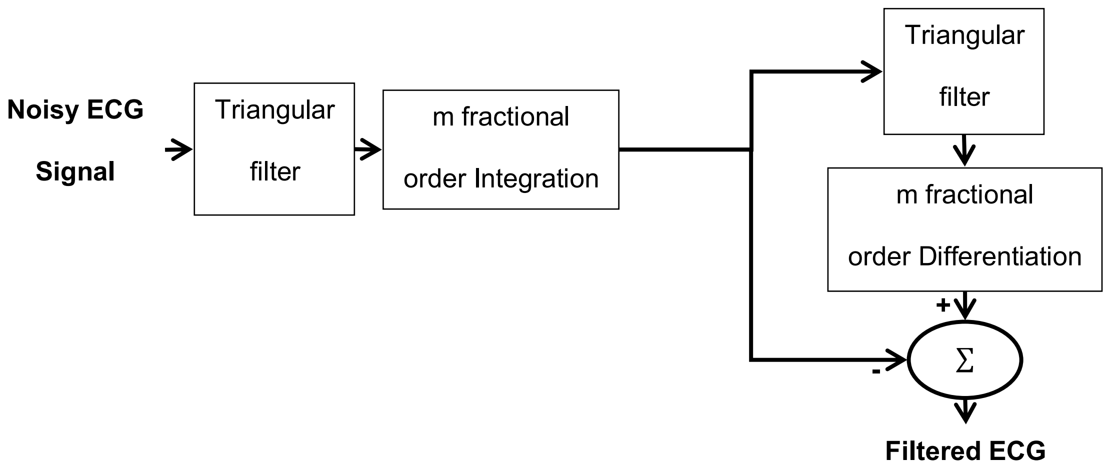

Fig. 7 : Digital Band-pass Filter Diagram for the method of [6]

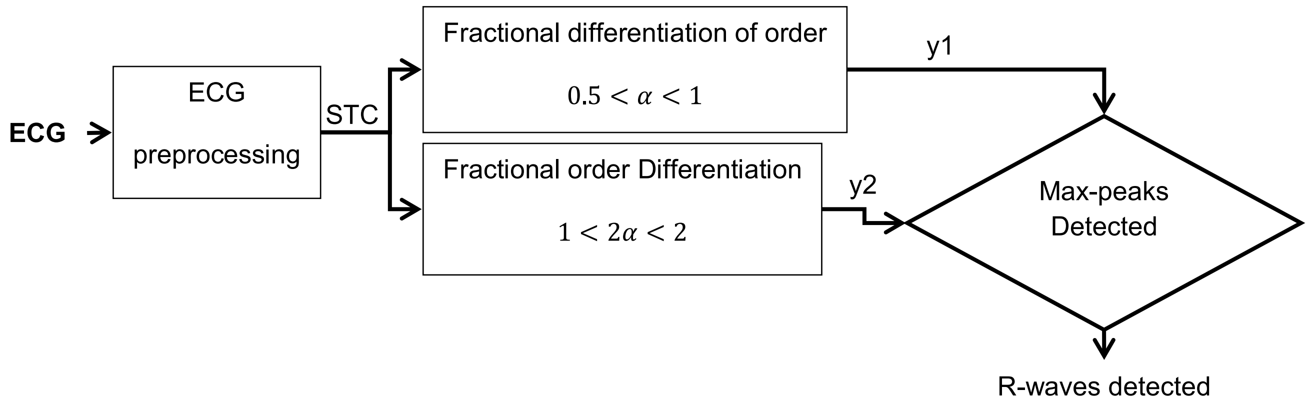

Fig. 8 : Block diagram of the R-wave detector for the method of [6]

estimate the appropriate QRS positions are shown in Fig. 10. The input ECG signal is first de-noised with an FIR bandpass filter removing components outside the interval [5,22] Hz, the main goal of this processing is to enhance the QRS complexes and reduce noise components. Bandpass and lowpass filters have been designed to do this task; in addition, absolute value is applied to make the polarity positive. Then, smoothing operation consisting of an FIR average filter with an order of 8 is carried out to center the signal and gather all ECG waves on a unique slope. QRS complexes are identified making use of a search back procedure. This procedure exploits RR intervals estimations for long and short time and identifies QRSs from prescribed rules. Yakut and Bolat [11] proposed a very light QRS detector in terms of computation, the same thing for Tekeste et al. [12] where a low complex method for QRS detection and ECG compression has been developed. In [13], Nguyen et al. proposed the triangle template matching for the finding the QRS positions. Three different schemes have been proposed for QRS detection by Poli et al. [14], genetic algorithm optimization approach has been utilized to optimize the coefficients of linear and nonlinear filters introduced to detect QRSs and a final decision stage estimate the positions.

Time-domain methods involve a variety of developed detectors. Of particular interest is the Pan and Tompkins algorithm [4], which is one of the widely used algorithms for QRS detection. It is an accurate method utilizing only differentiation, integration, and nonlinear transformation in addition to a thresholding strategy. It keeps a running estimation of the signal and noise levels. It uses a search back procedure to look for missed positions by initial knowledge of the interval between two successive beats. Christov et al. [15] used two adaptive approaches to distinguish between QRSs and no QRSs; the first approach computes the difference between amplitudes sum of one or more leads and a defined adaptive threshold. The second approach takes into consideration the interval between two successive beats. In [16], a wavelet denoising was used to suppress additive noise. In addition to a second noise suppression stage with a low and high pass filters. Finally, a decision stage is used to determine the QRS positions. Besides, the method of Suarez et al. [17] is based on the geometrical distance. It detects the QRS positions based on the knowledge of complex geometry represented by a genetic algorithm optimized model, then the signal is segmented using moving window, when a classifier extract the QRS complexes positions.

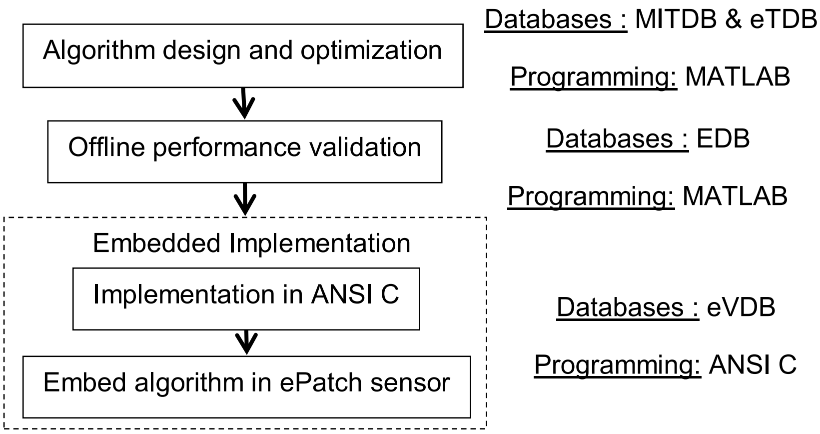

Fig. 9 : Saadi's schematic overview of the study design [10]

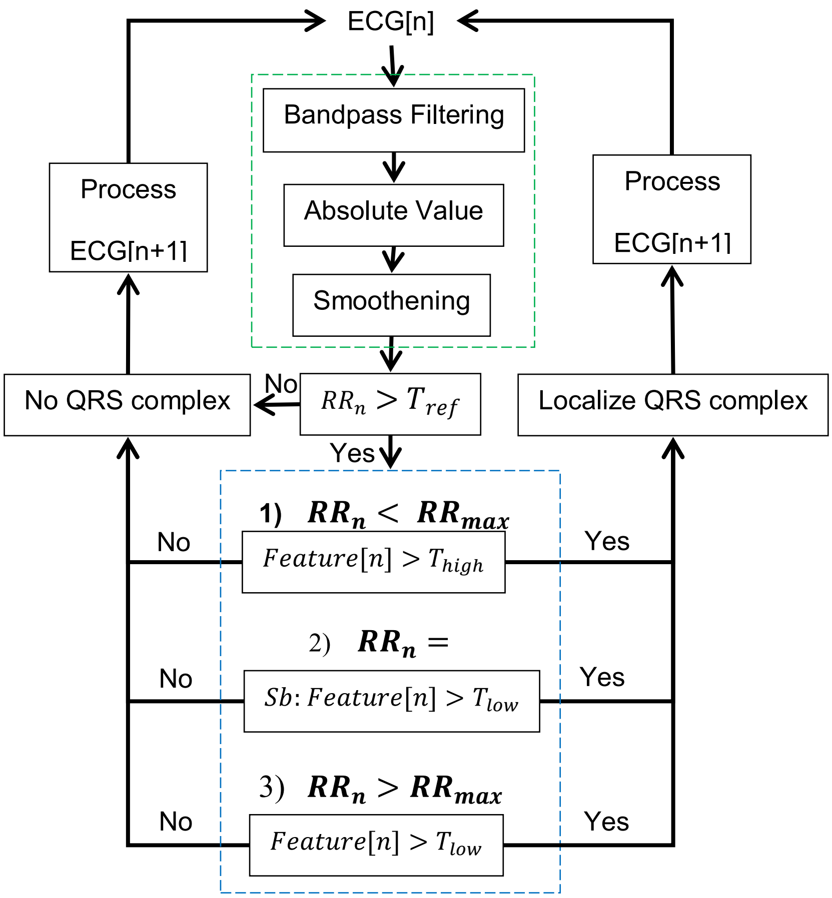

Fig. 10 : Schematic overview of the designed QRS complex detection algorithm of Saadi's method. RR_n indicates the current RR interval, if a QRS complex is detected at the current sample, n [10].

Arzeno et al. [18] used differentiation, integration, and nonlinear transformation; their processing steps resemble Hamilton and Tompkins work [3] and the Hilbert transform. Morphological filters have been used for the detection of the QRSs by Zhang et al. [19]. Their thresholding strategy is based on the maximum amplitude. The method of [19] is illustrated by the processing blocks shown in Fig. 11. In particular, a 3M morphological filter extracts the shape and size information from the input signal, the differentiator works as a baseline drift removal, then differential absolute value is computed, similar to energy transformation,

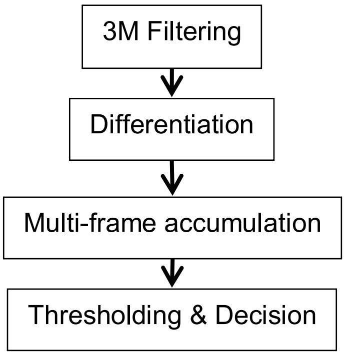

Fig. 11 : Block diagram of Zhang's QRS detection algorithm [19]

this aims to attenuate extra QRS complexes waves influence, and finally, rules based on maximum regions amplitudes are fixed to decide about the final output, and the estimation of the appropriate QRS complex positions. In [3], a QRS detection scheme has been proposed involving a low pass filter, a high pass filter, an integrator and a nonlinear transformation. Zhang et al. [20] contributed to the QRS detection field by the implementation on an FPGA device of a designed QRS detector. Manikandan et al. [21] made use of a noise removal, and a Gaussian function for R peaks location extraction.

II. 3. Frequency Domain

Frequency analysis based methods generally produce poor performance. This is due to the nonstationary behavior of the ECG signal. However, some researchers attempted the QRS detection using frequency domain representation. The use of the standard Fourier transform is not possible because the time information is totally lost in the frequency domain. Alternatively, a time-frequency approach is used, which is the short time Fourier transform (STFT). The STFT preserves the time information over a predefined window. Uchaipichat et al [22] applied thresholding on the resulting STFT components to keep dominant frequencies only. Then R peaks decision stage is apply to identify the R peaks positions. Manikandan et al [23] detected QRSs in the frequency domain, making use of Shannon energy and Hilbert transform.

II. 4. Time-Scale Domain Methods

Time-scale domain methods are characterized by their accuracy and high ability of slopes identification, which is the main feature of the R peak. In addition, by scale variation, frequency range variation is guaranteed. While wavelet-based methods could change their basis to match the analyzed input signal, the Fourier transform bases are restricted to sinusoidal functions only. Time-scale domain techniques demonstrated their efficiency in more than a field of application, such as image processing (Road extraction, object detection…). In general, very interesting works have been proposed for QRS detection. For instance, Shivappriya et al. [24] relies on the detection of R waves at the second scale from the de-noised ECG signal, employing approximation coefficients at the third decomposition level. In addition to a differentiator, squaring operation, and a moving window average process were used. Merah et al [25] method involves a number of processing steps based on wavelets for the identification of the center of the QRS complex, the R peak. They used the Stationary Wavelet Transform (SWT) at the ninth decomposition level with the Symlet-4 mother wavelet. In [26], the same mother wavelet as [25] and SWT have been used till the sixth decomposition level. Then, an inverse SWT is performed after zeroing/modifying some coefficients, before final identification of the QRS positions using a well-known thresholding strategy. Li et al [26] utilized the decomposition levels from 1 of the discrete wavelet transform to separate the QRS from P and T waves, and then thresholding was applied to extract QRS positions. Also, we can find one of the first wavelet-based methods, Kadambe et

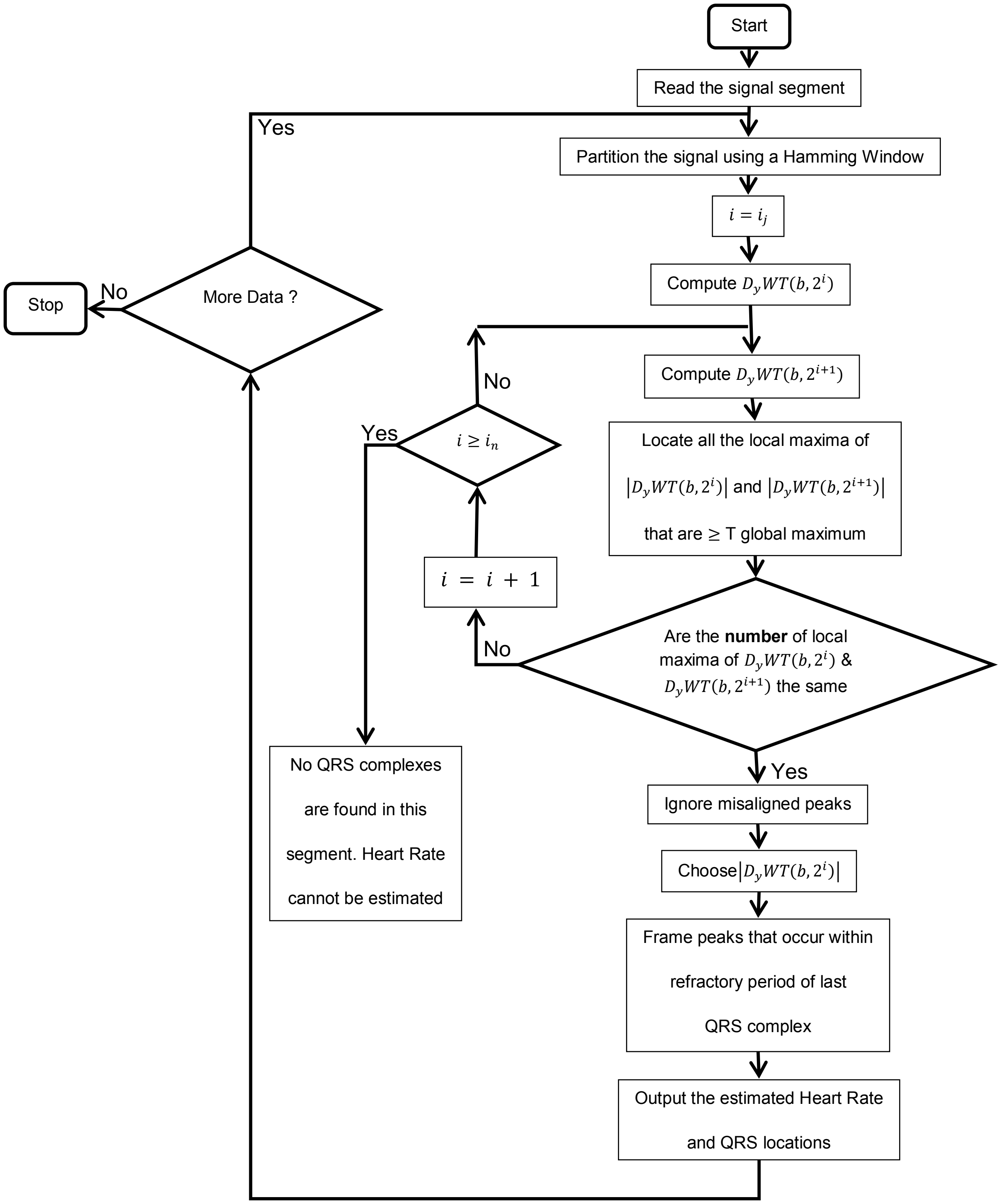

Fig. 12 : Flow chart of Kadambe's DyWT-based QRS detector [27]

al [27], which segments the input signal using a hamming window as depicted in Fig. 12, so the detection of QRSs is performed employing a cubic split mother wavelet. The level of decomposition is estimated instantly by comparing the results of different decomposition levels. Bouaziz et al [28] proposed the detection strategy shown in Fig. 13 and made use of the Daubechies 6 mother wavelet and the detailed coefficients at levels from one to seven for the identification of the different QRS complexes present on the input signal; decomposition levels one, two and eight have been used for noise identification and suppression. Power spectrum computation of the fourth and fifth decomposition levels allow the detection of the QRS complexes by the thresholding rules shown in Fig. 14. The decomposition steps for this method were performed using the discrete wavelet transform (DWT), also from thresholding diagram (see Fig. 14), thresholding level is fixed to be 10% of a computed function value g, and this threshold is applied to determine QRS positions. The detection is achieved by considering the maximum amplitude for segments of 58 samples (about 0.161 seconds). Behbahani et al [29] and Haddadi et al [30] also employed multi-level decompositions for the identification of the QRS complexes. Behbahani et al [29] used the levels from three to five, in addition to a new thresholding scheme as a decision rule. Haddadi [30] exploited the approximation coefficients of levels one to eight to de-noise the signal with the 'db4' mother

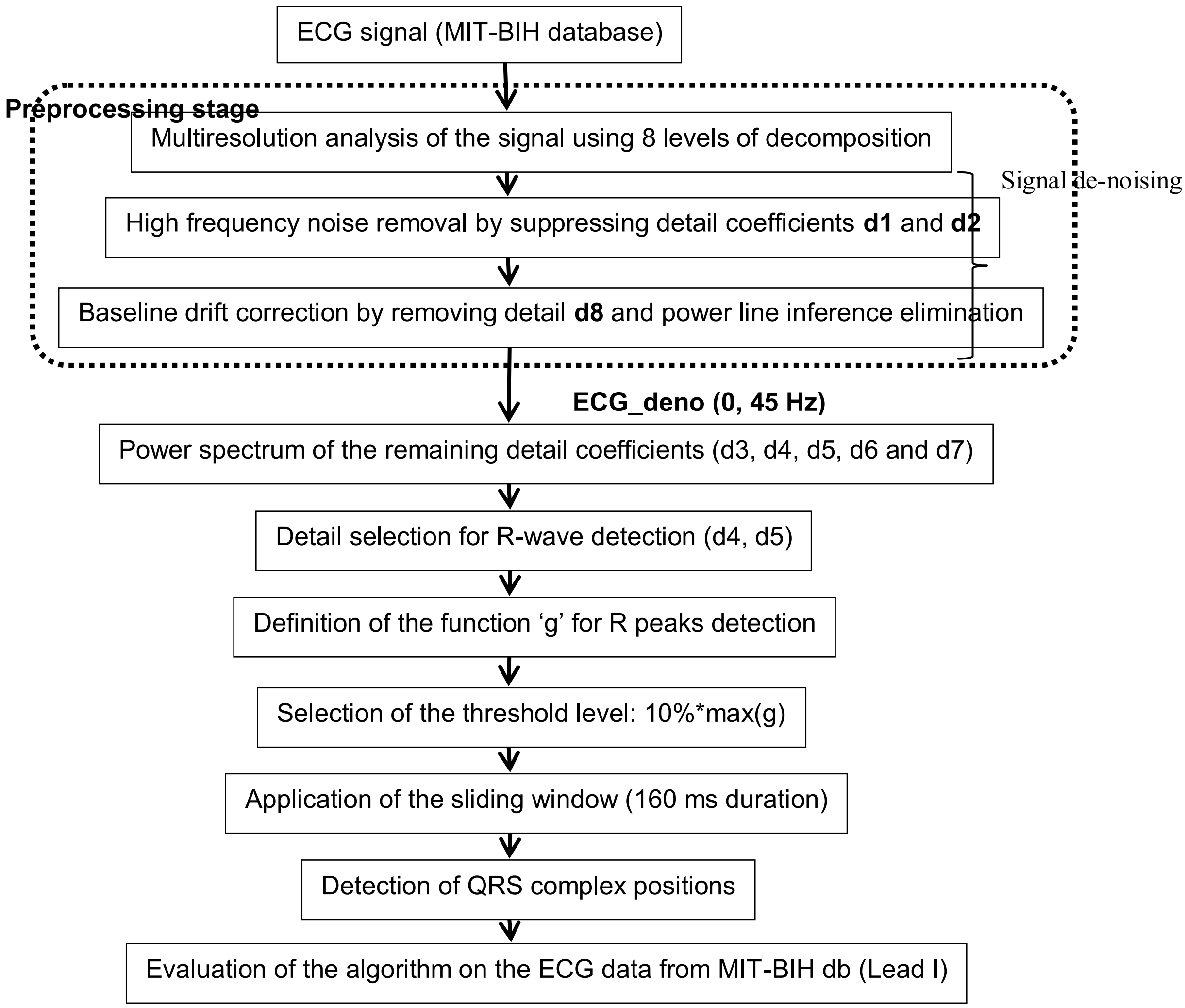

Fig. 13 : Block diagram of Bouaziz's QRS detection algorithm [28]

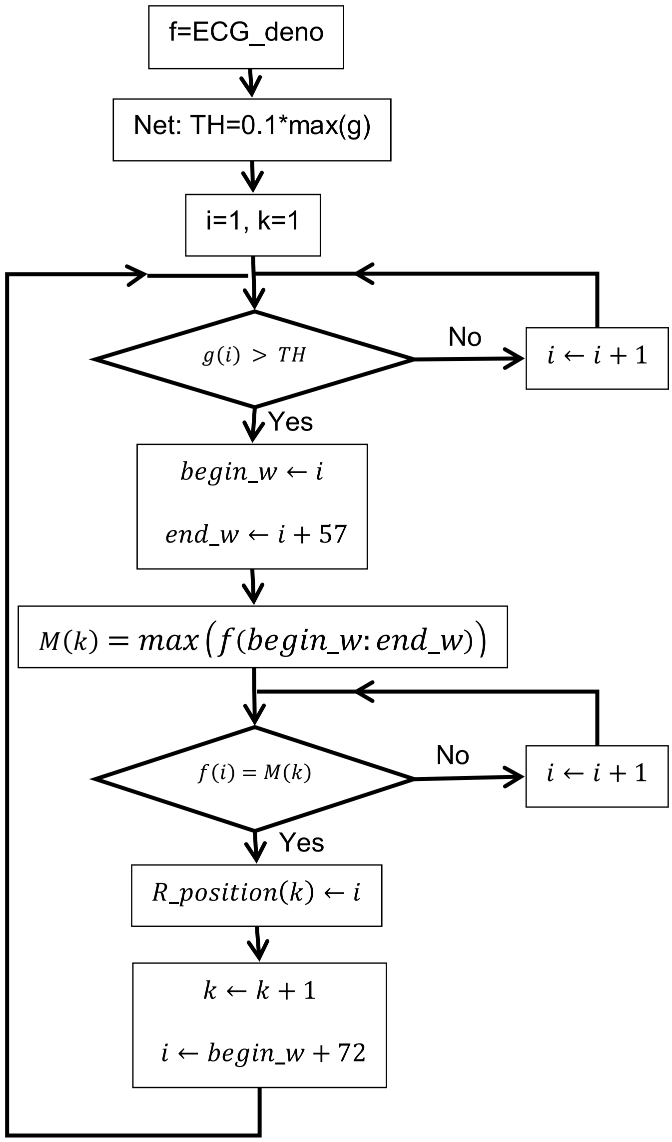

Fig. 14 : Flowchart of R-wave detection algorithm for Bouaziz's method [28]

wavelet, and then level four details coefficients are computed for QRS complex dominance. A new thresholding strategy was developed for the identification of QRS complexes. Jenkal et al [31] used first and second level details coefficients for the de-noising of the input signal. Then, third, fourth and fifth levels were used for thresholding to determine the QRS complexes. In [32], authors utilized the fourth and fifth levels of decomposition for the detection of QRSs, and the seventh for de-noising; the 'db6' has been used for this algorithm, and a thresholding scheme has been proposed taking into consideration the amplitude and the interval between two successive R peaks. Martínez et al [33] made use of the DWT with levels from 1 to 4, before final estimation using thresholding rules. Karimipour et al. [34] proposed a new QRS detection algorithm; they used wavelets for de-noising and detected QRS using curves interpretation as shown in Fig. 15. The input signal is segmented with a window length of 256 samples, corresponding to a sampling frequency of 360 Hz to 711 ms, so wavelet de-noising using the discrete wavelet transform (DWT) is done on the window for noise suppression by means of the daubechies 4 (db4). They used the decomposition levels from one to eight, first derivative curve, area and average curve in addition to arc length

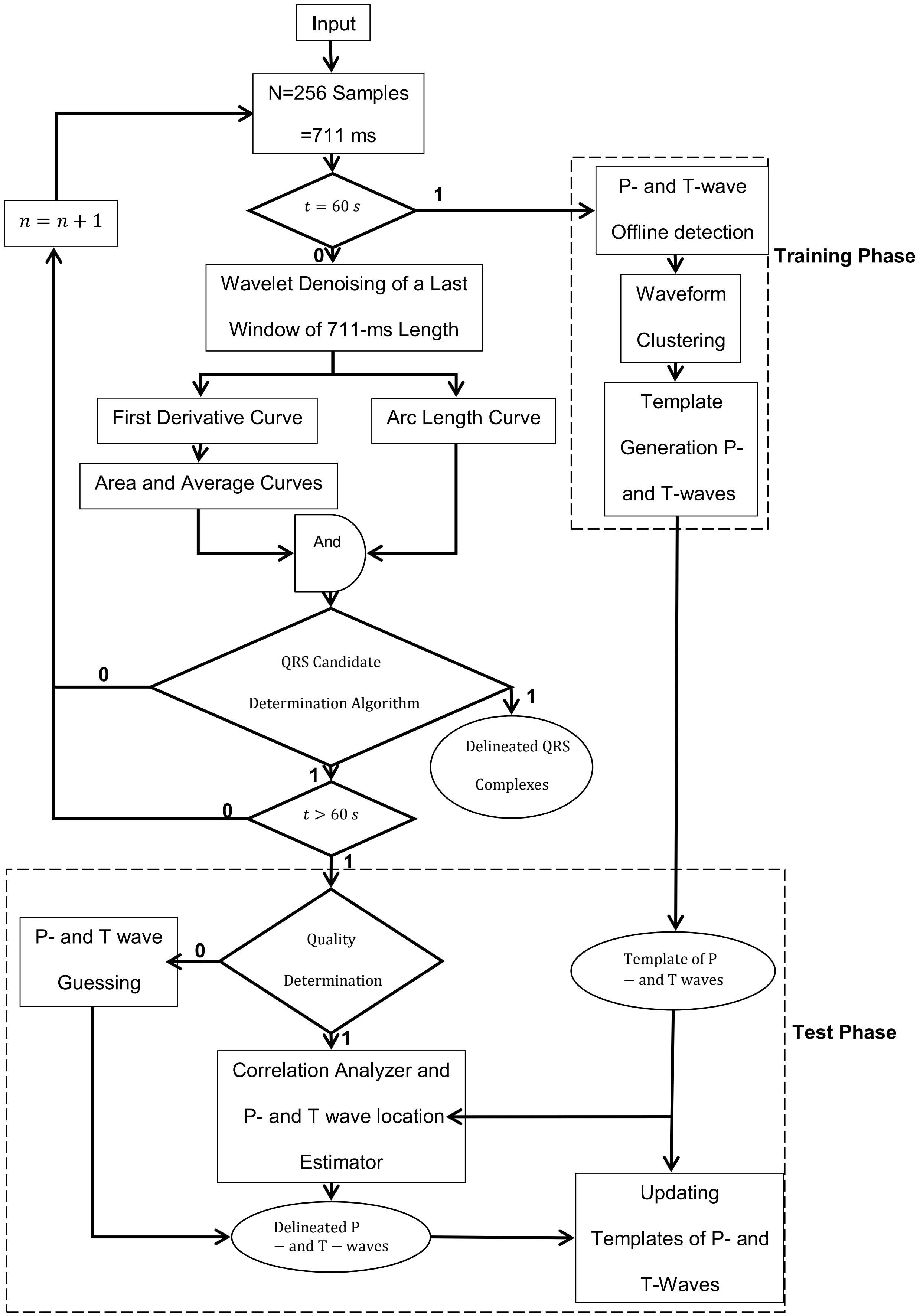

Fig. 15 : Block diagram of Karimipour's real-time P-QRS-T detection–delineation algorithm [34]

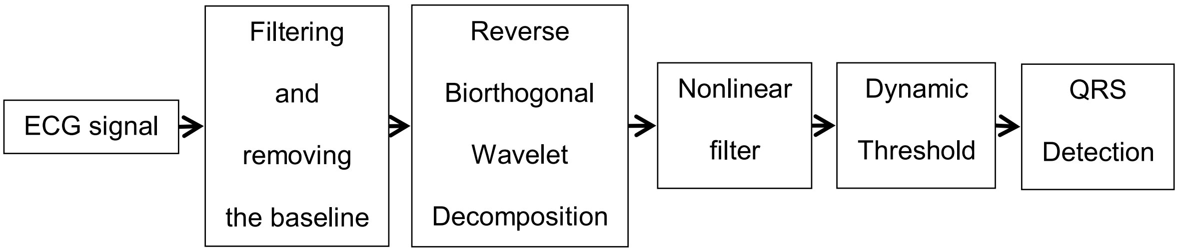

Fig. 16 : Kholkhal's QRS complex detection approach [35]

curve, estimating the necessary elements for this scheme to decide about the presence of the QRSs. A number of rules were used to estimate the exact QRS complex positions. Kholkhal et al. [35] detected the QRS complex from the scheme illustrated in Fig. 16; they detected the QRS from wavelet coefficients after filtering for de-noising. They fused two filters, the first is a median filter for noise removal, and the second is a low-pass filter with a cutoff frequency of 25 Hz for better purification. To make QRS complex waves dominant for efficient thresholding, they used the continuous wavelet transform (CWT) with a reverse biorthogonal wavelet mother, especially the 'rbio2.2'. It has been found that scale 3 is appropriate for detection with good attenuation of the P and T waves. The nonlinear filtering involved an absolute function for positive parity, an averaging filter with a window length of 10, a median filter with a window length of 20, and a dynamic threshold over periods of length T = 2s.

II. 5. Learning Technics

II. 5. 1. Traditional Artificial Intelligence Technics

The number of published algorithms based on traditional artificial intelligence is limited compared to the signal processing approaches. The traditional artificial intelligence methods can be organized into two categories, namely, the Hidden Markov Models (HMM) and the Artificial Neural Networks (ANN). Therefore, our description considers only those two categories. As a sample of the HMM-based approach to QRS detectors, Andreão et al [36] manually selected samples from different databases for the training and the construction of the detection models. Then, the input signal is preprocessed using the continuous wavelet decomposition (CWT) for signal waves taking form for training and testing. The Gaussian density function deviation was used to model P, QRS, and T wave characteristics forms from a structured architecture for HMMs states. Later, the same author Andreão et al [36] presented a new work which can be considered as an extension of the previous one [37]. The first part is similar to the previous one, while the second consists of a set of stages. Generally, models illustrated in Fig. 17 and Fig. 18 provides an overview of the schematic and modeled ECG waves by the authors to describe and predict all the ECG cycle occurrences. Six states have been modeled, namely, isolation (ISO) corresponding to the transition from the T to the P wave, P, QRS and T states represent the P, QRS and T waves, and transition to one of those states when being on the PQ or ST states correspond to a transition state between ECG waves. Thomas et al [38] trained six knowledge-based models to represent the different QRS wave forms and non QRS wave forms. They conditioned the input signal using the CWT transform with Haar mother wavelet. In [39], the authors developed a number of architectures with a dynamic running recursive model parameters adaptation. They improved their initial proposal

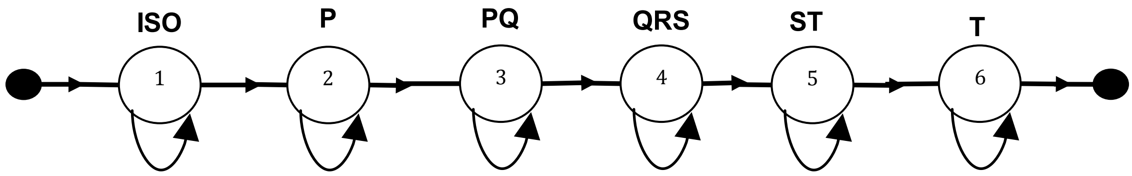

Fig. 17 : Andreão's et al Left-right HMM model of a normal beat [36]

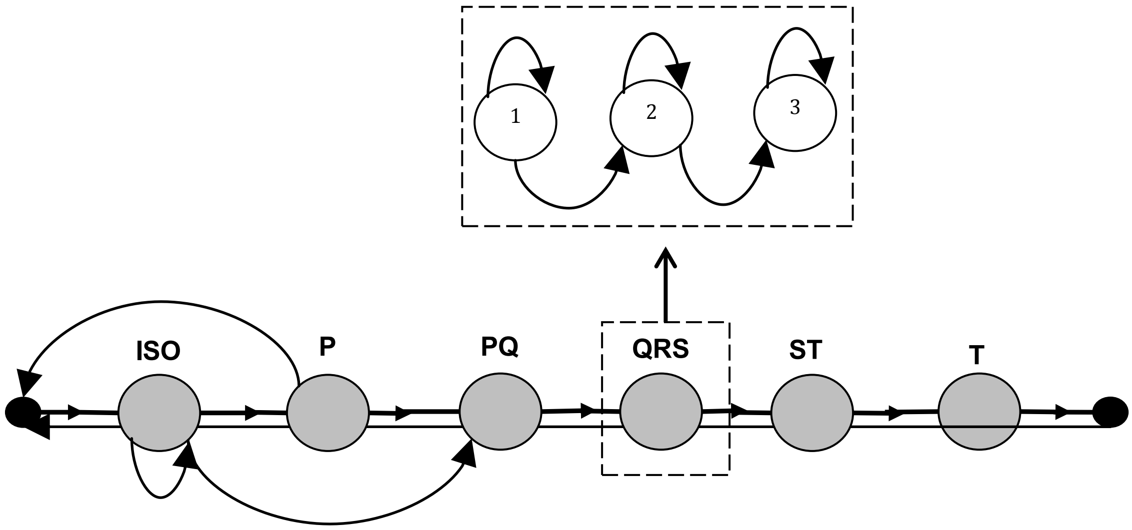

Fig. 18 : Beat model composed of connected HMM of each beat waveform and segment. The transition from P to ISO models ECG signals with P waves not conducted by a ventricular activity. The transition from ISO to PQ models ECG signals with supraventricular arrhythmias without visible P wave. [36]

by time-domain preprocessing where they trained the HMMs models by forward-backward algorithm; a model for QRSs and another for non-QRSs. They considered the QRS process as Markovian and defined an HMM states machines for it. The detection is based on Viterbi algorithm and maximum probabilities following the maximum-likelihood rule, with a consideration of minimum durations of the QRSs and the non-QRSs.

On the other side, detection through Artificial Neural Networks (ANN) is faster and low cost compared to HMM-based methods. Unfortunately, this method is far from being accurate, which is its main drawback. However, many methods have been proposed in the literature based on ANNs. For example, Xue et al [40] one of the first works introducing ANNs to QRS detection. This method consists of an ANN network and a de-noising filter to identify QRSs with processing steps shown in Fig. 19. The processing scheme of this approach consists of FIR filters and artificial neural networks. The two adaptive filters remove noise and feed a matched neural network filter. In [4], authors employed squaring, moving averaging and thresholding. Saini et al. [41] used the K- nearest neighbor (KNN) classifier to detect the QRSs from the gradient curve of a bandpass-filtered signal as depicted in Fig. 20. They pre-trained the KNN classier on record MA1-001 of the CSE database and record 100m of the MIT database. The QRS complexes were detected by binary classification.

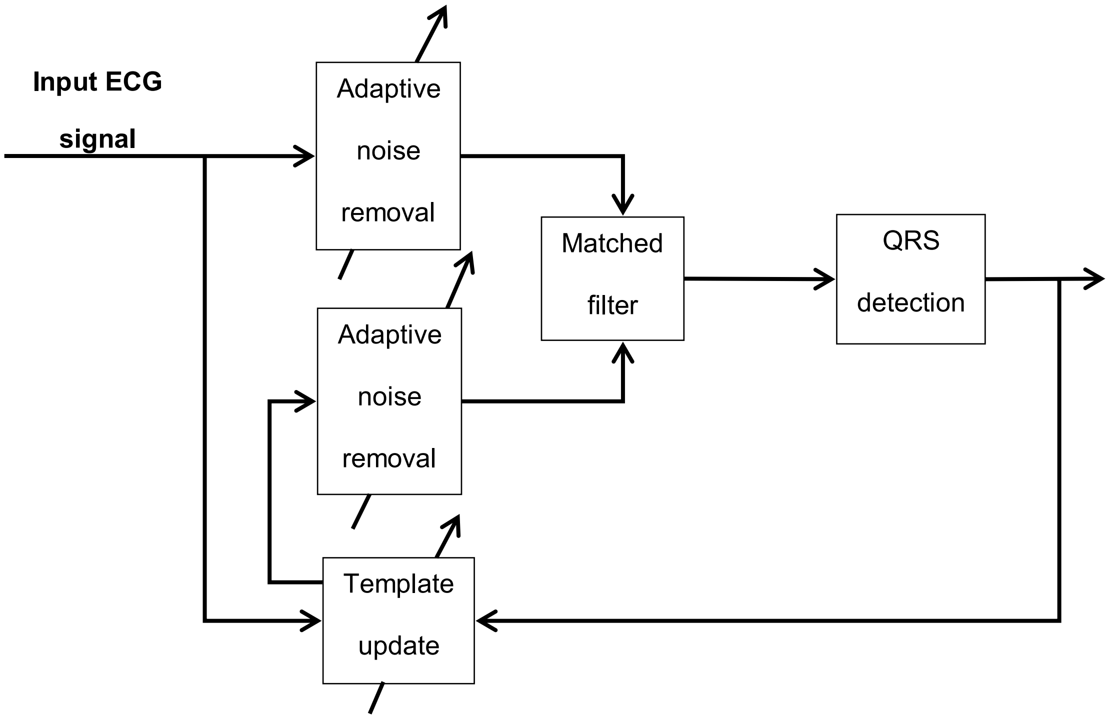

Fig. 19 : Block diagram of ANN-based adaptive matched filter for detection of QRS complexes [40]

II. 5. 2. Deep Learning Techniques

The deep learning (DL) approaches improve by far the classification of QRSs and non QRSs. Indeed, they offer new opportunities to developers and researchers to push further the frontiers to new limits. DL approaches enable researches to determine the appropriate class to an input attribute directly without any preprocessing, whereas traditional algorithms perform very poor. Actually, DL approaches are able to determine autonomously the appropriate features without any intervention of humans. Furthermore, DL requires large number of training samples and produces high generalization of the extracted features. Also, deep learning techniques began to be largely used in the ECG signal processing and classification field. Thus, the use of deep learning approaches started invading the field of biomedical signal processing. Subsequently, we will try to present some prominent works in this domain. Šarlija et al. [42] developed a 300-points convolutional neural network (CNN) and clustering on the neural output for QRS detection, the input signal is preprocessed using baseline wander removaland normalization is used to prevent incomprehensible results. Zhong et al. [43] used a CNN architecture for a reliable fetal QRS complex detection using only a single channel or single lead, without preprocessing the incoming ECG signal. The CNN has been used another time for QRS detection by Xiang et al. [44], this time employing its 1D variant. They used a temporal domain differentiation as an input feature to the deep neural, see Fig. 21, and two CNNs with architecture shown in Fig. 22 to determine the appropriate automatic features for detection. The first used differentiation input and the second used differentiation and averaging. Finally, the extracted features fed a multi-layer perceptron (MLP) classifier for the estimation of QRS positions.

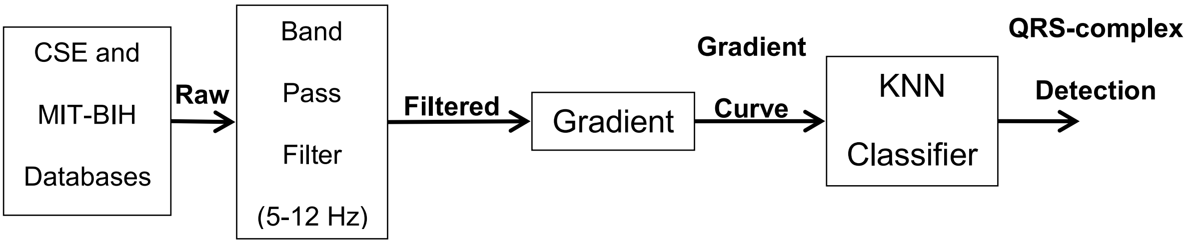

Fig. 20 : Saini's et al Schematic representation of intermediate steps for KNN algorithm implementation [41]

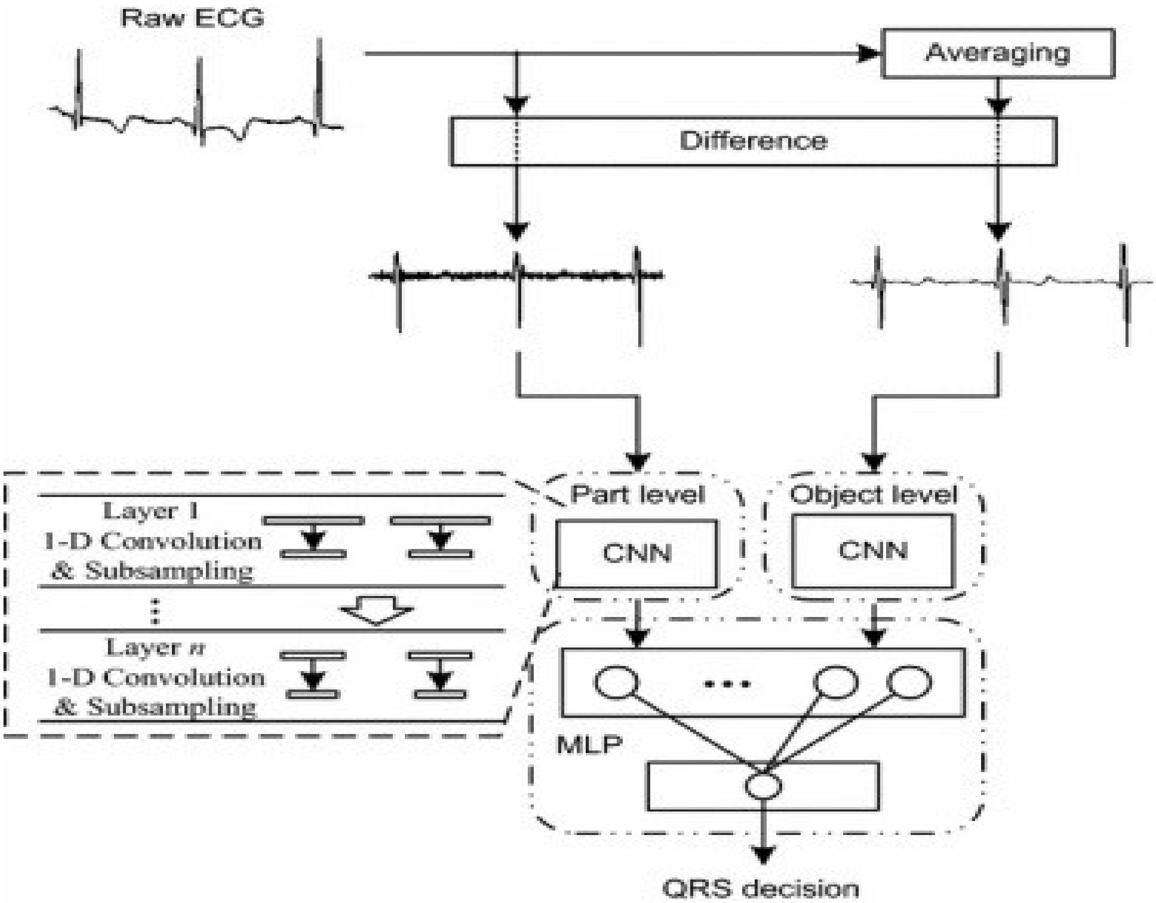

Fig. 21 : Xiang's QRS complex detection method [44]

II. 1. Conclusion

Several automatic techniques for the QRS detection have been reviewed throughout this chapter. A brief description of each method, its main features and some results have been presented. Many challenges have been overcome during the last three decades in term of QRS or R peak detection, accurate techniques have been proposed to resolve this physiological obstacle toward perfect heart state health analysis and interpretation. Now, a solid background of knowledge has been constructed. Among these methods, Martínez et al [33], Saadi et al [10], Gutiérrez-Rivas et al [5] and Kholkhal et al [35] achieved high accuracy when assessed on validation sets. However, disregarding achievements, many developed methods produce catastrophic results on certain scenarios of ECG signals. Also, high complexity of the processing steps of many algorithms increases significantly the detection time, which makes them unsuitable for real-time applications. Therefore, many improvements of those methods can be considered. Hence, this field of research is still open to contributions and developing new methods that hopefully would overcome the present shortcomings. The coming chapters are an attempt to fill this gap. Indeed, we proposed three methods for the QRS detection.

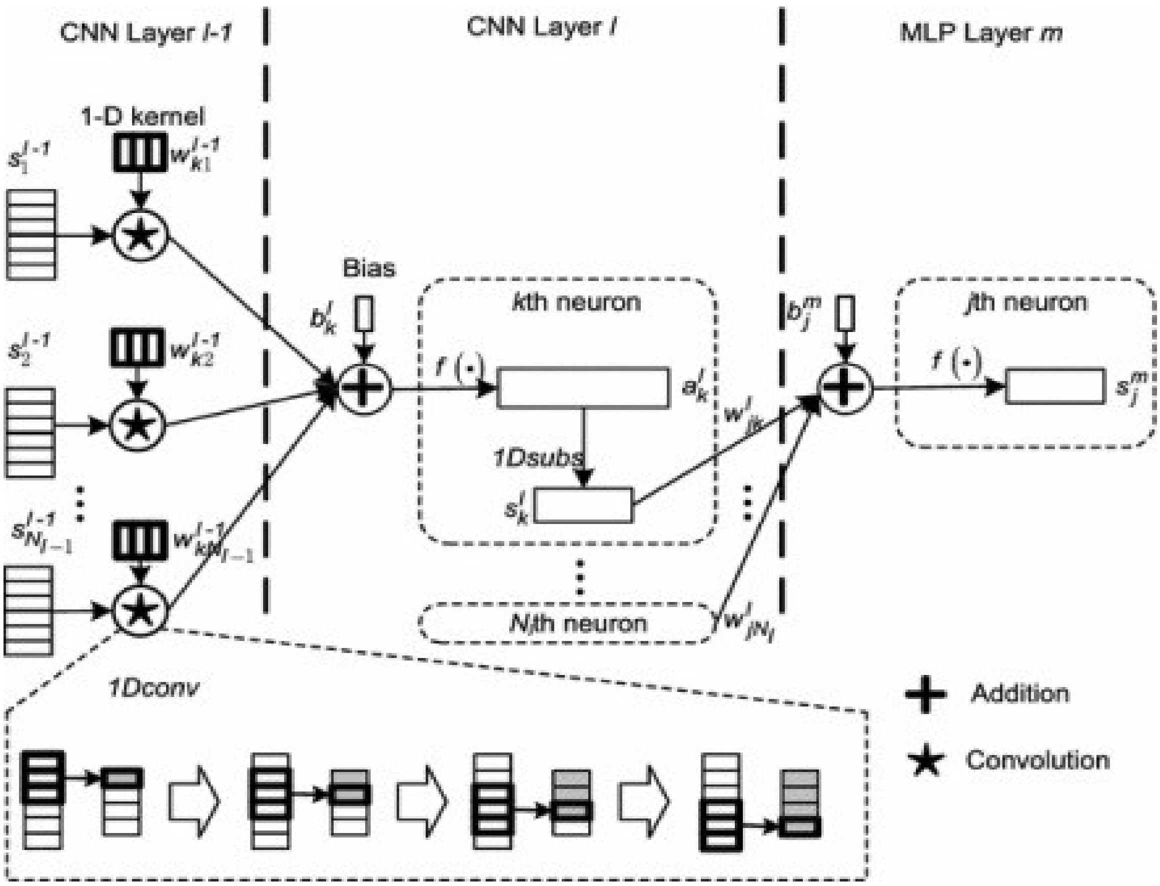

Fig. 22 : Xiang's 1-D CNN structure of the QRS detection [44]

CHAPTER III

SWARM INTELLIGENCE APPROACH TO QRS DETECTION

III. Swarm Intelligence Approach to QRS Detection

III. 1. Motivations and Approach

Among the accurate QRS detection algorithms that have been introduced to the literature during the last decades is the Pan-Tompkins algorithm. Its main features are the simplicity of implementation and low algorithmic complexity. At the aim of investigating the time-domain field, which does not require high skills and advanced transformations, we believe that many parameters of the well-known Pan and Tompkins algorithm were not optimal. Therefore, we used the particle swarm optimization algorithm to search for the set of the parameters that produce the minimum error of QRS detection.

III. 2. Introduction

New method development requires the choice of the appropriate development model. I used the cyclic model shown on Fig. 23 for the design and development of the different proposed algorithms during my dissertation. The adopted approach is advantageous compared to other models like spiral or V models. It allows feedback to rectify imperfections and perform enough tests to ensure the efficiency of the developed algorithm. Further, for the development of each method, a thorough literature review is carried out, then we choose appropriate tools and datasets. After that, we design and code independently the different units. Finally, we evaluate the obtained results, if they are competetive, we pass to the development of another method, otherwise, we improve the present one.

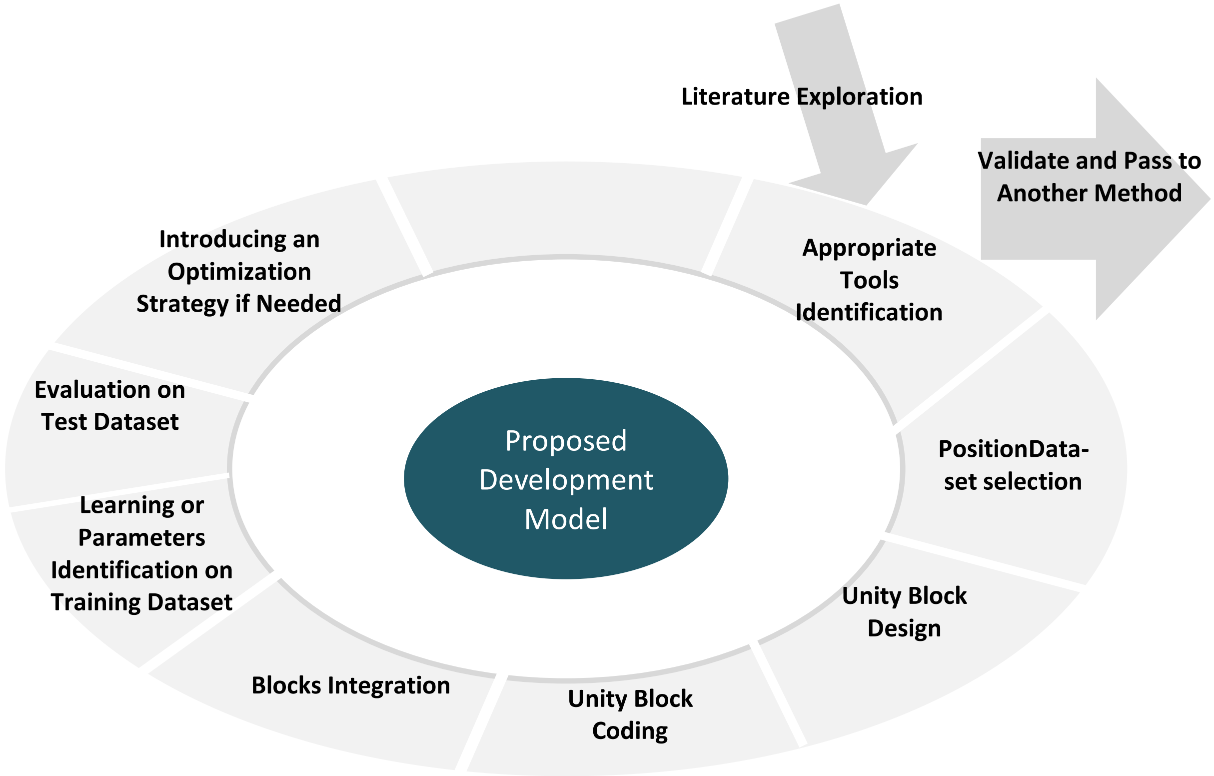

-

Fig. 23 : Follow cyclic development model

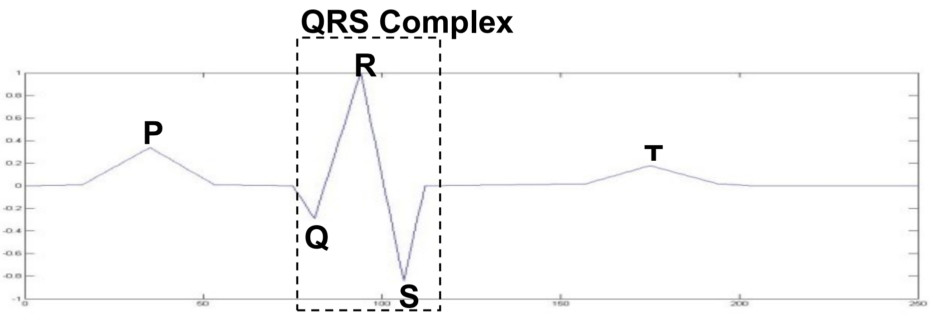

Fig. 24 : One cycle of a typical synthetic ECG signal

A great importance is given to the detection of the QRS wave shown on Fig. 24, comprising Q, R, and S waves, as it is essential for heart rate determination and beat type segmentation and recognition. The detection of the R wave, which is the peak of the QRS, is tricky since it has a time-varying morphology and is subject to physiological variations due to the patient state and noise [16]. The RR interval is the interval between two successive R peaks; identifying RR intervals permits to segment the ECG records.

Usually, the ECG signal is corrupted by many sources of noise. Among common types of noise, we name the $50/60$ Hz power line interference, the baseline drift due to respiration, and the electrode contact noise. To attenuate these disturbances and enhance the QRS components, many suggestions of the bandpass filtering have been proposed with the following frequency ranges, $[5, 15]$ Hz, $[8, 15]$ Hz or $[8, 20]$ Hz, etc. [54].

A variety of processing steps have been adopted for QRS detection before the decision process, which is usually carried out by thresholding. These processing steps can be categorized according to the domain in which the detection is done. The two major categories are the signal processing category and the learning techniques category. In this chapter, we explore time-domain methods. The ECG signal is not exclusively composed of the QRS

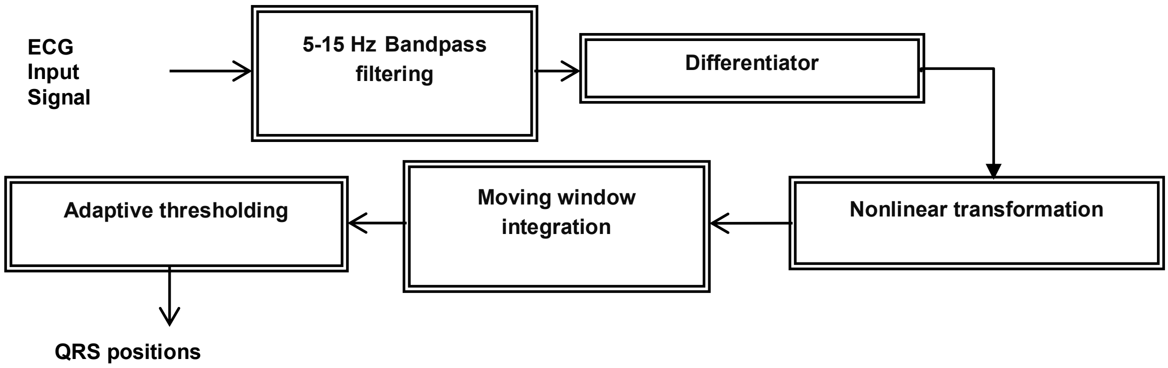

Fig. 25 : The five operations of the Pan-Tompkins algorithm.

complex wave alone. Hence, we need to attenuate the P and T waves and enhance the QRS complex wave. Usually, the signal processing steps consist of differentiation, integration and nonlinear transformation. The only remaining issue to implement the detector is the type of filters and their frequency range, as well as the number of samples per window for integration.

We think that the performance of many existing algorithms could be enhanced if the filtering parameters were optimized. In particular, many parameters of the Pan and Tompkins algorithm [4] are selected empirically. For example, the cutoff frequencies of the bandpass filter were determined by knowledge of an estimated band frequency of different sources such as muscle artifacts and stress. Also, the length of the averaging window and the parameters of the threshold are selected empirically. Since the problem at hand cannot be formulated in a closed-form formula, traditional optimization methods that rely on the computation of the gradient cannot be used. Therefore, we resort to evolutionary computational optimization methods. Among these methods, Particle Swarm Optimization (PSO) has gained a lot of popularity during the last two decades. The popularity of the PSO may be due to its simplicity, few code lines, and it provides potential solutions in many complex situations. Thus, we propose to use the particle swarm optimization algorithm to look for the best values of the parameters of the popular Pan-Tompkins algorithm such as cut off frequencies of the bandpass filter, the length of the averaging window, the threshold, etc, to improve its capability of detection for the QRS complexes.

III. 3. Pan & Tompkins Algorithm

Since our contribution is about improving the Pan-Tompkins algorithm, we start by describing the main steps involved in this algorithm. The main steps of the original Pan-Tompkins algorithm are depicted in Fig. 25. The algorithm comprises five steps which we will briefly describe in the following. The bandpass filter eliminates noise from the input raw ECG signal. The differentiator is introduced to detect abrupt variations in the signal. The nonlinear transformation is the square of the differentiated signal used to reduce the amplitudes of the T and P waves compared to the R peak amplitude wave (after normalization) and to make the values of the signal positive. The aim of the moving window integration is to make the P, Q, R, S, and T peaks appear together in a unique peak in order to reduce the number of false detections.

The decision strategy relies on the use of two main parameters which are the signal level and the noise level. The former is computed from a running estimation of the signal level whereas the latter is computed from a running estimation of the noise level. In particular, the first type of thresholding which is a running level of the separation between the amplitudes of the signal and the amplitudes of noise is formed by combining the estimated levels of the signal and noise. This type is used in normal cases. When no R peak is detected in a long time using the first type of thresholding, a search back procedure is launched with another type of thresholding. This second type of thresholding uses new rules for R peak detection.

In the training phase of our optimization algorithm, we estimate the threshold levels of the signal and noise from the few first seconds of the ECG input signal. First, we search for all the peaks present in this time interval and the minimum interval between them. We decide that a peak is an R wave if its amplitude is greater than the threshold level, and we update the level of the signal. Otherwise, if the amplitude of the peak is greater than the threshold level and the mean of amplitudes in this region is less than or equal to a certain percentage of the mean of amplitudes in the region of the previously detected R wave, and the interval between the current peak and the last detected R peak is within a certain value, then the current peak is a T wave and we update the noise level. If the amplitude of the current peak is less than the level of the search back threshold, it is a noise peak; we update the level of noise then. At each peak, we test if a search back is needed, and we update the threshold levels according to the levels of the signal and noise.

The search back procedure checks if the current RR interval is within a predefined interval. Otherwise, we reduce the level of the signal, if the current RR interval is greater than a predefined limit, then a search back is needed, we update the level of the signal. If the maximum amplitude between the last detected peak and the current peak is greater than or equal to the threshold level of the search back procedure, the corresponding position is considered as an R peak.

III. 4. The Particle Swarm Optimization (PSO)

PSO is a heuristic algorithm, inspired by fish flocking and birds flying. It has been used in a variety of optimization problems and usually delivers interesting results. It involves many characteristics that are common to heuristics search algorithms such as initial population, calculation of the current outputs, and mutation of the population to potentially reach better solutions. The PSO algorithm has many advantages; among them, we cite fast convergence, simplicity of implementation using only a few lines of code, and a reduced number of parameters. The potential solutions of the population of the PSO are called particles; they are usually initialized with random values. Each particle (pi) has its proper knowledge of its environment, represented by the present values that are the input values to the fitness function, and the values that are the best set of parameters that give the best output value (pbi) for a certain particle. The present values of a particle are adjusted at each generation by the velocity vector (vi).

The algorithm possesses a global best (pg), which is updated during each generation; it represents the best solution found so far, which is social knowledge. The steps involved in the

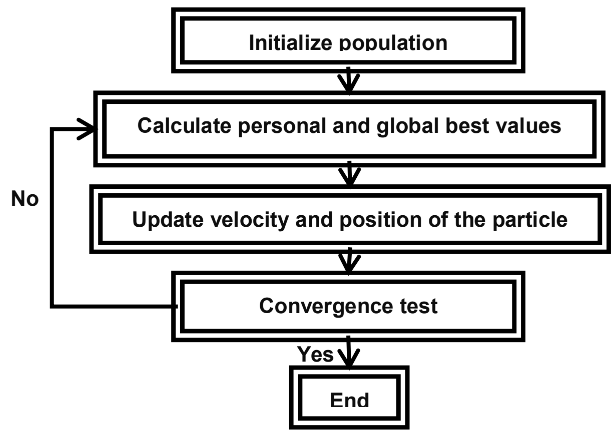

Fig. 26 : The steps involved in the PSO algorithm.

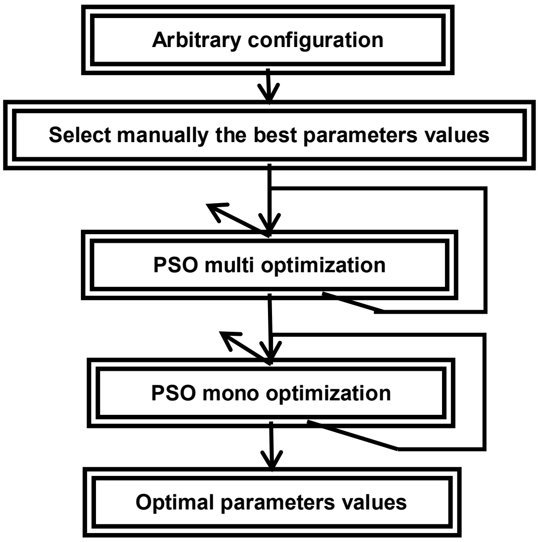

Fig. 27 : Optimization strategy particle update diagram.

PSO algorithm is illustrated in the block diagram of Fig. 26.

During each generation, the PSO algorithm updates its velocity vector and particles positions according to the following two equations.

$$v_i(t+1) = wv_i(t) + c_1r_1(t)\left(p_{bi}(t) - p_i(t)\right) + c_2r_2(t)\left(p_g(t) - p_i(t)\right) \quad \ldots(3)$$

$$p_i(t+1) = p_i(t) + v_i(t+1) \quad \ldots(4)$$

Where w stands for the inertia factor introduced as a regularization factor in (1) to prevent premature convergence. r1 and r2 are random numbers drawn from a uniform distribution in [0, 1], c1 and c2 are constants.

III. 5. The Proposed Optimization Approach

III. 5. 1. PSO Setup

As mentioned above the parameters of the PanTompkins are selected empirically. In particular, the coefficients involved in the design of the low pass and high pass filters are

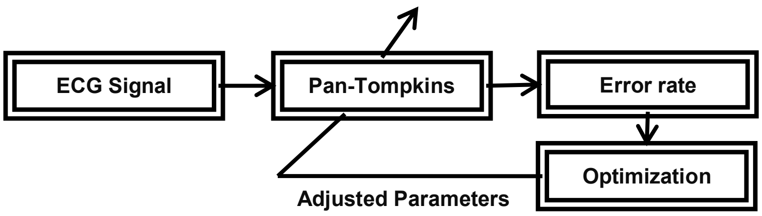

Fig. 28 : Flowchart showing the steps involved in the proposed optimization scheme.

chosen to be integers in order to reduce the computation load of the algorithm and make it appropriate for real-time implementation on microprocessors.

Also, the frequency response of the final resulting bandpass filter is approximately 5-11 Hz [4]. We think that this range is so narrow to represent the QRS wave complex which needs a wider range to represent its abrupt change in the time domain. Hence, we propose a new procedure to look for optimal values of the Pan-Tompkins algorithm which allows better QRS detection. For this purpose, we formulate the optimization problem as a space of parameters searched employing the PSO algorithm.

We opted to a multi-mono optimization approach as shown in Fig. 27. The multi optimization approach drives the algorithm near the global optimum. Then the mono optimization approach minimizes the error of each parameter.

Given the raw ECG signal which contains 24 hours of recording of the MIT-BIH Dataset, we applied the Pan-Tompkins algorithm with initial values of [4]. Our PSO-based algorithm tries to change the values of the Pan-Tompkins parameters to look for potential new best values for the next iteration. The main steps of the proposed optimization procedure are depicted in Fig. 28. The proposed scheme is driven by the performance of the ability of the Pan Tompkins algorithm to detect the QRS complex. The PSO adjusts the parameters of the Pan-Tompkins algorithm in such a way that the detection of the QRS complex improves with time.

In general, the most challenging thing in the application of the PSO is finding the appropriate fitness function. In our optimization scheme which relies on the PSO algorithm, in order to explore the solution space which depends on many parameters, we investigated three different fitness functions. The first fitness function is the total error, the second and the third ones use the sensitivity and the positive predictive value with different weights. In particular, the first fitness function is given by

$$\mathrm{F_1(X)} = \frac{\mathrm{FP+FN}}{\mathrm{TP+FP+FN}} \qquad \ldots(5)$$

Where X is the vector of the parameters, $\mathrm{F_1(X)}$ considers only the total detection error. In Equation (5), TP stands for true positive beats, which is the number of beats effectively present in the record and effectively detected by the algorithm. False Positive (FP) is the number of beats detected by the algorithm, but not effectively present in the record. False Negative (FN) is the number of beats not detected by the algorithm, but present in the record. The second fitness function is given by

$$\mathrm{F_2(X)} = (100 - \mathrm{Se})^2 + (100 - \mathrm{PPV})^2 \qquad \ldots(6)$$

It is the Euclidian distance of the error based on the Sensitivity (Se) and the positive predictive value (PPV). The third fitness function is given by

$$\mathrm{F_3(X)} = 0.75 * (100 - \mathrm{Se})^2 + 0.25 * (100 - \mathrm{PPV})^2 \qquad \ldots(7)$$

It is the weighted Euclidian distance of the error. In Equation (7) more importance is given to the sensitivity as compared to the positive predictive value due to the major attention given to this ratio by medical practitioners. In Equations (6) and (7); the sensitivity and the positive predictive value are defined as

$$\text{Se} = \frac{\text{TP}}{\text{TP+FN}} \qquad \dots(8)$$

$$\text{PPV} = \frac{\text{TP}}{\text{TP+FP}} \qquad \dots(9)$$

Sensitivity expressed by Equation (8) measures the ability of our detector to extract QRS complex positions. Indeed, the sensitivity increases with the reduction of the number of missed beats. Likewise, the positive predictive value described by Equation (9) measures the ability of our detector to reduce false detections; this is reflected by an increase in positive predictive value when FP decreases. Equations (8) and (9) are exploited in Equations (6) and (7) with different weights to measure their effectiveness in driving the optimization algorithm.

Applying our proposed procedure using the adopted three fitness functions on the MIT-BIH dataset has led to the results shown in Fig. 29. It is the variation of the fitness value as a function of the iteration number. We can see that $\text{F}_3(\text{X})$) converges faster than $\text{F}_1(\text{X})$ and $\text{F}_2(\text{X})$. Moreover, from Fig. 30, Equations (6) and (7) minimize better the error rate, and Equation (7) converges much faster than Equation (6). Furthermore, from Fig. 31 and 32, which represent the evolution of the sensitivity and positive predictive value, respectively, it is clear that using Equation (7) for optimization allows both the sensitivity and the positive predictive value increasing faster, while Equation (5) does not achieve a considerable improvement of the positive predictive value which gives rise to higher error rate than the other variants.

In summary, after extensive simulations, for the rapid convergence, and the best approximation of the minimum error rate, we selected (7) as a fitness function for our proposed optimization approach.

III. 5. 2. Procedure

The main steps of the proposed scheme are detailed in the following algorithm.

Initialization

- Set initial values for different parameters of the Pan-Tompkins algorithm (e.g., low cutoff frequency, high cutoff frequency, filter order, number of samples for the integration window, etc.,) to be the initial population of the PSO algorithm.
- Choose a random initial value for the velocity vector. For each particle, evaluate the fitness function given by (5).
- Store the position of each particle and label it as the best local position.
- Save the position of the particle with the largest fitness function value as the best global position.

Search Process (Parameters Update)

- Update the values of the velocity of each particle using (1).
- Update the position of each particle using (2).
- Using the new particle coordinates compute the new fitness function of each particle.

- Update the best local positions and save the coordinates of the particle with the minimum fitness function as the best global position.

Convergence check

- Repeat the "search process" steps until the user pre-defined number of iterations or predefined accuracy is reached (convergence check).

III. 6. Experimental Results and Discussions

III. 6. 1. Dataset Description

For the sake of the assessment of the proposed optimization procedure, we conducted experiments based on the benchmark MIT-BIH dataset available online at [45]. It consists of

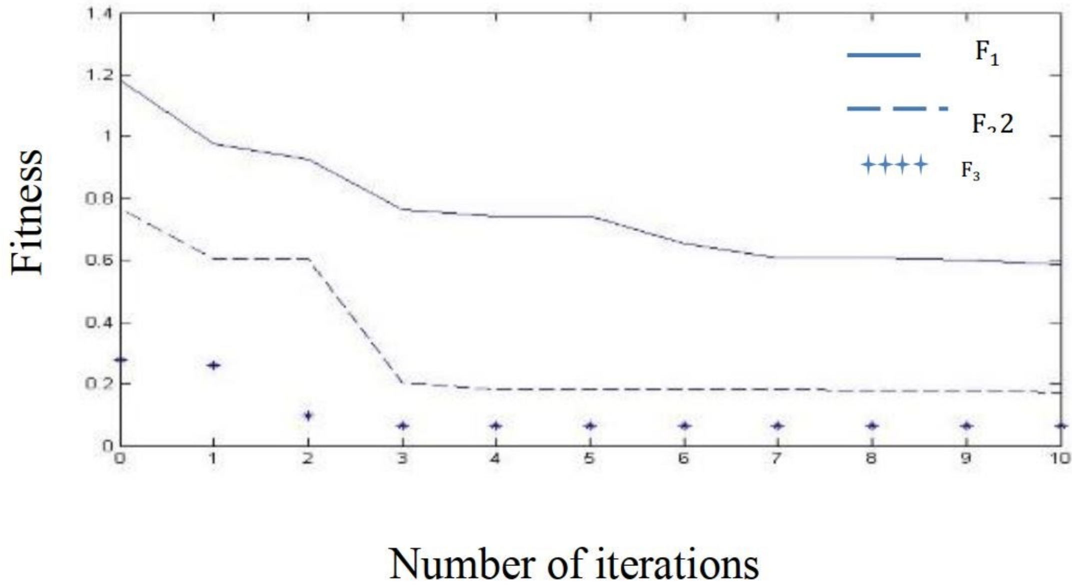

Fig. 29 : The fitness function vs. the number of iterations.

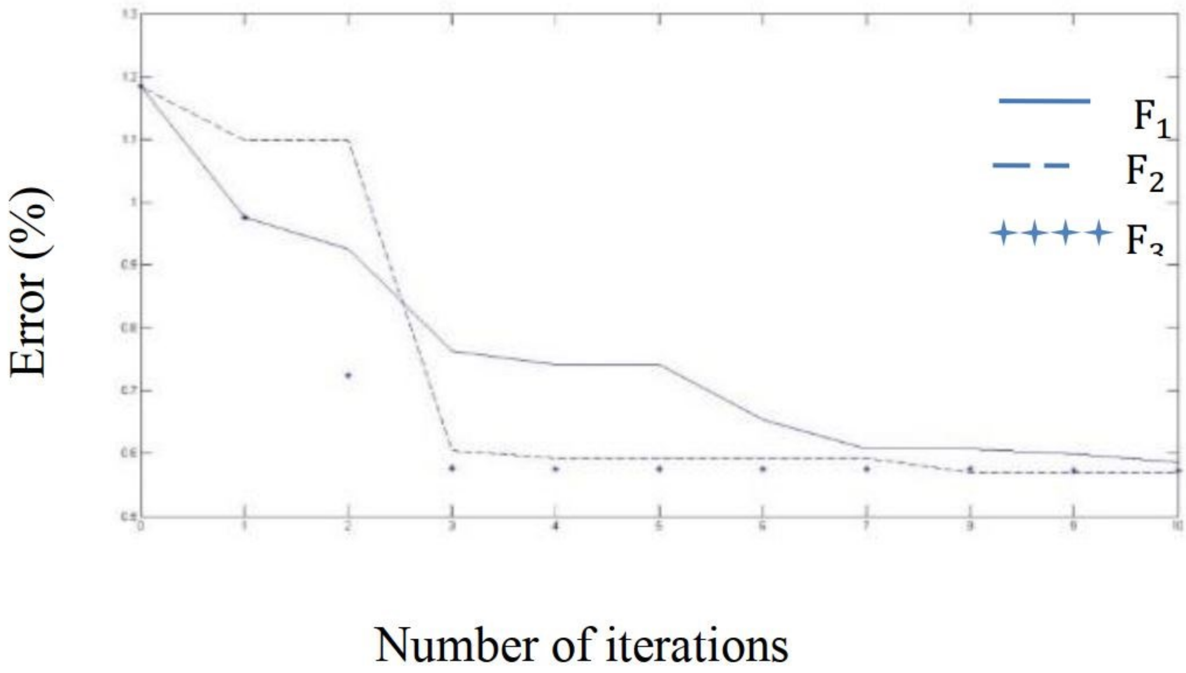

Fig. 30 : The total error vs. the number of iterations.

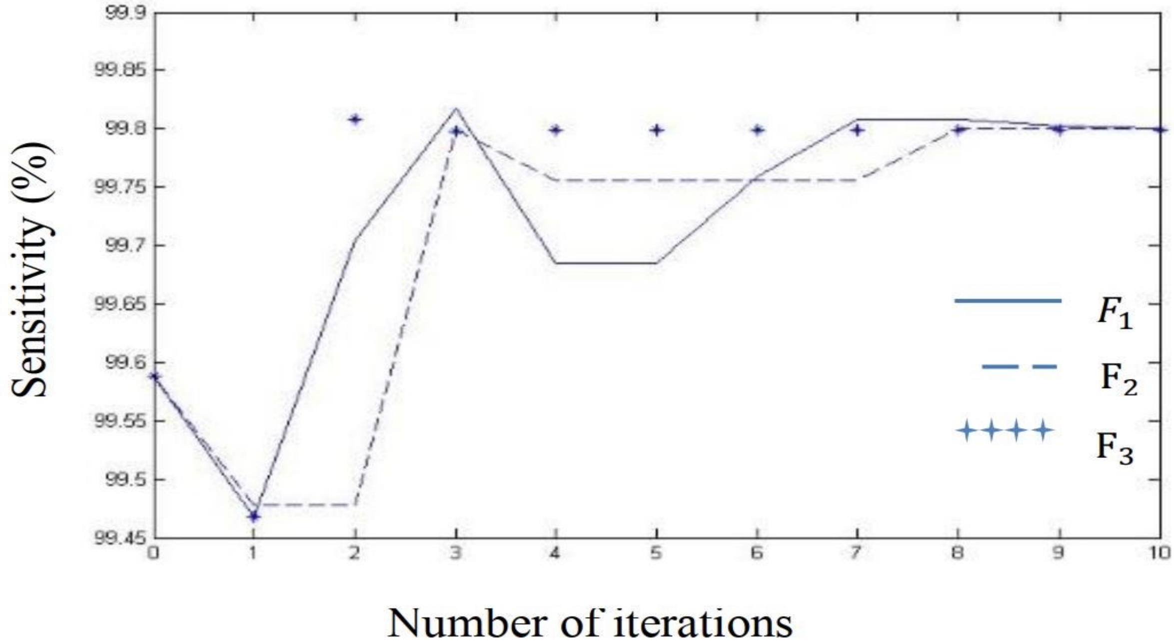

Fig. 31 : The sensitivity vs. the number of iterations.

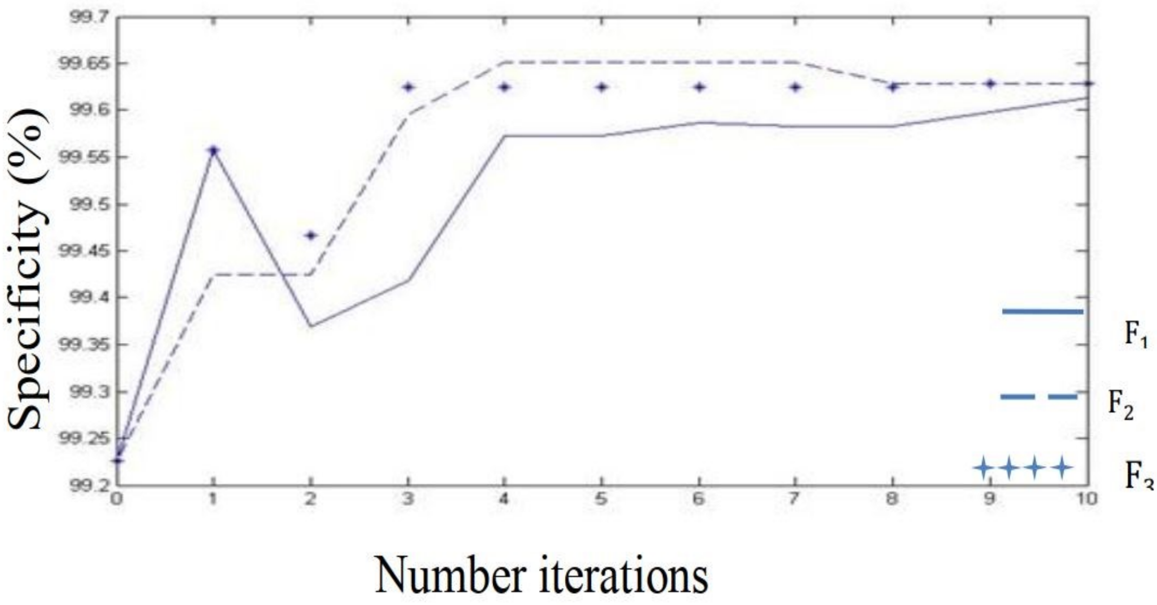

Fig. 32 : positive predictive value vs. the number of iterations.

48 records acquired from 47 subjects. Each record is 30 minutes long. The total number of beats used in our experiments is 109494.

It covers a wide range of arrhythmia; hence, it contains a wide range of QRS shapes that constitute a big challenge for any detection system. The dataset was annotated independently by two experts.

III. 6. 2. Experimental Setup

The PSO empirical parameters were selected according to the following configuration: The size of the swarm was fixed to 20 and the number of iteration was set to 550. The number of iterations has been set after many trials where it has been observed that the proposed algorithm converges after 500 iterations. The inertia weight was set to w=0.4 and both the cognitive coefficient c1 and the social coefficient c2 are set to 1.

It is worth noting that the band-pass filter used in our optimization scheme is a Finite Impulse Response (FIR) filter. We preferred the FIR filter because of its intrinsic characteristics of stability. Though Infinite Impulse Response (IIR) filters design results in a lower filter order, it is necessary to check for stability every time the filter coefficients are updated.

It is common to adopt as measures for the performance assessment of any QRS detection algorithm three measures, which are the total error represented by Equation (3), the sensitivity represented by Equation (6), and the positive predictive value given by Equation (7).

III. 6. 3. Results

The obtained results at convergence for the optimized parameters of the Pan-Tompkins algorithm are summarized in Table 1. We note that most of the original Pan-Tompkins parameters were not optimal as the obtained results confirm. This is because the parameters were selected empirically. Our claim is supported by the results obtained by the proposed optimization scheme evaluated on the MIT BIH dataset shown in Table 2. As expected, the obtained bandpass filter cutoff frequencies by our procedure [4, 24] Hz are wider than the ones of the original Pan-Tompkins algorithm, [5, 15] Hz. This allowed the detection of many QRS waves that were missed by the Pan-Tompkins algorithm. Overall, our scheme failed in detecting 185 beats only. Whereas, the optimization scheme converged to the same length of the averaging window (30 samples) and the same number of the average RR intervals (8 intervals).

Table 1 : The obtained Parameters of the Pan-Tompkins Algorithm at Convergence Using the Proposed Optimization Scheme. Initial Value Refers to The Value of The Parameter In Pan-Tompkins.

Parameter	New value(initial guess)(Unit)
The low cutoff frequency of the bandpass filter	4 (5) (Hz)
The high cutoff frequency of the bandpass filter	24 (15) (Hz)
Order of the FIR bandpass filter	250 (3 IIR)
Window length of the integrator	30 (30) (samples)
Minimum two successive peaks distance	99 (72) (samples)
Length of the window RR averaging	8 (8) (samples)
Search back signal level percentage from the normal signal level	1.5326 (2)
Current peak update factor in the search back procedure	0.4427 (0.25)
Signal level update factor in the search back procedure	0.7546 (0.75)
Distance between the current sample and the last detected R peak in the search back procedure	139 (72) (samples)
Distance between the current sample and the current peak in the search back procedure	83 (72) (samples)
RR LOW LIMIT percentage from RR AVERAGE2	90.7% (92%)
RR HIGH LIMIT percentage from RR AVERAGE2	116.74 % (116%)
RR MISSED LIMIT percentage from RR AVERAGE2	160.44 % (166%)
Distance between the current peak and the last detected R peak	119 (130) (samples)
Length of the current peak region	31 (27) (samples)
The factor of mean amplitudes of the R peak region	0.5634 (0.5)
Current peak update factor for noise level estimation	0.2316 (0.125)
Signal level update factor for noise level estimation	1.8228 (0.875)

Table 2 : Obtained Results over MIT/BIH Arrhythmia for the Optimal Proposed Scheme. The error is determined by DER(%) = 100*(FP+FN)/(TP+FP+FN).

File	Nb beats	TP	FPs	FNs	DER	PPV	Se
100m	2273	2272	0	1	0.04	100	99.96
101m	1865	1865	0	0	0	100	100
102m	2187	2187	0	0	0	100	100
103m	2084	2084	0	0	0	100	100
104m	2229	2229	5	0	0.22	99.78	100
105m	2572	2571	21	1	0.86	99.18	99.96
106m	2027	2027	0	0	0.1	100	100
107m	2137	2134	0	3	0.14	100	99.86
108m	1763	1763	8	0	0.45	99.54	100
109m	2532	2532	0	0	0	100	100
111m	2124	2123	0	1	0.05	100	99.95
112m	2539	2539	0	0	0	100	100
113m	1795	1794	4	1	0.28	99.78	99.94
114m	1879	1878	4	1	0.27	99.79	99.95
115m	1953	1952	0	1	0.05	100	99.95
116m	2412	2398	0	14	0.58	99.96	99.42
117m	1535	1535	0	0	0	100	100
118m	2278	2278	1	0	0.04	99.96	100
119m	1987	1987	0	0	0	99.95	100
121m	1863	1862	0	1	0.05	100	99.95
122m	2476	2476	0	0	0	100	100
123m	1518	1518	0	0	0	100	100
124m	1619	1619	0	0	0	100	100
200m	2601	2599	2	2	0.15	99.92	99.92
201m	1963	1953	3	10	0.66	99.85	99.49
202m	2136	2133	0	3	0.14	100	99.86
203m	2980	2963	3	17	0.67	99.9	99.43
205m	2656	2653	0	3	0.11	100	99.89
207m	1860	1855	4	5	0.48	99.79	99.73
208m	2955	2945	2	10	0.41	99.93	99.66
209m	3005	3005	0	0	0	100	100
210m	2650	2643	1	7	0.3	99.96	99.74
212m	2748	2748	0	0	0	100	100
213m	3251	3250	0	1	0.03	100	99.97
214m	2262	2261	0	1	0.04	100	99.96
215m	3363	3360	0	3	0.09	100	99.91
217m	2208	2208	0	0	0	100	100

219m	2154	2154	0	0	0	100	100
220m	2048	2048	0	0	0	100	100
221m	2427	2426	0	1	0.04	100	99.96
222m	2483	2483	19	0	0.77	99.24	100
223m	2605	2605	0	0	0	100	100
228m	2053	2052	8	1	0.44	99.66	99.95
230m	2256	2256	0	0	0	100	100
231m	1571	1571	0	0	0	100	100
232m	1780	1780	11	0	0.73	99.39	100
233m	3079	3078	0	1	0.03	100	99.90
234m	2753	2753	1	0	0.04	99.96	100
Total	**109494**	**109406**	**97**	**88**	**0.169**	**99.91**	**99.92**

For a fair comparison with the existing methods, we compared our optimization scheme with the state-of-the-art methods. As shown in Table 3, our optimization scheme outperforms all time-domain methods including the well-known Pan-Tompkins algorithm when using approximately the same number of test beats. The only exception which produced the best result (0.15% of error) used only 101579 beats, which is less than our total number of test beats by more than 7900 beats. It is worth noting that our optimization scheme produced 99.92% of sensitivity and 99.91% of predictivity. We developed this optimization approach to enhance the monitoring of heart disease which is the leading cause of death and to contribute to the improvement of the detection process. Generally, repeated failures of the QRS detector influence the disease detection process and this has a bad influence on the diagnosis result. The obtained results for QRS detection presented in this manuscript give us more confidence in the computerized methods for disease identification.

Table 3 : Comparison of the Performance of the Proposed Scheme with State-of-the-Art Methods. Here DER (%)=100*(FP+FN)/(TP+FP+FN).

Method	**Nb of beats**	DER **(%)**	**Se %**	**PPV %**
Geometrical matching [17]	60431	2.92	97.94	99.13
Zero crossing [8]	109428	1.71	97.44	99.13
Short Time Fourier Transform [22]	109982	1.3	99.1	99.6
Moving average [16]	102654	0.96	99.6	99.78
STFT using Adap. Threshold [46]	109011	0.93	99.56	99.52
MaMeMi filter [9]	109494	0.88	99.68	99.44
Adaptative Thresholding [5]	109949	0.72	99.54	99.74
Pan-Tompkins [4]	109809	0.68	99.76	99.56
Hamilton [3]	109267	0.54	99.69	99.77

Low cost [13]	109494	0.49	99.8	99.71
Morphological filtering(VLSI) [20]	109510	0.43	99.76	99.82
Multiscale morphological filtering [19]	109510	0.39	99.81	99.8
Two moving averages [47]	109985	0.35	99.78	99.87
CNN Detector [44]	105078	0.32	99.77	99.91
Efficient Detection [35]	106310	0.29	99.76	99.95
Fractional order operator [6]	107632	0.29	99.86	99.86
Shannon energy envelope estimation [23]	109809	0.2	99.93	99.88
Proposed optimized	**109494**	**0.17**	**99.92**	**99.91**
Wavelet Detection [26]	101579	0.15	99.89	99.94

Concerning the execution time, the proposed scheme requires 1.3 seconds to detect 2273 beats from the 100m MIT/BIH record, which has a duration of 30 minutes and contains 650000 samples, using an Intel i5 M480 2.67 GHz with 4GB of RAM running on MATLAB software, corresponding to 57.19 ms to detect a beat, or 2 µs to process a sample, making our scheme suitable for real-time and embedded systems. Our detector outperforms all existing methods except two works, Nguyen et al. [13] with 0.16 seconds to process 30 minutes of recording, and 0.43 seconds at mean reported by Elgendi [47]. However, the proposed scheme is superior in detection and accuracy. On the benchmark MIT arrhythmia, our algorithm generates 0.17% of DER error, where Nguyen et al. [13] reported 0.49% of error. Also, in terms of sensitivity and positive predictive value, the work of Elgendi [47] is inferior to ours with 99.78% of sensitivity and 99.87% of positive predictive value, where our detector achieved 99.92% of sensitivity and 99.91% of positive predictive value.

For the other knowledge works, no method is faster than our scheme. For instance, the method of Bal et al. [48] spends 1.92 seconds, Hashim et al. [49] spends 2.97 seconds, Xiang et al. [44] spends 14.53 seconds, and Karimipour et al. [34] spends 18.18seconds to process 30 minutes of ECG record, respectively. Also, the algorithm of Kholkhal et al. [35] requires 1476 seconds to detect 15027 beats, which means that it needs 223.26 seconds to process 2273 beats. Finally, the work of Saadi et al. [10] requires 2.3 hours to process 4271185 samples, which is equivalent to 1260.07 seconds to process 650000 samples. Therefore, our scheme is the best and is suitable for low cost and mobile devices.

III. 7. Conclusions

In this chapter, we proposed an optimization scheme that exploits the features of the PSO algorithm to search for the optimized parameters of the well-known Pan-Tompkins algorithm. Despite the simplicity of the PSO algorithm, it allowed us to find a set of optimal parameters for enhancing the QRS complex and then setting the value of the thresholding to minimize the number of false detection all in only one global optimization approach. In particular, the proposed scheme efficiently determines a set of parameters using an optimization algorithm driven by sensitivity and positive predictive value. The main contribution of our paper [50] is the generation of the parameters of the detection algorithm automatically. Whereas, the parameters of other algorithms are set empirically.

To the best of our knowledge, the PSO algorithm has not been used to optimize the parameters of the QRS detection scheme. Our proposed scheme outperforms the state-of-the-art time-domain algorithms that are published in the literature so far.

The accuracy and low complexity of the developed algorithm are features that allow the embedding of the presented scheme on ambulatory instruments. In particular, the low complexity feature offers the opportunity to integrate this algorithm on emergency and healthcare low energy consumption instruments. Thus, our proposed algorithm can be exploited as an efficient module for medical healthcare to help practitioners in their daily tasks. Also, the developed scheme could be incorporated in the Holter arrhythmia detection chain.

The high detection rate achieved by our proposed approach may help clinicians in improving the heartbeat segmentation process which is time-consuming if done manually. Further work could be something related to developing a parallel scheme to further reduce the processing time.

The next chapter uses the transform domain to detect the QRS waveform.

CHAPTER IV

A ROBUST QRS DETECTION APPROACH USING STATIONARY WAVELET TRANSFORM

IV. A Robust QRS Detection Approach Using Stationary Wavelet Transform

IV. 1. Motivations and Approach

The Wavelet Transform (WT) is widely used in the literature for QRS detection. Most of the existing QRS detectors are based on the dyadic discrete wavelet transform (DWT) [51]. Few works have exploited the stationary wavelet transform (SWT) for QRS detection. We will show through this contribution that the SWT provides almost the same accuracy as the DWT, yet it is more robust in noisy environments. Moreover, the developed method in the present work used solely the first decomposition level, hence it is computationally efficient.

IV. 2. Introduction

The popularity of wavelet transforms in the signal processing field has attracted researchers to utilize this tool to develop automatic algorithms for ECG signal analysis. The wavelet transform offers the possibility to explore the signal characteristics in different scales. In this work, to address the problem of environment change, we develop a simple algorithm that tackles the QRS complex detection in normal recordings, long term recordings, and noisy environments. The developed algorithm is robust, delivers high accuracy, and has low complexity. Indeed, we present an extension of our previously developed approach for QRS detection [52]. We propose a noise-robust scheme based on the accurate decomposition feature of the SWT to determine the QRS positions. We use solely the approximation coefficients of the first decomposition level. We emphasize that the details coefficients are not used; this reduces considerably the complexity of the proposed scheme. Then, a squaring operation is performed on the resulting coefficients. After this, the SWT is applied again. Finally, a dynamic thresholding procedure is used to identify QRS positions. The main advantage of the proposed approach, since only approximation coefficients of the first decomposition level are calculated, is reduced computational complexity. The proposed algorithm is tested on the whole benchmark MIT-BIH database without excluding any record from the assessment in contrast to many works that drop out some records in order to reduce the total error of their algorithms. Furthermore, our algorithm outperforms all state-of-the-art algorithms when tested on noisy records of the NSTMIT database.

IV. 3. Proposed method

Algorithms intended for QRS complex detection perform the ECG signal analysis whether in the time domain, frequency domain, or time-frequency domain. The time-frequency domain algorithms deliver the best performance. They are more appropriate for QRS detection because the QRS complex is localized in time and has a good frequency concentration. Fourier methods decompose the signal into a series of sine and cosine functions. The wavelet decomposition is more flexible because the mother wavelet shape can be selected to approximate the shape of the analyzed signal. Also, the Fourier-based methods are poor in the detection of localized events and slope localization. In the proposed scheme, the QRS detection is carried out in the scale domain. That is, no reconstruction is required. In the following, we will present some theoretical background of the wavelet transform.

IV. 3. 1. The Continuous Wavelet Transform

The continuous wavelet transform at a scale ‘a’ and shift ‘b’ is expressed by the following integral [53]

$$W_{\psi} f(a,b) = {}^{1}\!/_{\sqrt{a}} \int_{\mathbb{R}} f(t)\psi\left({}^{t\,-\,b}\!/_{a}\right) dt \qquad \ldots(10)$$

The function $\psi(\mathrm{t})$ is the mother wavelet and the function $f(t)$ is the input signal to be analyzed. One notices that the general form of the wavelet transform given by Eq. (1) is similar to the Fourier transform. The only difference is that the Fourier transform decomposes the signal of interest into a linear combination of sinusoids. While the wavelet transform decomposes the signal into a combination of wavelet functions at different scales. The wavelet transform is characterized by two parameters, the scale factor ‘a’ and the shift factor ‘b’. The factor ‘a’ introduces the compression/dilation in the shape of the mother wavelet. The influence of varying factors ‘a’ and ‘b’ is shown in Fig. 33 (b) and (c). Consequently, varying ‘a’ and ‘b’ results in different shapes and positions, this allows more flexibility in matching arbitrary signals. However, the selection of the right type of mother wavelet to analyze arbitrary signals remains an open issue in the signal processing community; in the present work, we used the Daubechies wavelet of order 14. Furthermore, the appropriate decomposition level highly depends on the information to be extracted from the analyzed signal; in this paper, we used the first decomposition level to reduce the algorithm complexity.

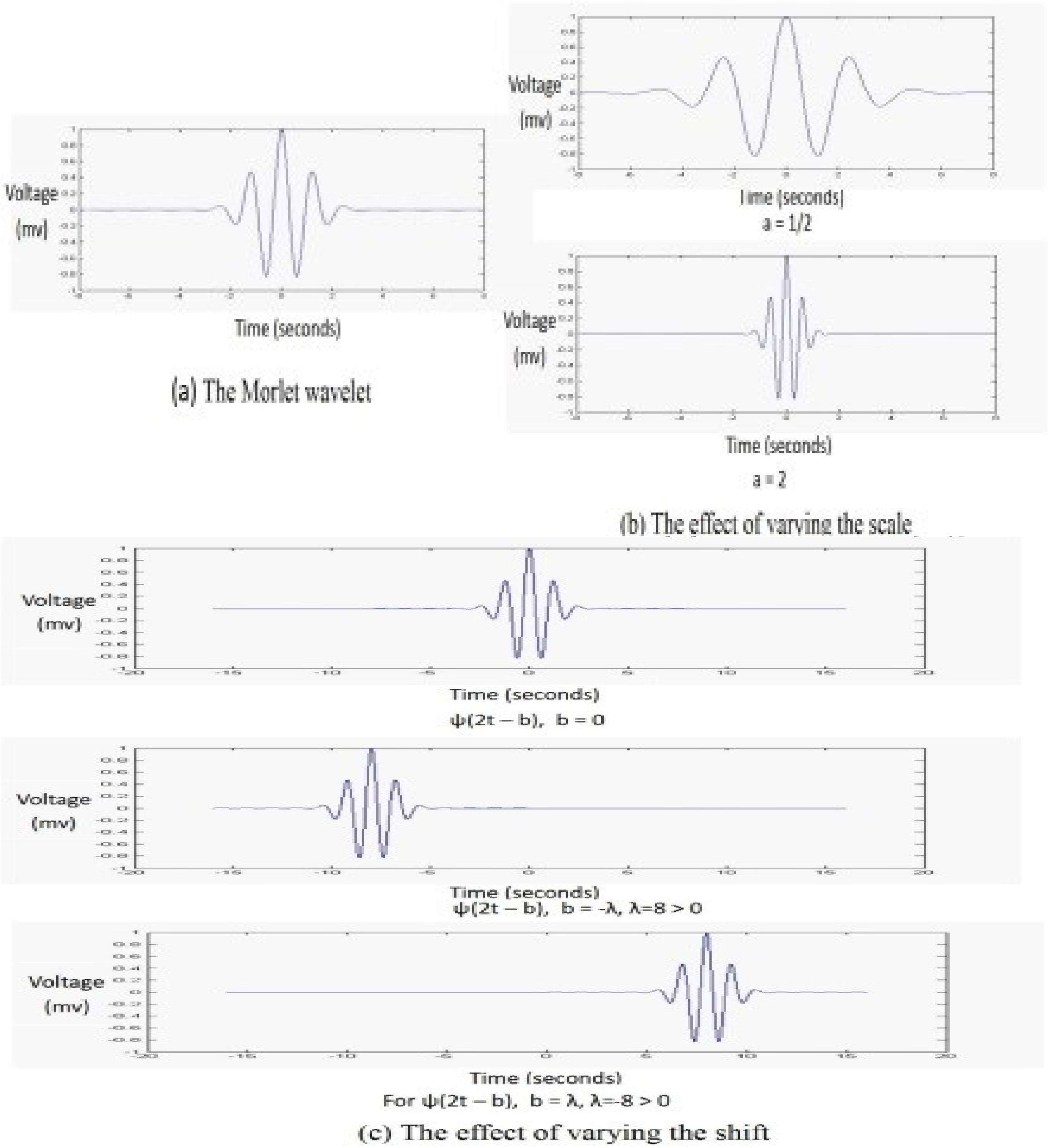

Fig. 33 : A typical example of a continuous wavelet.

IV. 3. 2. The Stationary Wavelet Transform (SWT)

The main drawback of the CWT is the presence of many parameters to be selected. Therefore, its application is not straightforward. Also, the CWT requires a high computational capability, which limits its application in signal processing and is used only when both the mother wavelet and the signal to be analyzed have closed-form formulae. The stationary wavelet transform (SWT) is a discrete wavelet decomposition that does not use decimation. The length of the output after the decomposition is twice the length of the input; this occurs as a result of using the filter bank structure (see Fig. 34). This length of the output results in the conservation of information which may be lost by the decimation of the coefficients. In continuous wavelet decomposition, the scale and shift factors vary over continuous intervals $\in \mathbb{R}^+ - \{0\}, b \in \mathbb{R}$. In the discrete wavelet decomposition, scale and shift factors range over discrete values $= 2^j, b = k2^j, (j,k) \in \mathbb{Z}^2$; where j is the decomposition level and k is the discrete-time index. A flowchart illustrating the steps involved in the SWT decomposition at different levels is shown in Fig. 34. The SWT decomposes signals into a low pass frequency component and high pass frequency component; the resulting coefficients after low pass filtering are referred to as approximation coefficients, while the resulting coefficients after high pass filtering are known as details coefficients. The decomposed signal at level j can be reconstructed by the sum of the approximations coefficients and details coefficients at level $j + 1$. That is

$$cA_j = cA_{j+1} + cD_{j+1} \quad \ldots(11)$$

Where $\mathrm{cA_j}$'s are the approximation coefficients at level j, $\mathrm{cA_{j+1}}$'s are the approximation coefficients at level $\mathrm{j+1}$, and $\mathrm{cD_{j+1}}$'s are the details coefficients at level $\mathrm{j+1}$.

IV. 3. 3. Methodology

In this part, we describe the proposed QRS detector along with we give the steps involved in the feature extraction. It is well-known that the time-frequency analysis is an effective tool for the analysis of the ECG signal. Therefore, we have applied the SWT to the ECG signal in order to detect QRS complexes. The proposed QRS detector consists of two main stages: 1) preprocessing, which involves bandpass filtering and squaring of the wavelet coefficients, 2) decision, which involves dynamic thresholding. The proposed method is illustrated by the flowchart shown in Fig. 35.

IV. 3. 4. Noise Cancelation

In this paper, we used a different interval of the bandpass filter, which is $[4, 24]$ Hz. We note that this frequency interval is used for the first time in our recently published paper [50] and it has not been used in the literature. This frequency band has been determined by a stochastic search method based on the particle swarm optimization (PSO) algorithm. We observed that this band of frequency enhances the QRS detection task. A finite impulse response (FIR) was used to implement the bandpass filter. The FIR filter was preferred because of its intrinsic stability as opposed to IIR filters.

IV. 3. 5. Wavelet Selection

The application of the SWT to the filtered ECG requires two things. First, which mother wavelet should be used? Second, at which level (scale) should we stop the decomposition of the signal? Ideally, it is intended to select a mother wavelet having a shape similar to the QRS wave shape and a level (scale) that contains the frequency band of the QRS wave. That is, the wavelet coefficients are obtained by convolving the mother wavelet and the ECG signal, this operation results in high coefficients amplitudes where the two signals match and low amplitudes where the two signals differ. To determine the appropriate mother wavelet that

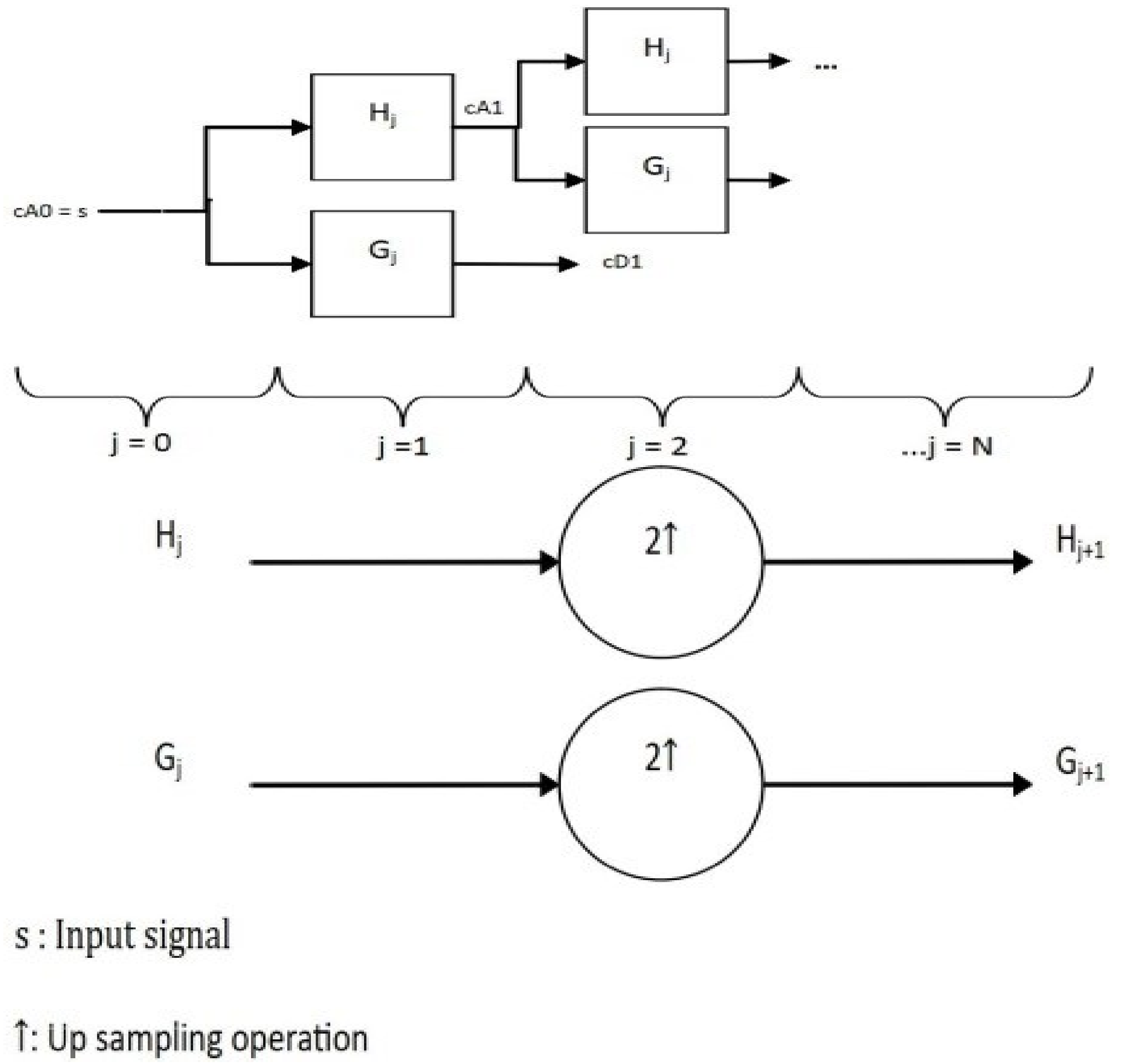

Fig. 34 : The stationary wavelet transform using multi-level decomposition.

resembles the QRS complex shape we sketch a synthetic shape of a typical cycle of an ECG signal as shown in Fig. 24 and the mean QRS of one record from the MIT-BIH database.

We note that it is not possible to find a single mother wavelet that fits all possible normal and abnormal ECG waveforms. After extensive experimentation, we observed that the Daubechies wavelet of order 14 is a suitable choice that delivers good performance. A close inspection of the Daubechies mother wavelet shown in Fig. 36, the QRS wave of Fig. 24, and the mean QRS of record 233 (MIT-BIH database) shown in Fig. 37, suggests a high similarity between the QRS shape and the adopted mother wavelet shape. The Daubechies mother wavelet of order 14 is shown with its scaling function in Fig. 36.

To explore the information content of different decomposition levels, especially purification of the signal from unwanted components, we computed the approximation coefficients of the ECG signal until level 6. By inspecting Fig. 38, it is clear that the response changes with the change in the decomposition level. In particular, we observe that we can distinguish the QRS wave positions starting from the first decomposition level to the fifth

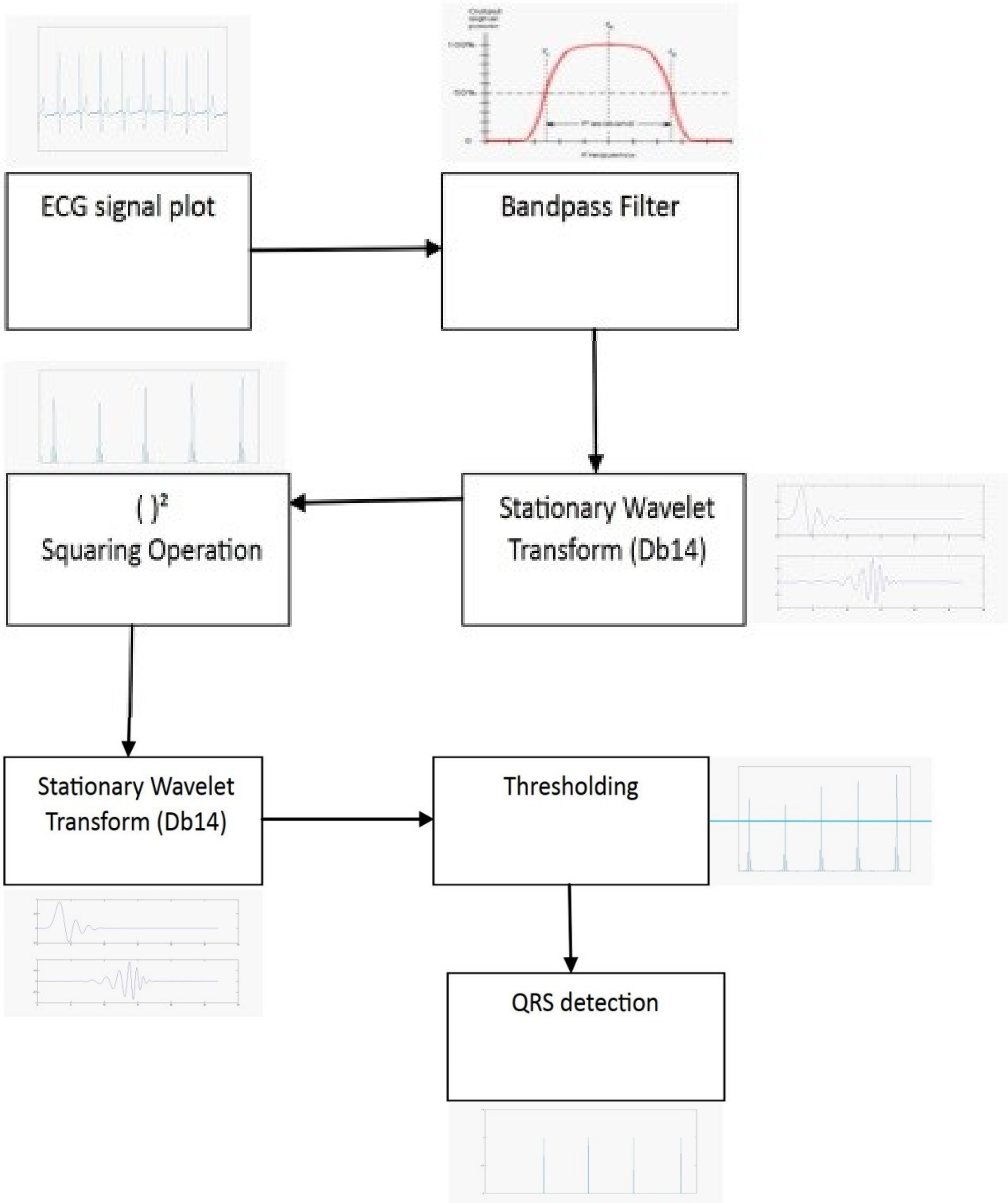

Fig. 35 : A block diagram of the proposed method.

decomposition level. This observation is justified by the high amplitudes of the coefficients obtained in these scales.

IV. 3. 6. Procedure

In this work, we use the time-frequency representation as a framework, from which we extract the QRS complex. In the following, we will detail the role of each step of the proposed algorithm. Our method is illustrated by the flowchart in Fig. 35. The raw ECG signal is first bandpass-filtered to eliminate the disturbances. The second step consists of transforming the signal to the time-frequency domain by the wavelet transform. The stationary wavelet transform is applied to the filtered signal, only approximations coefficients are stored for further processing. We used solely the first decomposition level in order to reduce the complexity of the detector. This makes our algorithm advantageous as others use very deep decomposition levels. Then, the obtained coefficients are squared to enhance the QRS wave and attenuate the P and T waves. To give more dominance to the QRS complexes, we applied another stationary wavelet transform to the squared coefficients. An example that illustrates graphically the steps an arbitrary signal undergoes using the proposed algorithm is shown in Fig. 39. We notice from Fig. 39 (b) that the wavelet coefficients of the bandpass-filtered signal enhance considerably the QRS complexes. The squaring operation (Fig. 39 (c)) clearly allows dominance of the R peaks that appear with high amplitudes. The application of the wavelet transform to the squared signal enhances more the QRS waves and attenuates high-frequency components as shown in Fig. 39 (d). Finally, the adaptive thresholding scheme of the well-known Pan-Tompkins algorithm is applied to determine the presence and locations of the QRS complexes. In the following, we will briefly explain the Pan-Tompkins thresholding scheme.

IV. 3. 7. Pan and Tompkins Thresholding

We have seen in the preceding steps that the ECG signal undergoes bandpass filtering and the application of the SWT followed by the squaring and another SWT applied to the approximation coefficients. At this stage, the obtained signal is ready for the QRS extraction by thresholding. Inspired by the adaptive thresholding of the pioneering paper of Pan-Tompkins [4], we are going to exploit the approximation coefficients of the SWT throughout thresholding to detect the QRS complexes. In the following, we give a brief description of the used thresholding method. The adaptive thresholding proposed in [4] is designed to float over the noise level. That is, from a running estimation of the signal and noise levels, the algorithm adapts the value of the threshold according to the changing values of the record under consideration. As a starting point, the level of the signal SPKI is fixed as half of the maximum amplitude of the first two seconds of the signal under consideration. Likewise, the level of noise NPKI is fixed at one third (1/3) of the mean value of the first two seconds. Each time a new QRS wave is detected, if the amplitude of the current peak PEAK_L is greater than the current level of the threshold, the level of the threshold is updated in the following way

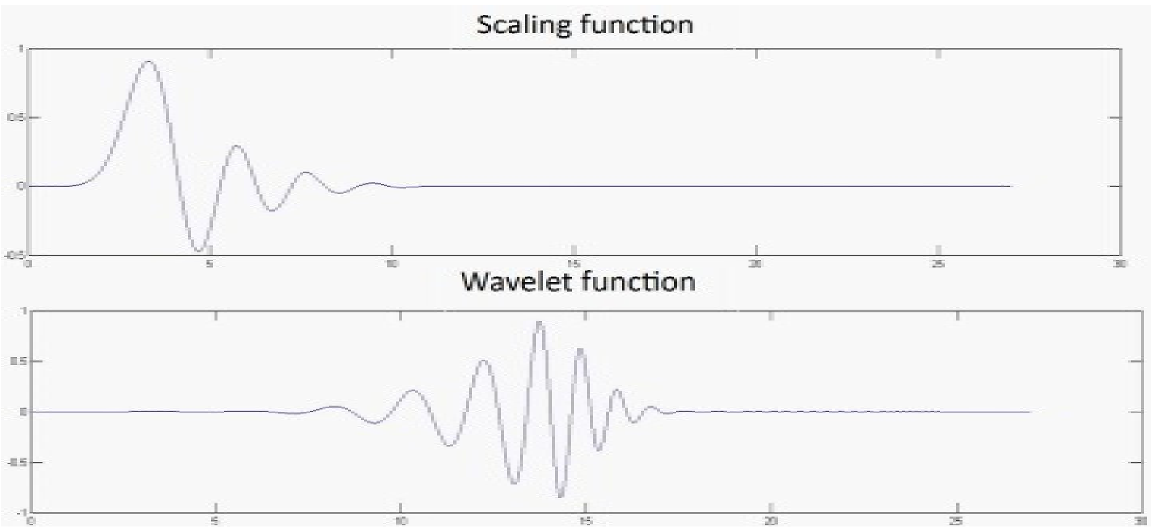

Fig. 36 : Waveforms of the Daubechies wavelet of order 14 'db14'.

$$\text{SPKI} = 0.125 * \text{PEAK\_L} + 0.875 * \text{SPKI} \quad \ldots(12)$$

Otherwise, the noise level is computed by:

$$\text{NPKI} = 0.125 * \text{PEAK\_L} + 0.875 * \text{NPKI} \quad \ldots(13)$$

During each iteration, we update the value of the threshold $THRESHOLD\ I2$ as:

$$\text{THRESHOLD I1} = \text{NPKI} + 0.25 * (\text{SPKI} - \text{NPKI}) \quad \ldots(14)$$

$$\text{THRESHOLD I2} = \text{THRESHOLD I1}/2 \quad \ldots(15)$$

An illustration of the algorithm workflow is shown in Fig. 40. The initial estimation of signal and noise levels is carried out by the pre-estimation stage, more precisely, maximum signal amplitude and mean signal amplitude of the first two seconds of the recorded signal as it clearly appears on the detailed analytic formula diagram of Fig. 41. Also, Fig. 40 and Fig. 41 make in evidence that the threshold level is necessary to identify QRS positions. Then, peaks positions with amplitudes greater than or equal to its instantinous thresholding level are designated as QRS positions, otherwise, the current peak position is a candidate to be T wave position and this assumption is validated if the amplitude is greater than or equal to the noise thresholding level value, so noise level is updated in this case.

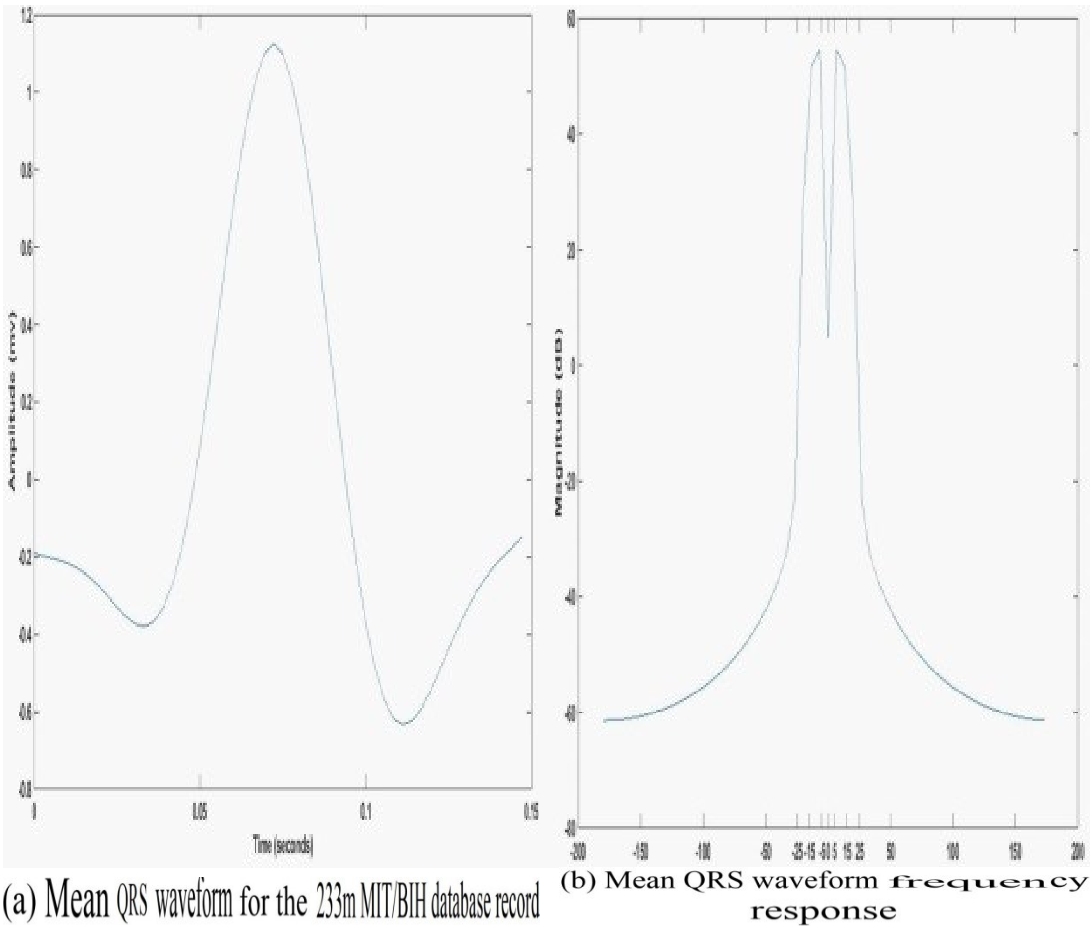

Fig. 37 : The mean of the QRS complex of record 203 and its frequency response.

If we encounter a long time duration segment without any QRS detection, then highly probably we missed a QRS wave. In this case, we search for missed QRSs. For this purpose, let us denote the interval between two successive R peaks by RR interval, and let us define three RR interval durations, namely $\mathrm{RR\ LOW\ LIMIT}$, which is the minimum length for the RR interval; $\mathrm{RR\ HIGH\ LIMIT}$, which is the maximum length for the RR interval; and an interval to decide that a QRS wave is missed denoted by $\mathrm{RR\ MISSED\ LIMIT}$. Let us denote the mean of the eight most recent RR intervals by $\mathrm{RR\ AVERAGE1}$. If $\mathrm{RR\ AVERAGE1}$ falls in the interval $[\mathrm{RR\ LOW\ LIMIT}, \mathrm{RR\ HIGH\ LIMIT}]$, then this value becomes the reference to decide about occurrences of RR interval and it is denoted by $\mathrm{RR\ AVERAGE2}$. Consequently, the parameters are determined in the following way

$$\mathrm{RR\ LOW\ LIMIT} = 92\%\ \mathrm{RR\ AVERAGE2} \quad \ldots(16)$$

$$\mathrm{RR\ HIGH\ LIMIT} = 116\%\ \mathrm{RR\ AVERAGE2} \quad \ldots(17)$$

$$\mathrm{RR\ MISSED\ LIMIT} = 166\%\ \mathrm{RR\ AVERAGE2} \quad \ldots(18)$$

If the $\mathrm{RR\ AVERAGE1}$ is greater than or equal to $\mathrm{RR\ MISSED\ LIMIT}$, a search back is needed and an R peak is potentially present between the last found R peak position and the current search position. Its position corresponds to the maximum amplitude in this region and is validated if its value is greater than or equal to the search back threshold level $\mathrm{THRESHOLD\ I2}$.

IV. 1. Results and Discussions

For the evaluation of the performance of the proposed algorithm, we used the most common metrics, which are: 1) Sensitivity (Se) is the proportion of QRS complexes that are correctly detected, 2) Positive predictive value (PPV) is the proportion of non QRS complexes that are correctly identified, and 3) Detection error rate (DER) is the total error percentage. Most of the published papers use the three metrics to give a quantitative measure of the obtained results [4][25][26][27][28]

$$\mathrm{Sensitivity}\ (\%) = \mathrm{TP} / (\mathrm{TP} + \mathrm{FN}) \quad \ldots(19)$$

$$\mathrm{Positive\ predictive\ value}\ (\%) = \mathrm{TP} / (\mathrm{TP} + \mathrm{FP}) \quad \ldots(20)$$

$$\mathrm{DER}\ (\%) = (\mathrm{FP} + \mathrm{FN}) / \mathrm{Total\ number\ of\ QRSs} \quad \ldots(21)$$

Where TP stands for true positives, which is the number of QRS complexes effectively present in the record and effectively detected by the algorithm. FP stands for false positives, which is the number of QRS complexes detected by the algorithm but not effectively present in the record. FN stands for false negatives, which is the number of QRS complexes not detected by the algorithm but exists in the record. We performed a thorough assessment of the proposed approach on three publicly available datasets. The first one is the MIT/BIH benchmark dataset. The obtained results show a total detection error rate (DER) of 0.228%, a sensitivity of 99.83%, and a positive predictive value of 99.94%, the detailed results for each record are given in Table 4.

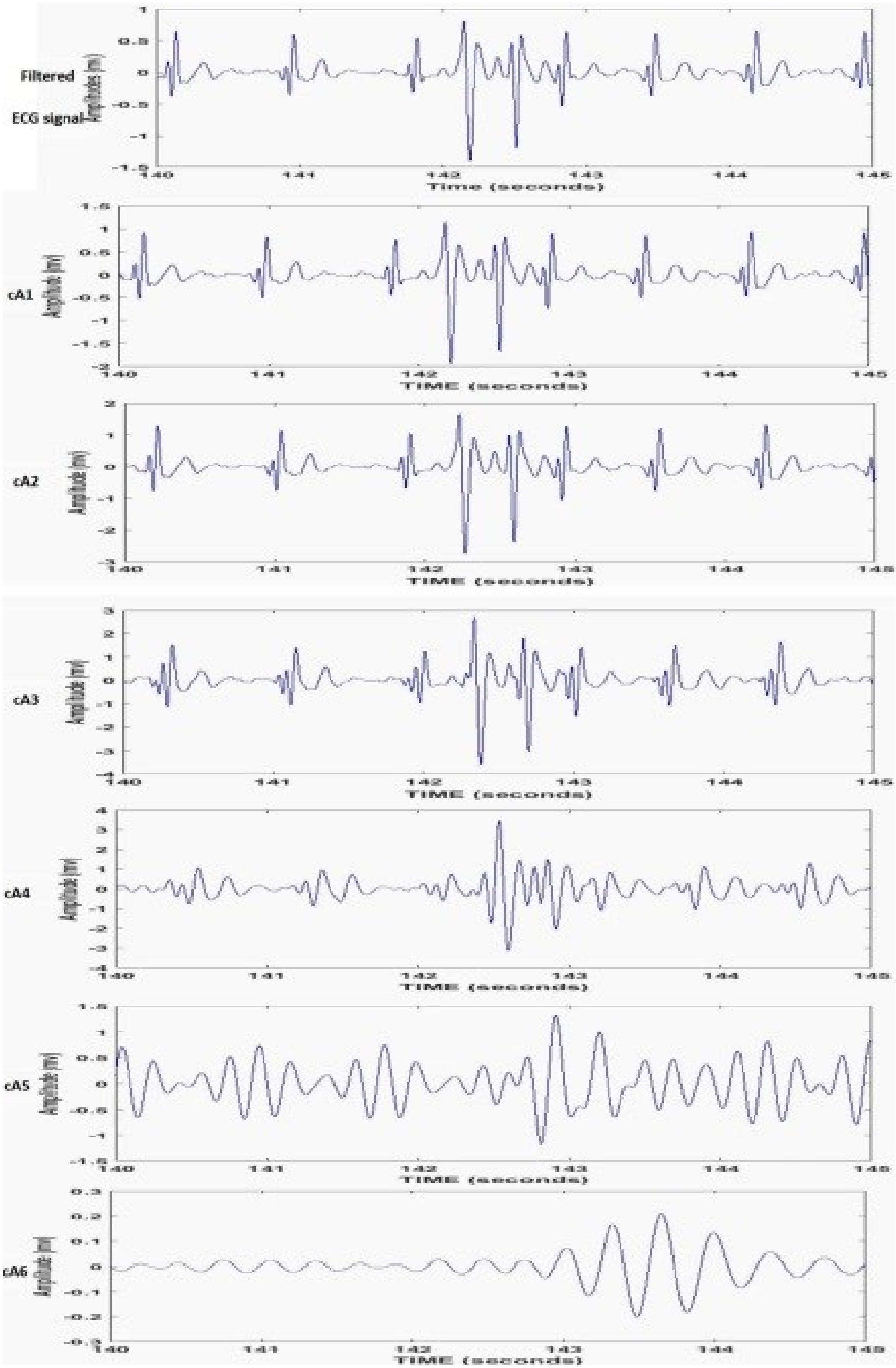

Fig. 38 : Plots of different levels using the SWT approximation coefficients for the record 203m from the 140th second to the 145th second.

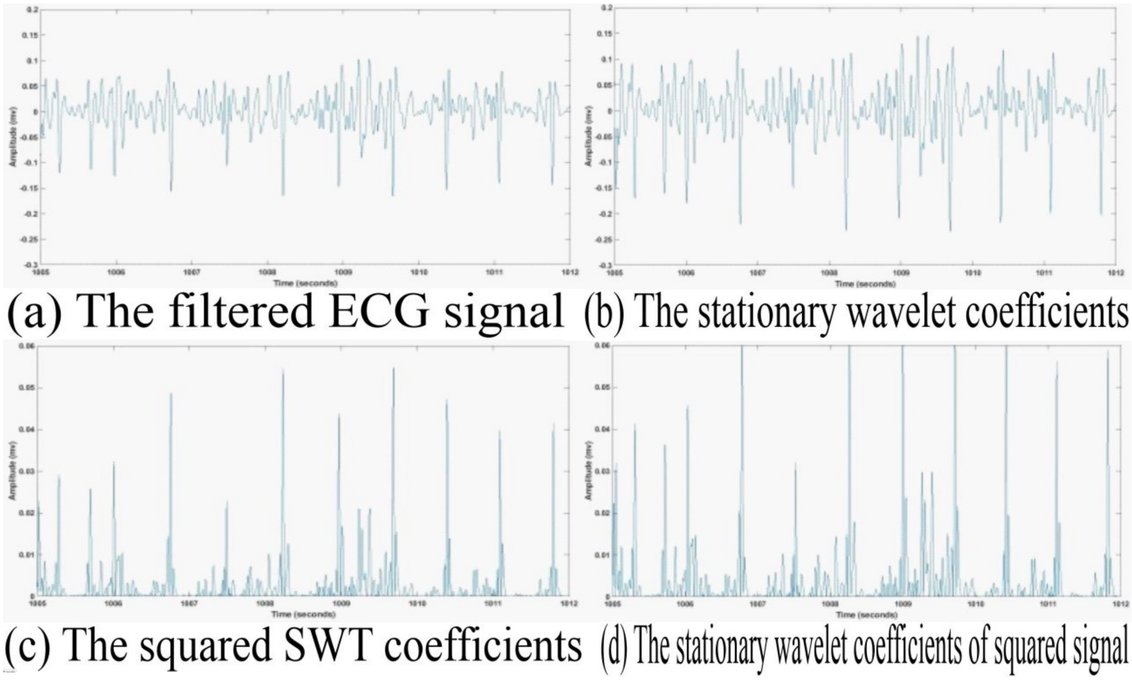

Fig. 39 : Feature extraction steps by the proposed method.

The results of Table 4 indicate that the proposed algorithm outperforms most state-of-the-art algorithms including the two pioneering works of the Pan-Tompkins algorithm [4] and Merah et al [25] and achieves similar performances in terms of QRS detection as state-of-the-art algorithms. In summary, there are only 64 false positives and 186 missed QRSs, a total detection failure of 250 beats. More interestingly, the proposed algorithm achieved excellent sensitivity (99.94%), positive predictive value (99.83%), and the detection error rate (0.22%). The obtained results are very satisfying and the detection error rate (DER) per record does not exceed 1% for all records of the database. Most of the errors occurred in record 203 (46 FN) which contains abrupt changes, and record 210 (53 FN) which contains irregular rhythmic patterns. In greater detail, while the proposed algorithm achieved perfect performance in 15 records, the Pan-Tompkins algorithm achieved perfect performance in 11 records only.

In particular, while the proposed algorithm produced FP+FN=9 for record 108m and FP+FN=6 for record 222m, the Pan-Tompkins algorithm produced FP+FN=223 and 182, respectively. This shows a significant improvement in records where most existing algorithms suffer from poor performance.

Furthermore, to confirm the robustness of our algorithm, and to test our method in abnormal conditions, we used the MIT-BIH noise stress test database (NSTDB), which contains records 118m and 119m of the MIT/BIH database disturbed by additional noise. The number after the letter 'e' in the name of the file for each record represents the signal to noise ratio ([file_name]e[SNR]m). As shown in Table 5, the proposed algorithm achieved very well results and shows robustness to QRS detection in the presence of noise. The proposed algorithm behaves very well and keeps the total detection error rate (DER) under 5% for a reasonable signal to noise ratios and exceeds 10% of DER only when the signal is totally

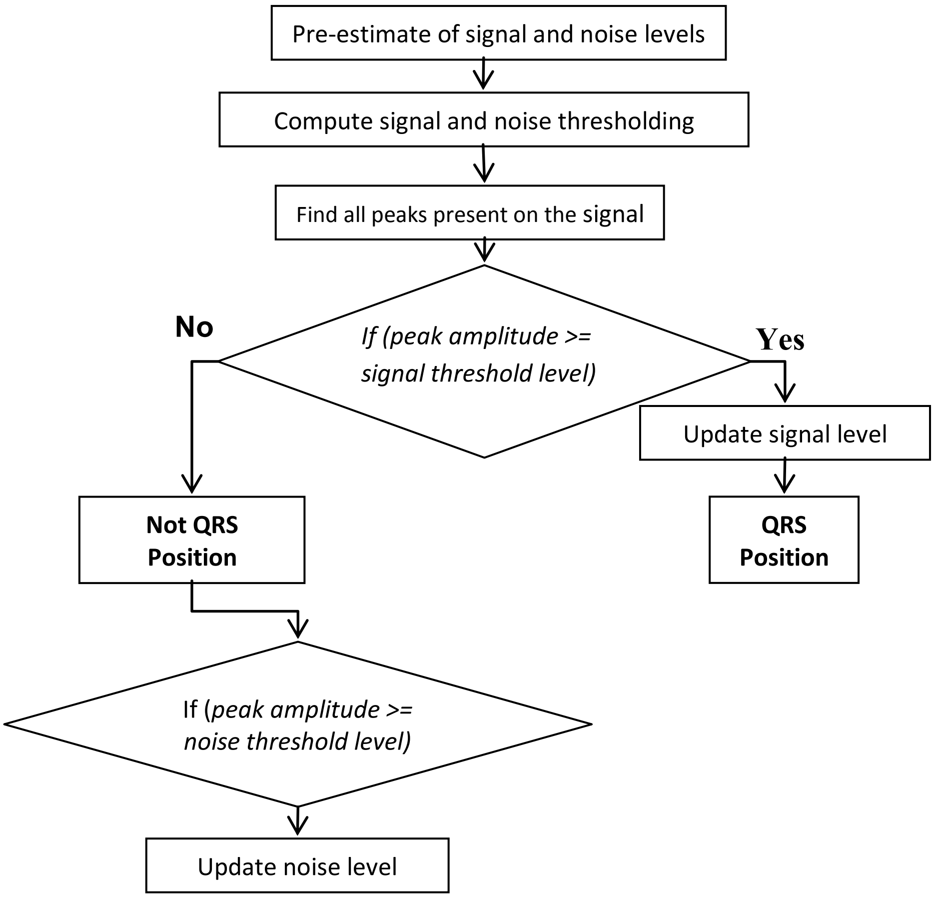

Fig. 40 : Pan & Tompkins algorithm thresholding strategy diagram

buried in noise. Our method fails in detecting 290 beats and produces 2300 false positive beats.

To sum up, our algorithm achieved 91.01% of sensitivity, 98.77% of positive predictive value, and 10.12% of error rate. Based on this result, the proposed approach outperforms state-of-the-art works in terms of the detection error rate in noisy environments.

Finally, we used a third dataset, which is the European ST-T dataset. This dataset is very large and is used to test the performances of the proposed approach on the Holter environment; it contains more than 790000 beats. The detailed results obtained by the proposed algorithm are summarized in Table 6. The proposed method achieved 99.91% of positive predictive value, 98.87% of sensitivity, and an error rate of 1.23% over 734555 beats. In light of these results, we can say that our method ranks very well compared with state-of-the-art methods.

The superiority of the proposed scheme in delineating the QRS positions either on MIT arrhythmia or MIT noise stress test databases is shown in Table 7. For the MIT arrhythmia, our method outperforms all existing QRS detection methods except the works of Slih et al [56] and Manikandan et al [23]. However, the authors of [56] said in the abstract:" Mostly used records in the online ECG database (MIT-BIH Arrhythmia) have been used to evaluate the new technique.", besides they did not mention explicitly the number of beats used in the

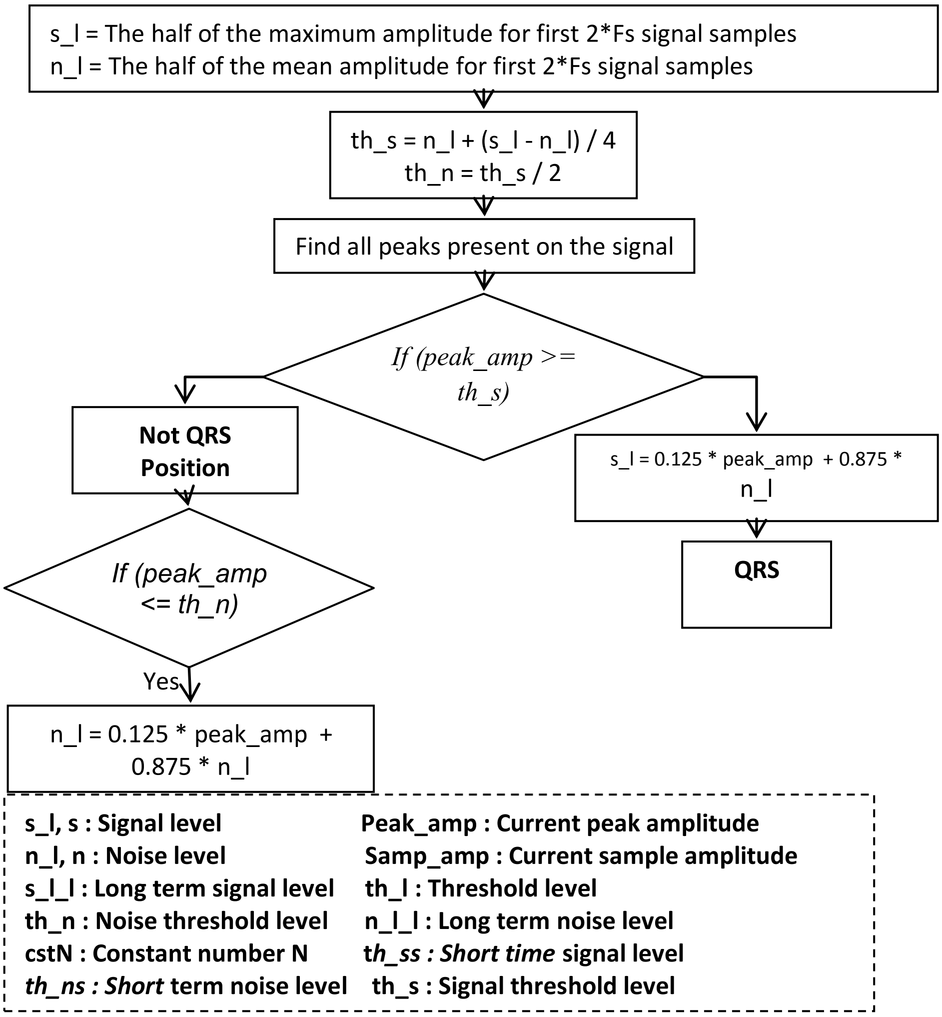

Fig. 41 : Detailed diagram of the Pan & Tompkins algorithm thresholding strategy

assessment of their algorithm. So, they excluded some records, maybe many of them, and the number of test beats in the assessment of their algorithm is limited. These two facts indicate that the real performance of their algorithm [56] is far less than the published results. Therefore, the algorithm of [23] does not outperform our algorithm. On the other hand, while the algorithm of [23] produces 86 false positives, our algorithm produces only 64 false

Table 4 : MIT/BIH results using the proposed SWT-based algorithms.

File	Nb beats	TP	FPs	FNs	DER	PPV	Se
100m	2273	2271	0	2	0.09	100	99.91
101m	1865	1863	0	2	0.11	100	99.89
102m	2187	2187	0	0	0	100	100
103m	2084	2084	0	0	0	100	100
104m	2229	2228	5	1	0.27	99.78	99.96
105m	2572	2572	6	0	0.23	99.77	100
106m	2027	2026	1	1	0.1	99.95	99.95
107m	2137	2134	0	3	0.14	100	99.86

108m	1763	1762	8	1	0.51	99.55	99.94
109m	2532	2532	0	0	0	100	100
111m	2124	2123	0	1	0.05	100	99.95
112m	2539	2539	0	0	0	100	100
113m	1795	1794	0	1	0.06	100	99.94
114m	1879	1877	3	2	0.27	99.84	99.89
115m	1953	1953	0	0	0	100	100
116m	2412	2398	1	14	0.62	99.96	99.42
117m	1535	1535	0	0	0	100	100
118m	2278	2277	1	1	0.09	99.96	99.96
119m	1987	1987	1	0	0.05	99.95	100
121m	1863	1863	0	0	0	100	100
122m	2476	2476	0	0	0	100	100
123m	1518	1517	0	1	0.07	100	99.93
124m	1619	1619	0	0	0	100	100
200m	2601	2599	1	2	0.12	99.96	99.92
201m	1963	1959	15	4	0.97	99.24	99.8
202m	2136	2131	0	5	0.23	100	99.77
203m	2980	2934	0	46	1.54	100	98.48
205m	2656	2651	0	5	0.19	100	99.81
207m	1860	1858	3	2	0.27	99.84	99.89
208m	2955	2939	1	19	0.68	99.97	99.36
209m	3005	3005	0	0	0	100	100
210m	2650	2597	0	53	2	100	98.04
212m	2748	2748	0	0	0	100	100
213m	3251	3249	0	2	0.06	100	99.94
214m	2262	2260	0	2	0.09	100	99.91
215m	3363	3359	0	4	0.12	100	99.88
217m	2208	2207	0	1	0.05	100	99.96
219m	2154	2154	0	0	0	100	100
220m	2048	2047	0	1	0.05	100	99.96
221m	2427	2426	0	1	0.04	100	99.96
222m	2483	2480	3	3	0.24	99.88	99.88
223m	2605	2604	0	1	0.04	100	99.96
228m	2053	2052	11	1	0.59	99.46	99.95
230m	2256	2255	0	1	0.04	100	99.96
231m	1571	1571	0	0	0	100	100
232m	1780	1780	0	0	0	100	100
233m	3079	3076	0	3	0.1	100	99.90
234m	2753	2753	0	0	0	100	100

Total	**109494**	**109308**	**64**	**186**	**0.228**	**99.94**	**99.83**

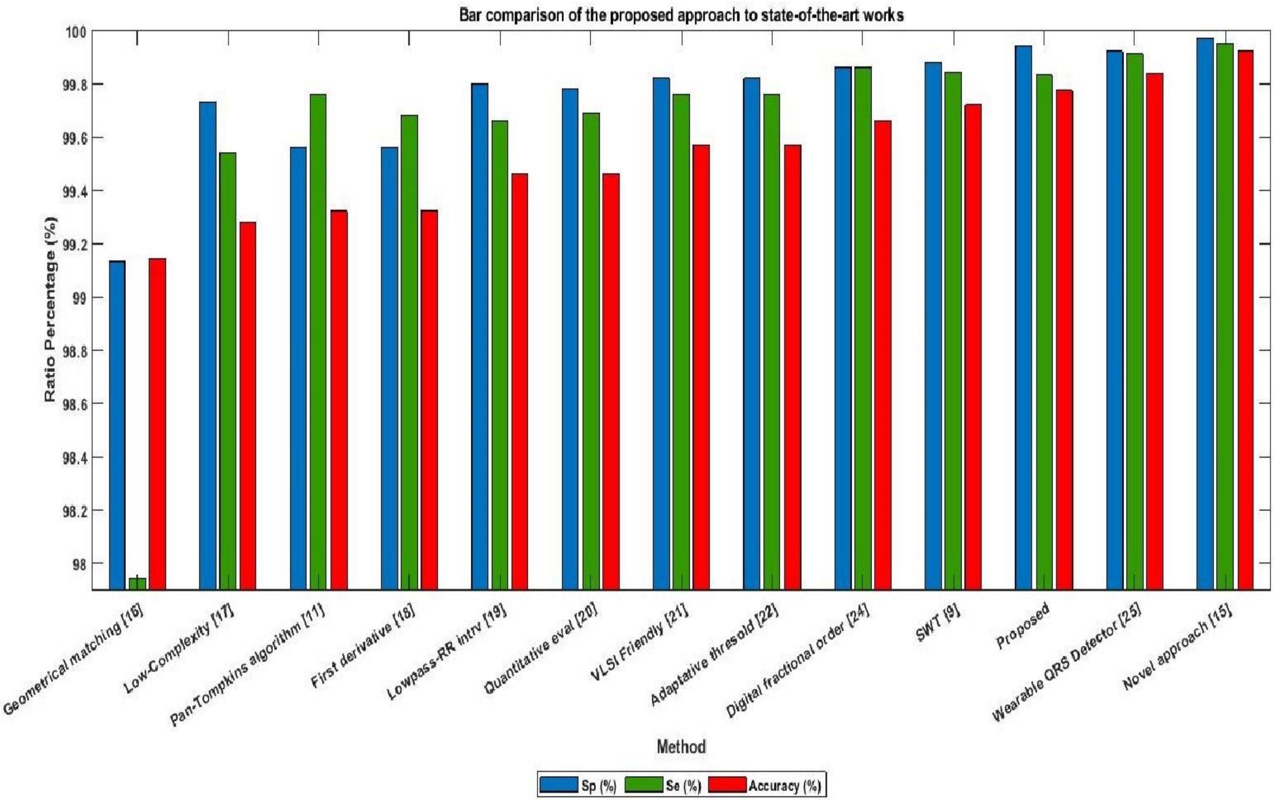

Fig. 42 : Bar performances graph.

positives. This shows that the proposed algorithm is the best in terms of positive predictive value (99.94%). For noisy environments, the proposed algorithm has the best performance (see Table 7). It is clear that the proposed SWT based method using only approximation coefficients resulted in a robust detection method over the MIT noise stress test database and outperformed state-of-the-art algorithms. The numerical results of Table 7 need some effort to be analyzed by the reader. To simplify the analysis and interpretation of the results,

Table 5 : Obtained results by the proposed algorithm on the MIT-BIH noise stress test database.

Record	Number of beats	TP	FP	FN	DER %	PPV	Se
118e24m	2278	2277	2	1	0.13	99.91	99.96
118e18m	2278	2277	3	1	0.18	99.87	99.96
118e12m	2278	2277	13	1	0.62	99.43	99.96
118e06m	2278	2277	130	1	5.75	94.29	99.95
118e00m	2278	2241	348	37	16.9	84.72	98.12
118e-6m	2278	2135	574	143	31.48	74.80	92.26
119e24m	1987	1987	1	0	0.05	99.95	100
119e18m	1987	1987	1	0	0.05	99.95	100
119e12m	1987	1987	7	0	0.35	99.65	100

119e06m	1987	1987	203	0	10.22	89.78	100
119e00m	1987	1976	433	11	22.35	78.20	99.30
119e-6m	1987	1892	585	95	34.22	70.56	93.65
Total	**25590**	**25300**	**2300**	**290**	**10.12**	**91.67**	**98.87**

we use the bar chart to allow a visual comparison of our algorithm with the existing algorithms. For this purpose, we plot the numerical results of Table 7 in Fig. 42. The bar chart is organized in increasing order, from the least to the best performance, from left to right. Also, we plot the percentage accuracy (Acc) instead of the detection error rate (DER), $[\mathrm{ACC}(\%) = 1 - \mathrm{DER}]$. From the visual inspection of Fig. 42, the proposed method outperforms state-of-the-art methods in many aspects.

Table 6 : Obtained results by the proposed algorithm over the European ST-T Database.

File	Nb beats	TP	FPs	FNs	DER	PPV	Se
e0103	7296	7274	0	22	0.3	100	99.7
e0104	7696	7686	0	10	0.13	100	99.87
e0105	6629	6622	3	7	0.15	99.95	99.94
e0107	7029	7005	2	24	0.37	99.97	99.69
e0108	6597	6592	0	5	0.08	100	99.92
e0110	6971	6970	3	1	0.06	99.96	99.97
e0111	7535	7448	92	87	2.38	98.78	98.84
e0112	5506	5480	153	26	3.25	97.22	99.52
e0113	8946	8939	0	7	0.08	100	99.92
e0114	5543	5540	2	3	0.09	99.96	99.95
e0115	11313	11307	0	6	5.39	100	99.95
e0116	4494	4477	62	17	1.76	98.62	99.62
e0118	7080	7076	9	4	0.18	99.87	99.94
e0119	7718	7698	32	20	0.67	99.56	99.97
e0121	10629	10618	0	11	0.1	100	99.9
e0122	11363	11353	0	10	0.09	100	99.91
e0123	9175	9175	0	0	0	100	100
e0124	9213	9208	0	5	0.05	100	99.95
e0125	9066	9064	0	2	0.022	100	99.98
e0126	8291	8290	0	1	0.012	100	99.99
e0127	9391	9391	0	0	0	100	100
e0129	5568	5560	35	8	0.77	99.37	99.86
e0133	6570	6547	16	23	0.44	99.76	99.65
e0136	7044	7040	3	4	0.1	99.96	99.94
e0147	6374	6369	0	5	0.08	100	99.92
e0148	6676	6640	13	36	0.72	99.8	99.46

e0151	7546	7545	0	1	0.013	100	99.99
e0154	6782	6764	17	18	0.52	99.75	99.74
e0155	8125	8076	32	49	0.99	99.61	99.4
e0159	9196	9005	66	191	2.79	99.61	97.96
e0161	8858	8855	0	3	0.03	100	99.97
e0162	10616	10597	1	19	0.19	99.99	99.82
e0163	7616	7607	3	9	0.16	99.96	99.88
e0166	6399	6397	0	2	0.03	100	99.97
e0170	8824	8821	1	3	0.045	99.99	99.97
e0203	10165	10163	0	2	0.2	100	99.98
e0204	11472	11435	1	37	0.33	99.99	99.68
e0205	11807	11778	1	29	0.25	99.99	99.76
e0206	10916	10816	0	100	0.92	100	99.09
e0207	7197	7186	4	11	0.21	99.94	99.85
e0208	8695	8688	2	7	0.1	99.98	99.92
e0210	8739	8731	4	8	0.14	99.95	99.91
e0211	14970	13428	0	1542	10.3	100	90.66
e0212	10829	10815	0	14	0.13	100	99.87
e0213	11070	10876	6	194	1.8	99.95	98.28
e0302	10340	10333	2	7	0.09	99.98	99.93
e0303	8874	8870	1	3	0.05	99.99	99.97
e0304	8358	8341	14	27	0.49	100	99.96
e0306	7903	7901	2	2	0.05	99.98	99.98
e0403	9297	9290	0	7	0.08	100	99.92
e0404	6940	6939	0	1	0.014	100	99.99
e0406	8945	8935	0	10	0.11	100	99.89
e0408	9037	9035	0	2	0.022	100	99.98
e0409	12885	10109	0	2776	21.54	100	82.27
e0410	7527	7522	0	5	0.066	100	99.93
e0411	9934	9898	0	36	0.36	100	99.64
e0413	8149	8141	0	8	0.098	100	99.9
e0415	11407	11226	15	181	1.72	99.87	98.44
e0417	9253	9250	0	3	0.032	100	99.97
e0418	11706	11701	0	5	0.043	100	99.96
e0501	7758	7751	0	7	0.09	100	99.91
e0509	8091	8089	0	2	0.022	100	99.98
e0515	10694	10680	1	14	0.14	99.99	99.87
e0601	8769	8742	0	27	0.023	100	99.69
e0602	11128	11009	1	119	1.8	99.99	98.94
e0603	7935	7927	2	8	0.13	99.97	99.9

e0605	11386	10613	0	773	6.79	100	93.64
e0606	9624	9553	0	71	0.74	100	99.27
e0607	10266	10261	0	5	0.049	100	99.95
e0609	9321	9313	0	8	0.09	100	99.91
e0610	7999	7993	0	6	0.075	100	99.93
e0611	5812	5809	1	3	0.07	99.98	99.95
e0612	6887	6874	0	13	0.19	100	99.81
e0613	7726	7721	0	5	0.065	100	99.94
e0614	11107	10600	0	507	4.56	100	95.64
e0615	7193	7189	0	4	0.06	100	99.94
e0704	9718	9677	0	41	0.42	100	99.58
e0801	9388	9383	0	5	0.05	100	99.95
e0808	11075	11050	18	25	0.39	99.84	99.77
e0817	7554	7332	24	222	3.26	99.68	97.14
e0818	10129	10126	0	3	0.3	100	99.97
e1301	8740	8584	13	156	1.93	99.85	98.24
e1302	8350	8347	1	3	0.05	99.99	99.96
Total	**734555**	**726184**	**647**	**8371**	**1.23**	**99.91**	**98.86**

Table 7 : Comparison of the proposed approach to state-of-the-art works.

Method	Number of beats	TP	FP	FN	DER %	PPV	Se
MIT arrhythmia Database							
Geometrical matching [17]	60431	59185	-	-	0.86	99.13	97.94
Low-Complexity [5]	109949	109447	289	502	0.72	99.73	99.54
First derivative [18]	109504	109150	405	354	0.69	99.63	99.68
Lowpass-RR intrv [55]	109336	108960	218	376	0.54	99.80	99.66
Quantitative eval [3]	109267	108927	240	340	0.54	99.78	99.69
VLSI Friendly [20]	109510	109311	279	199	0.43	99.82	99.76
Adaptative thresold [15]	110050	109811	240	239	0.43	99.78	99.78
Optimize [47]	109985	-	-	-	-	99.87	99.78
Digital fractional order [6]	109494	109338	153	156	0.34	99.86	99.86
SWT [25]	109494	109316	126	178	0.28	99.88	99.84
Proposed SWT-based	**109494**	**109308**	**64**	**186**	**0.228**	**99.94**	**99.83**
Wearable QRS Detector [21]	109496	109402	86	94	0.164	99.92	99.91
Novel approach [56]	116137	116073	31	64	0.08	99.97	99.95
Noise Stress Test Database							
Optimize [47]	26370	-	-	-	-	90.25	95.39
SWT [25]	25590	24388	1563	1202	10.81	95.3	93.98
Proposed SWT-based	**25590**	**25300**	**2300**	**290**	**10.12**	**91.01**	**98.77**

IV. 2. Conclusion

In this chapter, we developed a very simple yet efficient algorithm based on the stationary wavelet algorithm. In particular, the first contribution resides in exploiting solely the approximations coefficients of the SWT to enhance the QRS complex waveform and keep a low complexity scheme. The second contribution is the robustness of the developed algorithm to the environment change. Experiments were implemented to assess the performance of the proposed algorithm using three benchmark datasets. Indeed, the proposed algorithm outperformed state-of-the-art methods on the MIT noise stress test database by achieving 10.12% of DER and 98.77% of sensitivity. For normal functioning conditions, the proposed algorithm achieved 0.228% of DER, 99.94% of positive predictive value, and 99.83% of sensitivity. This result ranks our algorithm among the top algorithms for QRS detection. For long-term ECG recordings (Holter environment), we achieved 1.23% of DER, 99.91% of positive predictive value, and 98.87% of sensitivity over more than 734000 beats, this proves the efficiency of the developed algorithm. It turns out that our algorithm is simple and performs similarly to state-of-the-art algorithms on benchmark databases and outperforms state-of-the-art algorithms in noisy environments.

As a continuation of the current work, we intend to use other types of wavelets that match more the QRS shape. Also, we will try to develop new thresholding procedures.

CHAPTER V

AN APPROACH TO QRS COMPLEX DETECTION USING DEEP NEURAL NETWORKS AUTOENCODER

V. An Approach to QRS Complex Detection using Deep Neural Networks Autoencoder

V. 1. Motivations and Approach

Deep learning (DL) techniques outperform, in more than a field, traditional techniques in terms of classification and prediction. Moreover, DL methods extract abstract features directly from raw signals without any preprocessing. The success of DL in a variety of applications is behind our motivations to develop a QRS detector based on this promising technique. Indeed, an accurate QRS detector using Staked Autoencoder has been developed, characterized by a small number of layers and neurons. We trained the developed architecture by a huge number of training samples in order to build a system with high generalization characteristics. Furthermore, the hidden information in RR intervals is exploited to support the decision process.

V. 2. Introduction

Deep learning has revolutionized the field of machine vision, and human-machine imitation by new training rules [57]. In recent years, DL techniques won many contests and achieved superhuman vision performance [57]. DL architectures proved their superiority in many applications [58] such as road extraction [59-62], speech recognition [63-67], and biomedical signal processing [68-74]. In this paper, a DL approach is used to determine the QRS complex from the electrocardiogram (ECG) signal which is one of the widely used tools for precise healthcare. An ECG signal, properly recorded, purified from additive noise and distortions, is a reliable tool for identifying numerous diseases.

While conventional machine learning algorithms fail to process natural data in their raw form [2], deep learning is characterized by learning features directly from raw data without any intervention of an expert. Most of the QRS detectors preprocess the input ECG signal before deep neural features extraction, or model and extract signal features before deep neural features extraction. Hence, they do not take benefit of the advantage of using deep learning.

In this chapter, we propose a fully automated method operating directly on the raw recorded signal for QRS detection, making use of a semi-supervised stacked autoencoder. We train the proposed architecture on a huge number of beats to guarantee the good learning of the deep neural network to model all QRS and non QRS occurrences scenarios. The simplicity of implementation and low complexity were also crucial criteria in our development phase to accelerate the full arrhythmia identification process.

The main contributions of the proposed DL QRS detector are:

1) To the best of our knowledge, this is the first time a stacked autoencoder is used for QRS detection,

2) New simple and low complexity architecture,

3) Fully automatic feature extraction and QRS detection,

Table 8 : The Number of Training Samples from Four Datasets

Attribute type	MIT	EDB	INCART	SVDB	∑
QRS	**51043**	**111995**	**18773**	**23439**	**205250**
NOT QRS	231052	528460	80085	93791	933388
∑	282095	640455	98858	117230	**1138638**

4) It processes ECG signals with an arbitrary sampling frequency (no re-sampling is required),

5) It is trained on a huge number of beats.

6) It is tested on many unseen databases to prove the generalization of the developed architecture.

7) It works directly on raw data, without any preprocessing phase which, in general, slows down the execution of the algorithm.

8) There are no empirical parameters such as thresholding and search back procedure.

V. 3. Semi-Supervised Stacked Autoencoder

Deep learning techniques proved their efficiency in more than a domain. The stacked autoencoder neural network has been utilized in our detector; it is a concatenation of homogenous and heterogeneous neural networks. The homogenous networks are encoder layers. The heterogeneous part is the softmax classifier placed after the last encoder layer. A basic (shallow) autoencoder consists of three layers, namely, the first layer is the input, the second layer is the hidden layer, and the last layer is the reconstruction layer (output). Usually, if the autoencoder comprises more than one hidden layer, it is trained greedily. Fig. 43 shows general stacked autoencoder architectures. Given an input X, the corresponding output Y of a neural network is

$$Y = F(WX + B) \qquad \ldots(22)$$

Where the rows of the matrix W are the weights linking the input nodes to the corresponding node from the hidden layer, B is the bias vector, and F is the activation

Table 9 : The Number of Test Samples from Four Datasets

Attribute type	MIT	EDB	INCART	SVDB	∑
QRS	**49707**	**679387**	**160840**	**160402**	**1050336**
NOT QRS	233234	3187601	633488	633926	4688249
∑	282941	3866988	794328	794328	**5738585**

function. The aim of the optimization consists of finding the weight matrix W_e that maps the input to the hidden layer (encoder) and the weight matrix W_d that reconstructs the input from the hidden layer (decoder), that is

$$\min_{W_e,W_d}(F_d(W_d F_e(W_e X + B_e) + B_d) - X)^2 \qquad \ldots(23)$$

In essence, the autoencoder neural network is an unsupervised learning system that tries to reproduce a copy of its input at the output without the need for labeled samples. The main goal of building autoencoder architecture is to seek an inherent representation of the input which cannot be discovered by hand-crafted features. The bottleneck hidden layer is exploited as an efficient set of automatic features. As mentioned above, each hidden layer is pre-trained alone, and then all layers are stacked together to build the recognition system. In practice, only the encoder layers are used for the stacked autoencoder. After concatenating the softmax classifier layer to the encoder layers, the whole system is fine-tuned in a supervised setup.

The training of autoencoders is achieved by minimizing the sum of squared differences between the input and the output. That is

$$Error = \frac{1}{2}\sum_{i=1}^{N}(y_i - t_i)^2 \qquad \ldots(24)$$

Where y_i's represent the predicted outputs, t_i's the targets (desired outputs) and N is the number of outputs.

The scaled conjugate gradient optimization algorithm was used for greedy training phases. It was chosen for its simplicity of implementation and low algorithmic complexity. Besides, the scaled conjugate gradient is more robust, against initial guess choices, than a simple gradient descent approach. The gradient update of the weights is performed by the

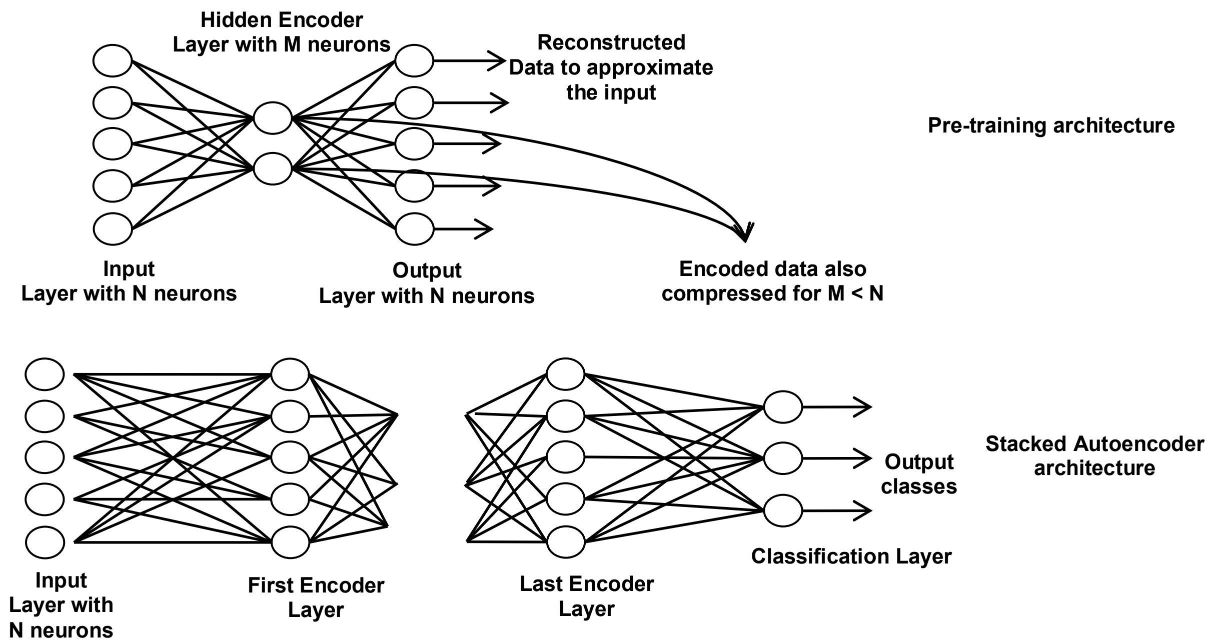

Fig. 43 : (Top) Single-Hidden layer, (Bottom) Multi-Hidden layer autoencoder architecture.

following equations:

$$W_{k+1}^{(i)} = W_k^{(i)} + \alpha \nabla G^{(i)} \qquad \ldots(25)$$

In eq. (177), the weights of layer i during the k^{th} iteration are updated by the gradient descent ∇G, following a step size α.

The gradient descent is computed starting from the output layer in the backward direction until reaching the input layer. This computation is repeated several times until convergence is reached. It has been proved in many studies that the back-propagation is very efficient in training multilayer architectures. The value of the gradient which minimizes the error is given by:

$$\nabla G^{(i)} = min_{W^{(i)}} E^{(i)} = -\frac{dE^{(i)}}{dW^{(i)}} \qquad \ldots(26)$$

Indeed, the encoder layers pre-training accuracy is not crucial. Always, a fine-tuning phase is performed involving all previously pre-trained neural network layers. However, for the final fine-tuning phase, the Levenberg-Marquardt is used instead for its high accuracy, convergence robustness, and semi-independency from the initial guess.

In practice, the back-propagation approach to minimizing the mean squared error attains good performance at the expense of slow convergence. To accelerate the convergence, the cross-entropy function was used to estimate the error at the output of the softmax layer, which is the final resulting feature from the encoder layers.

V. 4. Dataset Description

In an attempt to build a robust and reliable deep neural network, and knowing that deep neural networks require huge training sets, we used in this study many publicly available benchmark databases. Developing a method evaluated on a single database leads in many cases to poor results when tested on unseen data. This problem arises because the ECG signal differs from one person to another. In particular, ECG signal characteristics such as beat interval, shape, frequency content, vary not only from a given database to another but also from an individual to another, which raises several challenges for ECG signal analysis methods. To overcome these challenges, a big number of beats has been exploited for the training of the proposed deep neural network. Four datasets for training and test were used, namely, MIT/BIH Arrhythmia Database, MIT Supraventricular database, INCART database, and the European ST-T Database. The training and test samples contain 1255586 QRS waves embedded in 6877223 attributes (5621637 non QRS waves). More precisely, the training is composed of DS1 from MIT/BIH arrhythmia dataset following the AAMI recommendation [83], 11% of the INCART database, 13% of the Supraventricular database, and 14% of the European ST-T Database (see Table 8). The training samples were randomly selected except MIT/BIH Arrhythmia database; the remaining samples of each dataset were used to test the developed architecture (see Table 9). Furthermore, the considered datasets have different sampling frequencies; this proves that the proposed approach operates in different sampling frequencies fact makes our method applies to signals with arbitrary sampling frequency. In other words, there is no need for re-sampling different datasets to make them operate on a single sampling frequency as many existing methods do. As a further step to prove the robustness of the proposed deep network, six unseen databases have been used as validation, namely, QTDB, Apnea DB, NSRDB, LTSTDB, Fantasia, and Challenge 2014. This is to evaluate clinical environment potential issues.

In the following, we give a brief description of the four databases used in the training.

V. 4. 1. MIT/BIH Arrhythmia

MIT/BIH database is commonly used for QRS and arrhythmia detection. It is a two-lead ECG signal recording database. Lead I is recorded from MLII or V5, and lead II from V1, V2, V4, V5, or MLII. The database contains more than 110000 beats corresponding to 24 hours of recording. It consists of 48 records; each record is 30 minutes long, collected from 47 patients at a sampling frequency of 360 Hz. MIT/BIH database is divided into DS1 and DS2 according to the AAMI recommendation [198]. DS1 set is used solely for training, whereas the DS2 set is used for the test only (49707 beats).

V. 4. 2. European ST-T (EDB)

EDB contains more than 802000 beats, independently annotated by two cardiologists. This database required 79 patients to be constructed, for a total of 90 fully annotated records, all sampled at a frequency of 250 Hz with a duration of 120 minutes each. It contains two leads with a signal voltage level of ± 20 millivolts coded on 12 bits.

V. 4. 3. In Cardiology Saint Petersburg

INCART DB was developed for ischemia, coronary artery disease, conduction abnormalities, and arrhythmias. This database consists of 75 ECG fully annotated records sampled at 257 Hz. Each record is 30 minutes long. The database was collected from 32 patients; it comprises more than 175000 beats. A total of 11% of samples from INCART DB were randomly chosen to serve as training and the remaining 89% were used for the test. Moreover, the twelfth lead or V6 lead is used for the totality of this database for signal-to-noise ratio and signal waveform correspondence with the MLII or V5 lead.

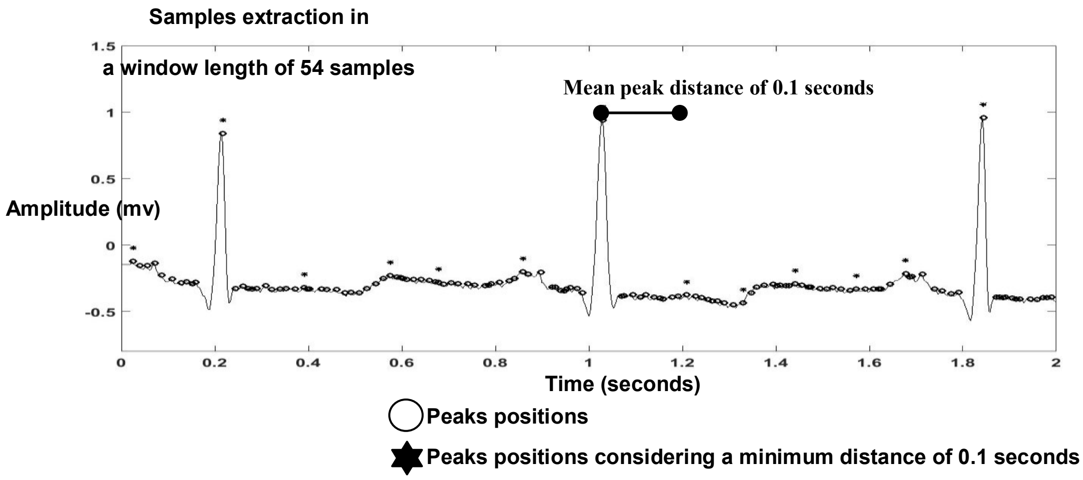

Fig. 44 : ECG attributes extraction rules plotting

V. 5. Proposed QRS Detection

The efficiency of an automated arrhythmia delineator depends on the accuracy of the QRS detector. Therefore, a robust QRS detector is vital for building a reliable ECG automatic recognition system. In this work, the proposed QRS detector is fed with 54 samples as input to the neural network. These samples are collected from the region around the peaks of a raw ECG signal. We keep only those peaks that are separated by at least 0.1 seconds (see Fig. 44).

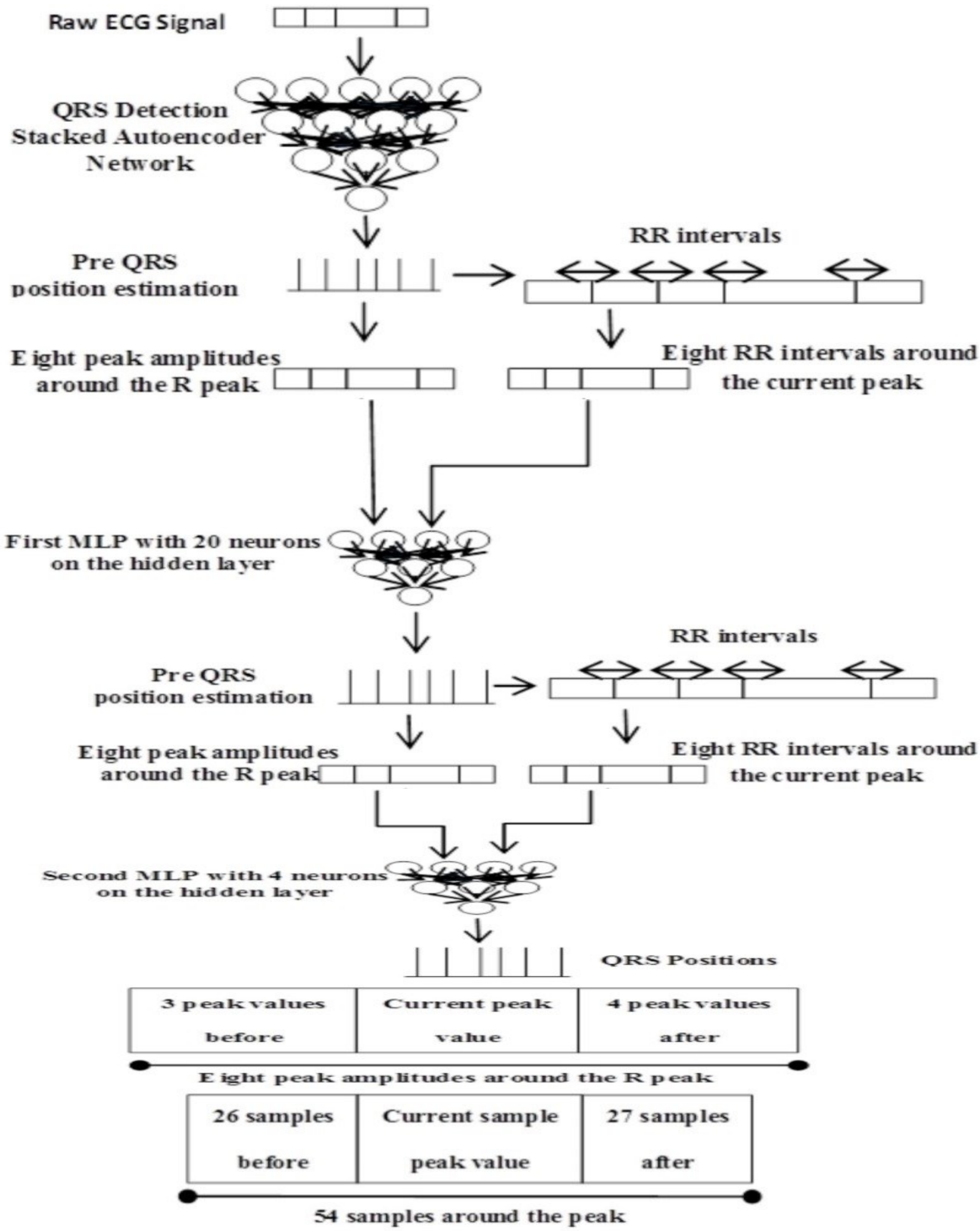

Fig. 45 : The proposed QRS Detection architecture.

The architecture of the proposed QRS detector is shown in Fig. 45. The design consists mainly of a stacked autoencoder, which is the most important part of the automatic feature extraction process, it contains two hidden layers. The autoencoder is followed by two multi-layer perceptrons (MLP) layers. The first MLP consists of 20 neurons and the second MLP consists of 4 neurons. The 20-neurons MLP is fed with the output of the autoencoder and the eight peaks around the peak under consideration (3 precedent peaks, current peak, and 4 peaks after). The second MLP is fed with the eight current peaks like the first MLP and the eight RR intervals. The QRS presence estimation is obtained from the output of the second MLP. Through extensive experimentation, we revealed that RR intervals and peaks amplitudes are important features for the detection of the QRS complexes.

We note that during the initialization of the detector, we wait for the four first peaks to occur, for our test set with a peaks interval of 0.145 seconds at the mean, the user needs to wait for less than 0.6 seconds until the system initialization finishes. Also, at the end of the recording, we create redundancy in the peak region to allow the processing of the last signal peaks.

V. 6. Experimental Results

Deep neural networks performance is seriously influenced by the number of layers and the number of neurons by layer. For this purpose, we investigated many configurations to select the optimal one. After extensive experimentation, we found that the best deep network configuration is achieved with two layers; 75 neurons in the first layer and 15 neurons in the second layer.

The assessment of the proposed scheme is carried out in terms of sensitivity (Se=TP/(TP+FN)), positive predictivity (PPr=TP/(TP+FP)), detection error rate (DER=(FN+FP)/(TP+FP+FN)), and overall accuracy (OA= (TP+TN)/(TP+TN +FP+FN)). In

Table 10 : Comparison of State-of-the-Art Algorithms Performance Obtained on the MIT/BIH Dataset

Method	**# of beats**	**Se**	**PPr**	**DER(%)**
Geometrical matching [17]	60431	97.94	99.13	2.92
2 Input CNN [76]	100724	99.36	98.99	1.64
Pan-Tompkins [4]	109809	99.19	99.41	1.39
Large CNN – LOO [77]	N/A	99.22	99.38	N/A
Proposed on DS2	**49707**	**99.76**	**99.24**	**1.00**
Wavelet Delineator [33]	109428	99.8	99.86	0.34
CNN [44]	105078	99.77	99.91	0.32
Preprocess CNN[42]	49653	99.81	99.93	0.25
Wearable Monitor [21]	109496	99.91	99.92	0.1644
Deep model [201]	N/A	99.94	99.97	0.09

general, the developed QRS detection scheme produced 0.82% of DER on six unseen datasets (Table 11) which contain more than 1470000 beats and produced 1.95% of DER on four test datasets (Table 12), which contain more than one million beats. These results prove the generalization of the proposed scheme.

In particular, the details of the results of the benchmark MIT/BIH arrhythmia dataset are shown in Table 13, where the proposed scheme produced 1.0% of DER and 99.8% of OA. Moreover, the accuracy by record is always greater than 99%. In Table 10, the performance of the proposed algorithms using the MIT/BIH dataset is compared with state-of-the-art methods (mostly deep CNN). It is clear that the developed scheme is competitive with all other algorithms. In our experiment, we followed the AAMI recommendations [83] that are violated by all shown methods except [42]. However, [42] utilized many preprocessing steps such as baseline wander removal and signal normalization. Also, [42] excluded the flutter segments of MITDB from the test and it is computationally demanding.

The achieved results of the proposed scheme using EDB sound good as shown in Table 12. We note that EDB contains a big number of beats and the real challenge with this dataset resides in the poor quality of the signal and the diversity of the ST-T wave change and the diversity of arrhythmia. Although Martinez et al. [33] attained a good result, their method uses empirical thresholds and search back procedure, also they use deep wavelet decomposition levels, thus increasing the complexity of their algorithm. Our scheme achieved 2.24% without any thresholding or search back. Totally, 1044598 beats were used in the test. The achieved total DER is 1.94% with high sensitivity (99.73%) and positive predictivity (98.31%). In particular, the proposed algorithm achieved 1.34% of DER on SVDB using 160402 beats. The result is a good achievement compared to Elgendi [47]. Likewise, the same performance is observed on the INCART dataset, where 1.46% of DER is achieved using 160840 beats. Table 12 shows the confusion matrix of the QRS detection evaluated on the four test datasets.

Finally, the results of the proposed algorithm on six unseen datasets are shown in Table 11. The obtained results on QTDB show low DER (1.03%) and very competitive Se (99.71%)

Table 11 : The Achieved QRS Detection Results Using Six Unseen Datasets

Validation set	**# of beats**	**Se**	**PPr**	**DER(%)**
Apnea	647816	99.27	99.47	1.26
NSRDB	191053	99.92	99.65	0.43
QTDB	80499	99.71	99.26	1.03
LTSTDB	357373	99.90	99.76	0.34
Fantasia	121128	99.50	99.85	0.65
Challenge 14	72415	99.74	99.91	0.34
Overall	**1470284**	**99.66**	**99.52**	**0.82**

Table 12 : The Obtained QRS Detection Results Using Four Test Datasets

Test database	# of beats	Se	PPr	DER(%)
SVDB				
This work	**160402**	**99.60**	**99.06**	**1.34**
Elgendi [47]	184744	99.96	99.80	N/A
INCART DB				
Elgendi [47]	175918	99.03	97.09	N/A
This work	**160840**	**99.73**	**98.82**	**1.45**
CNN [44]	170000	99.86	99.89	0.25
EDB				
This work	**677756**	**99.70**	**98.05**	**2.28**
Wavelet Delineator [33]	787103	99.61	99.48	0.9
Overall				
This work	**1042309**	**99.73**	**98.31**	**1.95**

and PPV (99.26%). Using NSRDB, we obtained Se (99.92%) and PPV (99.65%), these results outperform Elgendi [47]. The worst individual DER error is 1.26% (Apnea dataset), which is acceptable taking into consideration that 647816 beats were involved in the classification. The best performance is obtained on the LTSTDB and Challenge 2014 databases, with only 0.34% of DER. Overall; a very good DER of 0.82% is obtained using the six validation datasets. It is worth noting that the achieved results by the proposed algorithm outperform state-of-the-art results on Long Term ST and Challenge 2014 datasets. We remind here that Long Term ST and Challenge 2014 datasets were not involved in the training phase. This proves the generalization of the proposed algorithm.

Cross-validation on the training dataset prevents neural networks from overfitting. Thus, we divided the training set into 70% for pure training, 15% for validation, and 15% for test. Fig. 46 shows the decrease in the error for training, test, and validation. While Fig. 47 and Fig. 48 show the error for the first and second stages of MLP, respectively. The mean square error decays exponentially from the beginning until epoch 45 (Fig. 46). Then, the error slows down and optimization keeps refining the values of the optimal weights. The convergence is reached after 103 learning epochs. For the first and second MLPs layers, the decrease in the error is very fast during the three first iterations, and then a slow convergence is observed (see Fig.47 and Fig. 48).

Table 13 : DS2 (MIT-BIH) record detailed performance produced by our QRS detector.

File	Nb Beats	TP	FP	FN	Se	PPr	DER
100m	2273	2273	1	0	99.96	100	0.04
103m	2084	2084	0	0	100	100	0

105m	2570	2553	37	17	98.56	99.3	2.09
111m	2124	2124	5	0	100	100	0.24
113m	1795	1793	0	2	100	99.89	0.11
117m	1535	1535	1	0	99.94	100	0.07
121m	1863	1863	95	0	94.8	100	5.1
123m	1518	1517	3	1	99.8	99.93	0.26
200m	2601	2563	8	38	99.69	98.56	1.74
202m	2136	2135	7	1	99.67	99.95	0.37
210m	2647	2642	70	5	97.36	99.8	2.83
212m	2748	2746	0	2	100	99.93	0.07
213m	3251	3245	1	6	99.97	99.82	0.22
214m	2262	2261	10	1	99.56	99.96	0.49
219m	2154	2153	1	1	99.95	99.95	0.09
221m	2427	2425	9	2	99.63	99.92	0.45
222m	2483	2481	25	2	98.99	99.92	1.09
228m	2053	2018	69	35	96.64	98.27	4.98
231m	1571	1571	0	0	100	100	0
232m	1780	1776	1	4	99.94	99.78	0.28
233m	3079	3075	33	4	98.93	99.87	1.2
234m	2753	2753	2	0	99.93	100	0.07
Total	**49707**	**49586**	**378**	**121**	**99.24**	**99.76**	**1.00**

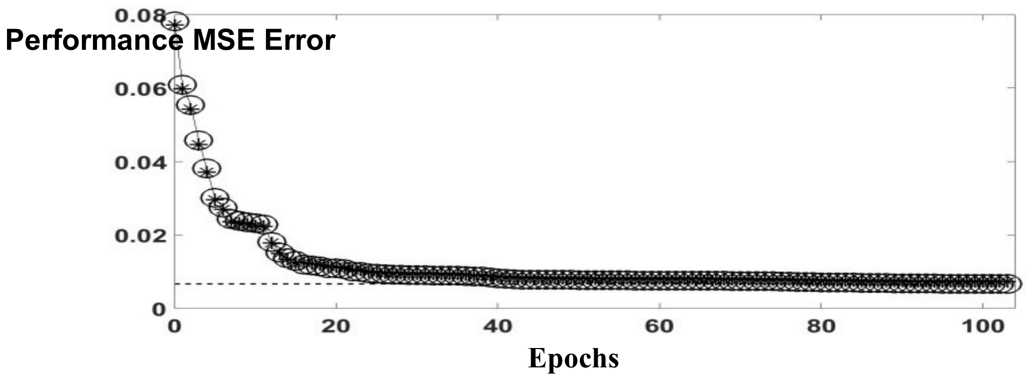

Fig. 46 : Error evolution during the deep learning phase.

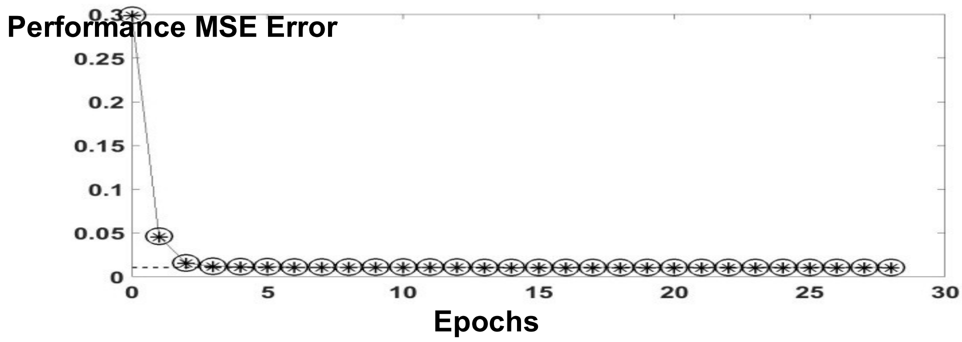

Fig. 47 : Error evolution during first stage MLP learning.

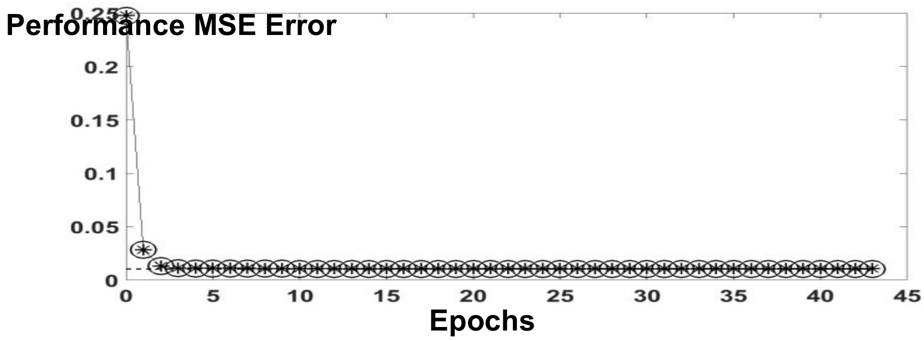

Fig. 48 : Error evolution during second stage MLP learning.

The real-time processing and the implementation of algorithms on embedded medical instruments with low processing capability and reduced memory are important in modern intelligent healthcare systems. Therefore, we evaluated the proposed detector time execution using CPU and GPU (Graphical processing unit).

On a computer that has an Intel i7-2670QM processor with 2.2 GHz and a GeForce 650 GTX 2GB graphical computation unit, the execution time required to process four datasets that contain 1044598 beats is 98.97 s (CPU), this corresponds to 94.95µs per one beat. Employing GPU CUDA acceleration, the execution time is reduced to 25.32 seconds for processing 1044598 beats, which corresponds to 24.23 µs per one beat. The reported values are the mean of three executions to overcome the execution time variations. To compare the proposed algorithm with state-of-the-art works, we collected some works that are based on deep learning in Table 15. In addition to the execution time spent by each method to detect

Table 14 : The Proposed QRS Detection Results on Four Test Datasets.

waveform	QRS	Not QRS	∑
QRS	**1026148**	**4150**	
NOT QRS	16161	4708971	
∑	1042309	4713121	**5755430**

Table 15 : Execution Time Comparison With State-of-the-Art works.

Method	**SE**	**DER**	**Execution Time for 30-minutes duration record (second)**
DEEP QRS [75]	N/A	1.1	1260
CNN [76]	99.36	1.65	810
2 LEVEL CNN [44]	99.77	0.32	14.53
Prep CNN [42]	99.81	0.25	30.6
DETEC [10]	99.87	N/A	19.44
CNN [79]	98.52	N/A	3.6
THIS WORK	**99.76**	**1.0**	**0.055**

the presence of the QRS complex on 30 minutes duration, we displayed the sensitivity and the detection error rate. It is clear that the proposed method outperforms all the methods shown in Table 15. In particular, in terms of overall accuracy, our method surpasses state-of-the-art works on two datasets, while being 65x faster on GPU inference than the fastest method of [79].

This offers the possibility of embedding this method on mobile devices. The low time-execution of our method is due to the simple deep architecture and the small number of weights of the stacked autoencoder.

V. 7. Conclusion

An automatic QRS detector is developed without any preprocessing. To the best of our knowledge, this is the first time a stacked autoencoder deep neural network is used for QRS detection directly from the raw ECG. Furthermore, the proposed architecture is simple and contains two hidden layers only with a reduced number of neurons. The proposed algorithm is faster than state-of-the-art methods and suitable for embedded systems implementation. The achieved experimental results, using many benchmark datasets, prove the generalization and high performance of the proposed algorithm.

As future work, the developed QRS detector will be incorporated in an automatic system for arrhythmia classification.

CHAPTER VI

MULTI-PLATFORM INTERACTIVE ARRHYTHMIA CLASSIFIER

VI. Multi-platform Interactive Arrhythmia Classifier

VI. 1. Motivations and Approach

The implementation of a stand-alone system, which could be used for diagnosis by health practitioners or non-specialized persons, has been a fundamental objective of this Ph. D. dissertation. This intelligent tool comprises many parts; each of which is still an open research area. Many methods have been developed for either QRS detection or arrhythmia classification. We attempted to integrate our own proposed algorithms to implement a reliable system. We selected the deep learning-based method for both QRS detection and arrhythmia classification. The fast feature of DL algorithms at inference motivates this choice. Besides, many features have been integrated into this software to meet users' requirements.

VI. 2. Introduction

The prediction and anticipation of physical and physiological events constitute a challenge to researchers and engineers. Physical and physiological phenomena are events recorded using transducers and detectors. These instruments provide information about the measured events. The objective of artificial intelligence and signal processing techniques is to improve the quality of the generated signal and extract useful information, which is used later for decision and monitoring. The implementation of developed algorithms aims at exploiting artificial intelligence in helping humans in their daily life. Another important factor is resource consumption, which alters directly the cost and mobility of the final product. Many features attract the attention of the customer, e.g., memory space, connection to the internet, reading external storage memories, connection to other instruments, easy to use, etc.

The developed system in the present chapter is intended to be able to detect precisely the ECG beats and deliver arrhythmia classification. The implemented system is a Holter Android arrhythmia classifier program, which comprises a graphical user interface with the possibility to observe the recorded signal and the result of segmentation and classification visually. The software saves the entire report of the estimated QRS positions and predicted arrhythmia for each beat.

VI. 3. Proposed System

During the realization of our diagnosis system, we have put a lot of effort to make the applications fully automatic. The developed system runs on PCs, MACs, or Android devices. The programming environment is programmed under the JAVA language. Then generated Byte code, interpreted with a virtual machine, can be executed under Windows, Linux, or Macintosh recent versions operation system. This flexibility allows using our product without migration to other hardware and permits also a large population of users.

The possibility of exploiting the developed system under Android devices offers wide mobility and users; especially cardiologists and veterinary personals will be able to decide about a patient's state of health directly from their Smartphone or Tablet automatically, no need to be in an office behind a monitor. Moreover, our software contains a big number of facilities (see Fig. 49), it offers the possibility to read ECG binary file stored on SD external memory or flash disk, or acquiring data from another device through a wireless connection. A variety of recording devices that are compatible with previously cited storage norms could be used for data acquisition. Also, an intuitive graphical user interface (GUI), integrated into our software, offers its users the possibility to choose the data acquisition mode. Therefore, we offer a signal plot to let the user enjoy the input signal shape. The developed system displays the normal or arrhythmia type for each detected beat. The detected arrhythmia is plotted on the top of the detection position. For post-decision, the software interface offers the user the possibility to save the resulting QRS positions and their identified pathologies on binary, pdf, or text file formats. Hence, the user has the opportunity to correct, if he is an expert, the wrong pathology or QRS position, after visualizing the plot. Another feature that the developed software provides is the computation of the Heart Rate (HR), which is the number of beats per minute. The graphical user interface shown in Figs. 50 and 51 of the developed software running on a Smartphone and emulated on PC gives an initial feeling of a user-friendly software that permits an easier manipulation. Employing icons for each feature, the user does not require advanced knowledge of medical or computer science disciplines.

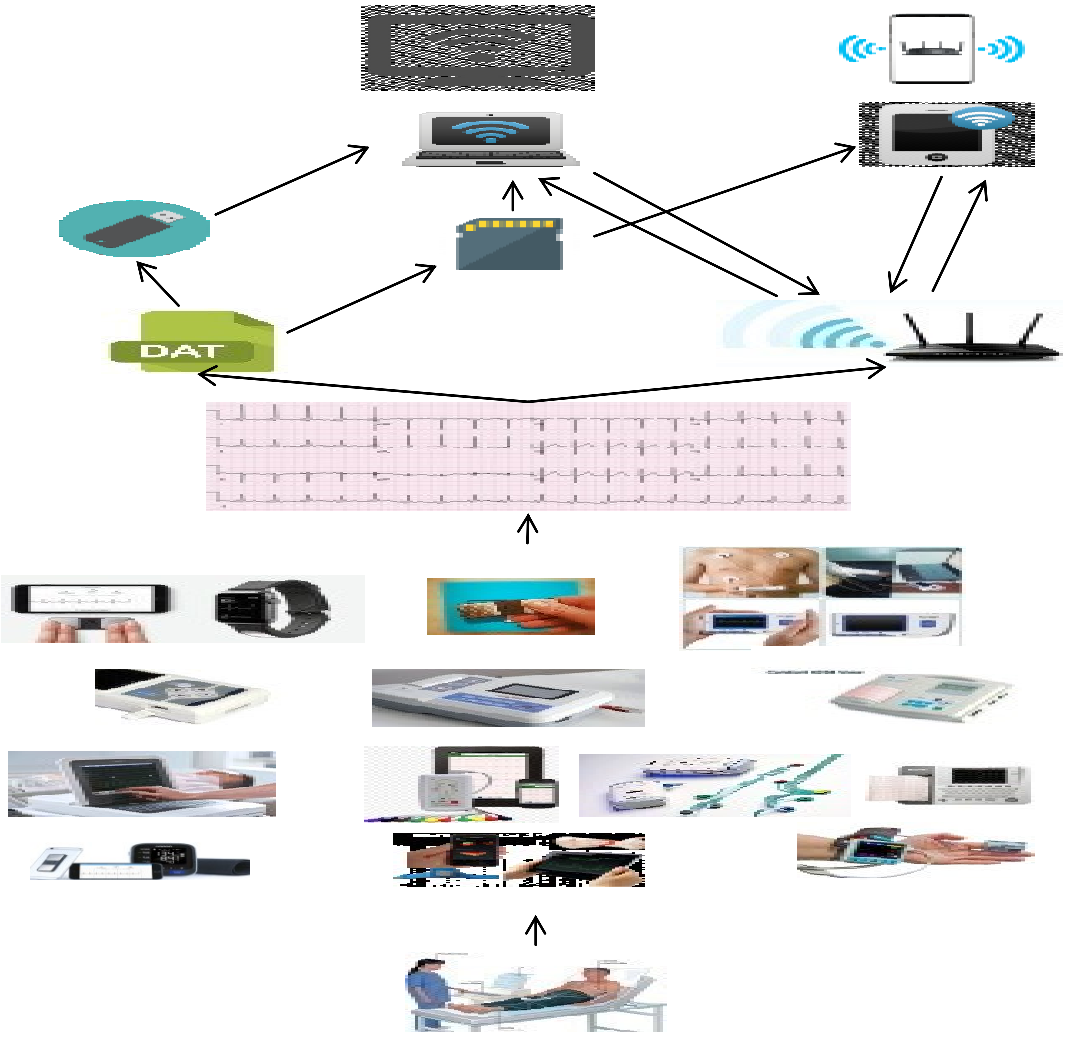

Fig. 49 : Software devices interactions.

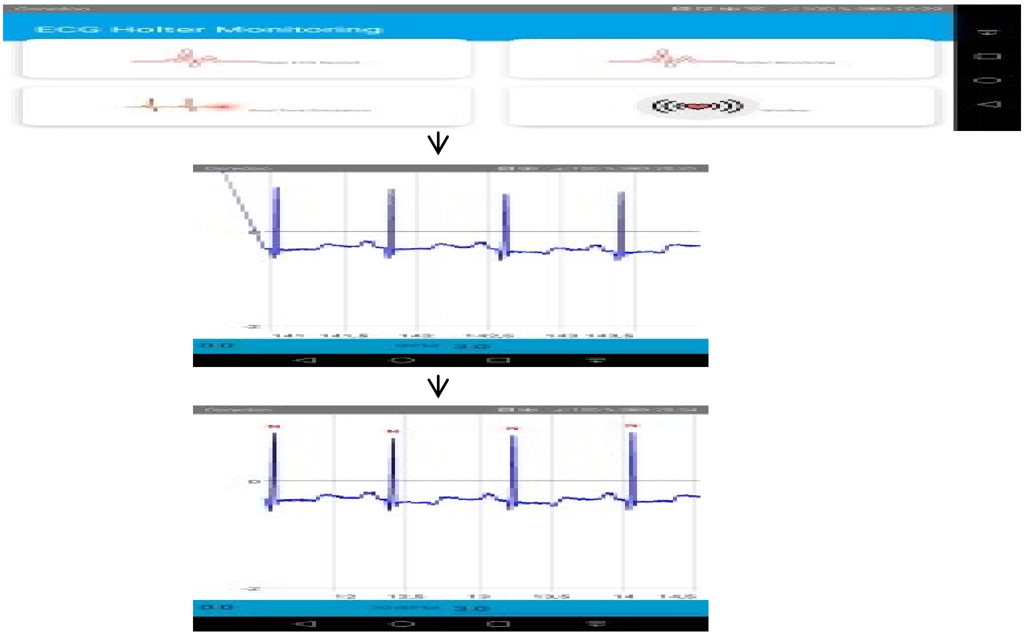

Fig. 50 : Overview of the Android software user interface.

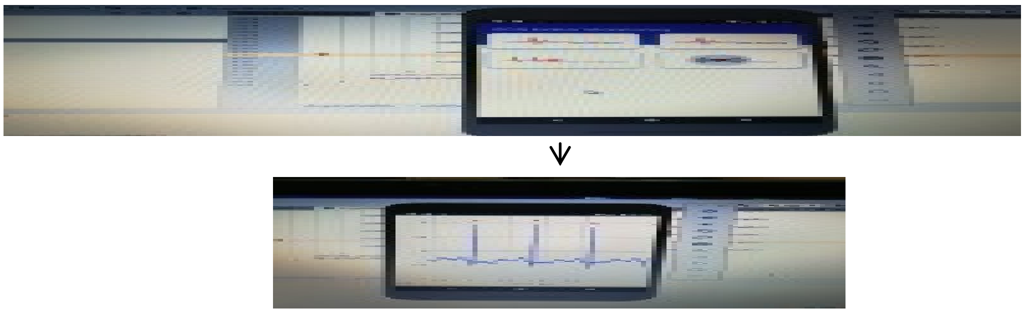

Fig. 51 : User interface overview on the PC emulator.

VI. 4. Numerical Results

While a user-friendly user interface and diverse functions for any software are indispensable, accurate QRS detection and arrhythmia classification are mandatory features. The classification accuracy is the main challenge in this kind of intelligent systems. The primary aim of utilizing this software by experts or any category of users is to determine the heart state health. Besides, the execution time is crucial; short processing time is required in order to have quick decisions. That is, if the processing time is greater than necessary, the cardiologists will not benefit from the software. In this case, the software will be useful only for analyzing long-duration recordings that require tedious work for their analysis.

Tables 16, 17, and 18 show QRS detection and arrhythmia accuracy performance. For the QRS detection, the proposed classification scheme is very accurate (0.82% of DER error, with 99.66% of sensitivity and 99.52% of positive predictive value) over more than 1400000 unseen beats, especially when the evaluation is done on databases completely not used on training, this proves the robustness of our method and the generalization of the proposed architecture.

Table 16 : The Achieved QRS Detection Results using Six Unseen Datasets.

Validation set	# of beats	Se	PPr	DER %
Apnea	647816	99.27	99.47	1.26
NSRDB	191053	99.92	99.65	0.43
QTDB	80499	99.71	99.26	1.03
LTSTDB	357373	99.9	99.76	0.34
Fantasia	121128	99.5	99.85	0.65
Challenge 14	72415	99.74	99.91	0.34
Overall	**1470284**	**99.66**	**99.52**	**0.82**

Table 17 : Test and Unseen sets Arrhythmia Classification Accuracies.

Approach	Accuracy
Test dataset	
MITDB	97.5
INCART DB	96.9
SVDB	98.6
EDB	99.7
Unseen dataset	
Challenge 2014	99.8
QTDB	84.3

For the arrhythmia classification, the proposed method achieved an overall accuracy of 99% over more than 670000 beats. The training and test beats were collected from four well-known databases for ECG signal processing and classification. Besides, the results of Table 17 indicate good learning of the signal characteristics and the accuracy of the proposed scheme on the different test and validation sets. More precisely, the accuracy on test sets is around an average of 98.5%; the accuracy on MITDB test set is 97.5%, 96.9% on INCART DB, 98.6% on SVDB, and 99.7% on EDB. Thus, the obtained results are very promising for arrhythmia classification. Moreover, 99.8% of accuracy for Challenge 2014 DB, and 84.3% for QTDB confirm the efficiency of our method on unseen data and the robustness of our method for ECG signal. The confusion matrix of Table 18 presents an overall view of the global arrhythmia classification results, including QRS detection.

VI. 5. Conclusion

The developed software can resolve many cardiologists’ problems; it can be a valuable tool for auto-diagnosis. Finally, we can say that we achieved most of the planned objectives. The developed system is accurate and fast. Moreover, it has a diverse number of functions and a short execution time. Also, mobility and multi-platform targeting constraints are met.

Table 18 : Confusion Matrix for Testing set Based on Subject-Oriented Representation

Pathology	0	N	Q	A	V	J	F	R	L	E	e	A	j	S	
0	**4708971**	86	0	0	22	0	0	0	5	0	0	0	0	1	
N	2964	**581734**	12	367	1125	14	121	27	24	1	3	15	59	1038	
Q	17	0	**0**	0	0	0	0	0	0	0	0	0	0	0	
A	17	126	0	**446**	5	0	1	33	0	0	0	2	4	1	
V	947	1497	6	36	**6969**	0	105	20	31	20	0	12	0	120	
J	0	0	0	0	0	**0**	0	0	0	0	0	0	0	0	
F	33	28	0	1	5	0	**49**	0	0	0	0	0	0	0	
R	16	40	1	34	12	3	0	**2004**	0	0	0	0	0	0	
L	91	51	0	13	10	0	0	1	**1560**	0	0	1	0	0	
E	8	0	0	0	0	0	0	0	0	**0**	0	0	0	0	
e	0	0	0	0	0	0	0	0	0	0	**0**	0	0	0	
a	58	0	0	0	0	0	0	0	0	0	0	**0**	0	0	
j	0	0	0	0	0	0	0	0	0	0	0	0	**0**	0	
S	0	1037	2	0	93	0	1	0	0	0	0	0	0	**1498**	
∑	**4713121**	**584599**	**21**	**897**	**8241**	**17**	**276**	**2085**	**1620**	**21**	**3**	**30**	**63**	**2658**	**5313652**

CHAPTER VI

GLOBAL RESULTS AND CONCLUSIONS

VII. Global Results and Conclusions

In this chapter, we report the achievements of our dissertation and a thorough comparison of the obtained results with state-of-art methods. In addition, we mention the remaining challenges and potential extensions of some methods.

VII. 1. QRS Detection Results

Table 19 : Comparison of the proposed methods with state of the art.

Method	# of beats	TP	FP	FN	PPV	Se	DER
MITDB							
Geometrical matching [17]	60431	N/A	N/A	N/A	97.94	99.13	2.92
Zero crossing [8]	109428	N/A	N/A	N/A	97.44	99.13	1.71
Short Time Fourier Transform [22]	109982	N/A	N/A	N/A	99.1	99.6	1.3
An Approach to QRS Complex Detection using Deep Neural Network Autoencoder	**49707**	**49586**	**378**	**121**	**99.24**	**99.76**	**1.00**
Moving average [16]	102654	N/A	N/A	N/A	99.6	99.78	0.96
MaMeMi filter [9]	109494	N/A	N/A	N/A	99.44	99.68	0.88
New QRS Detection Algorithm Using Discrete Wavelet Transform and Statistical Estimation [80]	**109494**	**109067**	**486**	**427**	**99.56**	**99.61**	**0.83**
An Improved QRS Detection Method Using Hidden Markov Models [81]	**44510**	**44232**	**52**	**278**	**99.38**	**99.88**	**0.741**
Adaptive Thresholding [5]	109949	109447	289	502	99.54	99.74	0.72
First dervitaive [18]	109504	109150	405	354	99.63	99.68	0.69
Pan-Tompkins [4]	109809				99.56	99.76	0.68
Lowpass-RR intrvals [18]	109336	108960	218	376	99.80	99.66	0.54
Quantitative evaluation [3]	109267	108927	240	340	99.78	99.69	0.54
C CUDA Acceleration of a New PSO Optimized Wavelet QRS Detector [81]	**109494**	**109201**	**309**	**293**	**99.72**	**99.73**	**0.5498**
Characteristic Templates [34]	116137	N/A	N/A	N/A	99.81	99.70	0.49
Morphological filtering(VLSI) [20]	109510	N/A	N/A	N/A	99.82	99.76	0.43
Adaptative thresold [15]	110050	109811	240	239	99.78	99.78	0.43
Optimize [47]	109985	N/A	N/A	N/A	99.87	99.78	N/A
Wavelet Delineator [33]	109428	N/A	N/A	N/A	99.8	99.86	0.34
Digital fractional order [6]	109494	109338	153	156	99.86	99.86	0.34
CNN [44]	105078	N/A	N/A	N/A	99.77	99.91	0.32
SWT [25]	109494	109316	126	178	99.88	99.84	0.28
Fractional order operator [6]	107632	N/A	N/A	N/A	99.86	99.86	0.29
Prep CNN[42]	49653	N/A	N/A	N/A	99.81	99.93	0.25
A New Method For QRS Detection Using Stationary Wavelet Transform	**109494**	**109308**	**64**	**186**	**99.94**	**99.83**	**0.228**
Embedded Detector [10]	91285	N/A	N/A	N/A	99.87	99.9	N/A
Swarm Intelligence Approach to QRS Detection [50]	**109494**	**109406**	**97**	**88**	**99.91**	**99.92**	**0.169**
Wearable Monitor [21]	109496	N/A	N/A	N/A	99.91	99.92	0.1644
MFO DFOD [204]	109949	N/A	N/A	N/A	99.93	99.92	0.1507
EDB							
Swarm Intelligence Approach to QRS Detection [50]	**704656**	**697169**	**827**	**7487**	**99.88**	**99.06**	**1.18**
An Approach to QRS Complex Detection using Deep Neural Network Autoencoder	**677756**	**674774**	**12445**	**2982**	**99.7**	**98.05**	**2.28**
A New Method For QRS Detection Using Stationary Wavelet Transform	**734555**	**726184**	**647**	**8371**	**99.91**	**98.87**	**1.23**
Wavelet Delineator [33]	983423	N/A	N/A	N/A	99.66	99.56	0.78
NSTDB							
Swarm Intelligence Approach to QRS Detection [50]	**25590**	**24803**	**4422**	**787**	**82.72**	**96.42**	**20.36**
Optimize [47]	26370	N/A	N/A	N/A	90.25	95.39	N/A

SWT [25]	25590	24388	1563	1202	95.3	93.98	10.81
A New Method For QRS Detection Using Stationary Wavelet Transform	**25590**	**25300**	**2300**	**290**	**91.01**	**98.77**	**10.12**
SVDB							
Optimize [47]	184744	N/A	N/A	N/A	99.96	99.80	N/A
An Approach to QRS Complex Detection using Deep Neural Network Autoencoder	**160402**	**159763**	**1514**	**639**	**99.6**	**99.06**	**1.34**
INCART							
CNN [44]	170000	N/A	N/A	N/A	99.86	99.89	0.25
Swarm Intelligence Approach to QRS Detection	**138891**	**137161**	**74**	**1730**	**99.95**	**98.82**	**1.3**
An Approach to QRS Complex Detection using Deep Neural Network Autoencoder	**160840**	**160432**	**1824**	**408**	**99.73**	**98.82**	**1.45**
Optimize [47]	175918	N/A	N/A	N/A	99.03	97.09	N/A
QTDB							
Swarm Intelligence Approach to QRS Detection	**80056**	**79989**	**957**	**67**	**99.92**	**98.82**	**1.279**
An Approach to QRS Complex Detection using Deep Neural Network Autoencoder	**80499**	**80266**	**597**	**233**	**99.26**	**99.8**	**1.03**
HMM [38]	61414	N/A	N/A	N/A	99.79	99.96	0.25
Wavelet Delineator [33]	86824	N/A	N/A	N/A	99.92	99.88	0.2
Optimize [47]	111201	N/A	N/A	N/A	99.99	99.67	N/A
Normal Sinus Rhythm							
Optimize [47]	183092	N/A	N/A	N/A	99.99	99.96	N/A
An Approach to QRS Complex Detection using Deep Neural Network Autoencoder	**191053**	**190896**	**669**	**157**	**99.92**	**99.67**	**0.43**
Adaptive Thresholding [5]	192389	N/A	N/A	N/A	99.97	99.99	0.04
Fantasia							
Adaptive Thresholding [5]	79484	N/A	N/A	N/A	99.99	99.94	N/A
An Approach to QRS Complex Detection using Deep Neural Network Autoencoder	**121125**	**120512**	**177**	**613**	**99.85**	**99.9**	**0.65**
Challenge 2014							
Adaptive Thresholding [5]	72309	N/A	N/A	N/A	99.94	99.75	N/A
An Approach to QRS Complex Detection using Deep Neural Network Autoencoder	**72415**	**72229**	**62**	**186**	**99.74**	**99.91**	**0.34**

Table 20 : The execution time of our developed algorithms.

Method	**Execution Time (100m) (2274 beats) (seconds)**
CPU	
Swarm Intelligence Approach to QRS Detection	1.3
An Approach to QRS Complex Detection using Deep Neural Network Autoencoder	0.216
GPU	
C CUDA Acceleration of a Newest PSO Optimized Wavelet QRS Detector	0.126
An Approach to QRS Complex Detection using Deep Neural Network Autoencoder	0.06

Our proposed QRS detection algorithms achieved a DER in the range of 0.169-1.0 % on the MIT/BIH arrhythmia database (see Table 1). This ranks the proposed algorithms among the best state- of- the-art algorithms. In particular, two of our introduced methods achieved the best performance over the MIT/BIH Arrhythmia database, namely, the swarm intelligence optimized method and the SWT based method, with 0.169% of error for the first, and 0.228% for the second. Thus, taken into consideration that the MITDB is a benchmark for the QRS detection, this achievement is a significant contribution to enriching the field of QRS detection research field.

For the assessment on the MIT Noise Stress database, for noise robustness evaluation, the proposed QRS Detection Using Stationary Wavelet Transform method outperforms state-of-the-art algorithms in terms of DER (10.12%). The result of the SWT based algorithm obtained under normal and abnormal noisy environments makes our algorithm unique in this field; while the algorithms designed for the QRS detection in noisy environments perform well only for this type of conditions, they produce very poor results for normal ECG signals. For instance, the error delivered by the swarm approach [50] is 20.36%, which is 2x the error of the SWT method. The SWT based method produced only 0.228% of DER on the MITDB set. The above results show that the SWT based algorithm is suitable for both normal and noisy environments. The assessment on long duration datasets has been carried out on the European database (EDB). The best offline result achieved by our SWT based algorithm is 1.23% of DER using more than 734000 beats, which confirms that our developed algorithm is appropriate for large validation datasets.

For Fantasia DB and challenge 2014 DB, our DL approach achieved 0.64% and 0.34% of DER, respectively. These achievements are state-of-the-art results in this domain. During our assessment, we used 121125 and 72415 beats, whereas Gutiérrez-Rivas et al [5] used only 79484 and 72309 beats. Therefore, our results are more reliable. For QTDB, SVDB and INCART, the reported results are not the best, but still rank well among state-of-the-art algorithms. Summing up, the deep learning proposed method achieved 0.82% of DER using more than 1470000 beats.

Among the developed methods throughout this dissertation, we believe that the deep learning approach is the most adequate for a potential implementation. This is due to the achieved high performance over a wide range of standard databases and the low execution time required at inference (Table 3).

VII. 2. Achievements and Perspectives

Throughout this dissertation, we developed many algorithms for QRS detection, an arrhythmia classification scheme, and a user-friendly diagnosis system. The first contribution is an optimization procedure of the Pan-Tompkins algorithm parameters. The second is a time-frequency method using the stationary wavelet transform, which is a state-of-the-art method for noisy ECG signals. The third is a new DL approach using stacked autoencoders. The DL approach produced very promising performance over a variety of standard datasets. Our proposed diagnosis system has many features and it is user-friendly. It can be used as a tool that helps the practitioners in delivering accurate and fast decision. In particular, it can help in the analysis of long duration recordings, which is a common method used to collect information about patients suffering from ECG disorders.

For further extensions, as the DL techniques are invading many fields of research, we believe that other architectures are possible based on CNNs in conjunction with LSTM. Besides, time-frequency performance might be improved if we use adaptive wavelets that are tailored to the ECG signal shape.

References

[1] Belforte G, De Mori R, Ferraris F, "A Contribution to the Automatic Processing of Electrocardiograms Using Syntactic Methods," IEEE Trans. Biomed. Eng. vol. BME-26, no. 3, pp. 230-236. https://doi.org/10.1109/TBME.1979.326470, March. 1979.

[2] Shackil A.F, "Microcomputers: Microprocessors and the M.D.: A new breed of smart medical equipment can diagnose, monitor, analyze, and rehabilitate," IEEE Spectrum, vol. 18, no. 4, pp. 45-49, Apr. 1981.

[3] Hamilton P. S., W. J. Tompkins, "Quantitative Investigation of QRS Detection Rules Using the MIT/BIH Arrhythmia Database," IEEE Trans. Biomed. Eng, vol. BME-33, no. 12, pp. 1157-1165, 1986.

[4] Pan J, Tompkins WJ (1985) "A Real-Time QRS Detection Algorithm". IEEE Trans. Biomed. Eng. BMS-32:230-236. https://doi.org/10.1109/TBME.1985.325532.

[5] Gutiérrez-Rivas R., García J. J., Marnane W. P., Hernández Á., "Novel Real-Time Low-Complexity QRS Complex Detector Based on Adaptive Thresholding," IEEE Sensors J, vol. 15, no. 10, pp. 6036-6043, 2015.

[6] Benmalek M., Charef A., "Digital fractional order operators for R-wave detection in eletrocardiogram," IET SIGNAL PROCESS, vol. 3, no. 5, pp. 381-391, 2009.

[7] Ruha A., Sallinen S., Nissila S., "A Real-Time Microprocessor QRS Detector System with a 1-ms Timing Accuracy for the Measurement of Ambulatory HRV," IEEE Trans. Biomed. Eng, vol. 44, no. 3, pp. 159-167, 1997.

[8] Ravanshad N., Rezaee-Dehsorkh H., Lotfi R., Lian Y., "A Level Crossing Based QRS-Detection Algorithm for Wearable ECG Sensors," IEEE Trans. Biomed. Eng, vol. 18, no. 1, pp. 183-192, 2014.

[9] Castells-Rufas D., Carrabina J., "Simple real-time QRS detector with the MaMeMi filter," Biomed Signal Process Control, vol. 21, pp. 137-145, 2015.

[10] Saadi D., Tanev G., Flintrup M., Osmanagic A., Egstrup K., Hoppe K., Jennium J., Iversen H., and Sorensen H., "Automatic Real-Time Embedded QRS Complex Detection for a Novel Patch-Type Electrocardiogram Recorder," IEEE J. Transl. Eng. Health Med., vol. 3, 2015.

[11] Yakut Ö., Bolat E. D., "An improved QRS complex detection method having low computational load," Biomed Signal Process Control, vol. 42, pp. 230-241, 2018.

[12] Tekeste T., Saleh H., Mohammad B., Ismail M., "Ultra-Low Power QRS Detection and ECG Compression Architecture for IoT Healthcare Devices," IEEE Trans. Circuits Syst. I, Reg. Papers, pp. 1-11, 2018.

[13] Nguyen T., Qin X., Dinh A., and Bui F., “Low Resource Complexity R-peak Detection Based on Triangle Template Matching and Moving Average Filter,” Sensors (Basel), vol. 19, no. 18, 2019.

[14] Poli P., Cagnoni S., Valli G., “Genetic Design of Optimum Linear and Nonlinear QRS Detectors,” IEEE Trans. Biomed. Eng, vol. 42, no. 11, pp. 1137-1141, 1995.

[15] I. I. Christov, “Real-Time Electrocardiogram QRS Detection Using Combined Adapted Threshold,” Biomed Eng Online, vol. 3, no. 28, Aug. 2004.

[16] Chen S. W., Chen H. C., Chan H. L., “A real-time QRS detection method based on moving-averaging incorporating with wavelet denoising,” Comput Methods Programs Biomed, vol. 82, no. 3, pp. 187-195, 2006.

[17] Suarez K. V., Silva J. C., Berthoumieu Y., Gomis P., Najim M., “ECG Beat Detection Using a Geometrical Matching Approach,” IEEE Trans. Biomed. Eng, vol. 54, no. 4, pp. 641-650, 2007.

[18] N. M. Arzeno, Zhi-De Deng, Chi-Sang Poon, “Analysis of First-Derivative Based QRS Detection Algorithms,” IEEE Trans. Biomed. Eng., vol. 55, no. 2, pp. 478-484, Feb. 2008.

[19] Zhang F., Lian Y., “QRS detection based on multiscale mathematical morphology, for wearable ECG devices in body area networks,” IEEE Trans. Biomed. Eng, vol. 3, no. 4, pp. 220-228, 2009.

[20] Zhang C. F., Tae-Wuk Bae, “VLSI Friendly ECG QRS Complex Detector for Body Sensor Netwroks,” IEEE Trans. Emerg. Sel. Topics Circuits Syst, vol. 2, no. 1, pp. 52-59, 2012.

[21] M. S. Manikandan, B. Ramkumar, “Straightforward and robust QRS detection algorithm for wearable cardiac monitor,” Healthcare Technology Letters, vol. 1, NO. 1, 2014, pp. 40 - 44.

[22] Uchaipichat N., Inban S., “Development of QRS Detection using Short-Time Fourier Transform Based Technique,” IJCA, pp. 7-10, 2010.

[23] Manikandan M., Soman K., “A novel method for detecting R-peaks in electrocardiogram (ECG) signal,” Biomed Signal Process Control, vol. 7, no. 2, pp. 118-128, 2012.

[24] S. N. Shivappriya; R. ShanthaSelvaKumari; T. GowriShankar, ECG Delineation Using Stationary Wavelet Transform, IEEE Int. Conf. Adv. Comp. and Comm., pp. 271-274. 2006.

[25] M. Merah, T.A. Abdelmalik, B.H. Larbi, R-peaks detection based on stationary wavelet transform, Comp. meth. Prog. in biomedicine 121 (3), 149-160, jun. 2015.

[26] Li C., Zheng C., Tai C., “Detection of ECG characteristic points using wavelet transforms,” IEEE Trans. Biomed. Eng, vol. 42, no. 1, pp. 21-28, 1995.

[27] Kadambe S., Murray R., Bordeaux-Bartels G. F., "Wavelet transform-based QRS complex detector," IEEE Trans. Biomed. Eng, vol. 46, no. 7, pp. 838-848, 1999.

[28] F. Bouaziz, D. Boutana, M. Benidir, "Multiresolution waveletbased QRS complex detection algorithm suited to several abnormal morphologies," IET Signal Process, vol. 8, pp. 774–782, September 2014.

[29] S. Behbahani, N. J. Dabanloo, "Detection of QRS complexes in the ECG signal using multiresolutionwavelet and thresholding method," IEEE. Hangzhou, China, pp. 805–808 September 2011 [Computing in Cardiology conference, 2011].

[30] R. Haddadi, E. Abdelmounim, M. El Hanine, A. Belaguid, "Discrete Wavelet Transform based algorithm for recognition of QRS complexes,". IEEE. Marrakesh, Morocco, pp. 375 379, April 2014 [International Conference on Multimedia Computing and Systems].

[31] W. Jenkal , A. Toumanari; A. Dliou; O. El B'charri, "Enhanced algorithm for QRS detection using discrete wavelet transform(DWT)," 2015 27th International Conference on Microelectronics (ICM), 2015, pp. 39 – 42.

[32] D. Sadhukhan, S. Pal, M. Mitra, "ECG delineation using multiresolution DWT and relative magnitude and slope comparison," 2016 2nd International Conference on Control, Instrumentation, Energy & Communication (CIEC), 2016, pp. 173 - 177.

[33] J. P. Martinez, R. Almeida, S. Olmos, A. P. Rocha, P. Laguna, "A Wavelet-based ECG Delineator: Evaluation on Standard Databases," IEEE Trans. Biomed. Eng., vol. 51, no. 4, pp. 570-581, Apr. 2004.

[34] Karimipour A., and Homaeinezhad M., "Real-time electrocardiogram P-QRS-T detection delineation algorithm based on quality-supported analysis of characteristic templates," Comput. Biol. Med., vol. 51, pp. 153-165, 2014.

[35] Kholkhal M., and Bereksi R., "Efficient Automatic Detection Of QRS Complexes In ECG Signal Based On Reverse Biorthogonal Wavelet Decomposition And Nonlinear Filtering," Measurement, vol. 94, pp. 663-670, 2016.

[36] R. V. Andreão, B. Dorizzi, J. Boudy. "ECG Signal Analysis through Hidden Markov Models". IEEE Transactions on Biomedical Engineering, vol.53, NO. 8, pp. 1541-1549, August 2006.

[37] R. V. Andreao, B. Dorizzi, J. Boudy, J. C. M. Mota, "ST-Segment Analysis Using Hidden Markov Model Beat Segmentation: Application to Ischemia Detection," IEEE Computers in Cardiology, 2004, pp. 381-384.

[38] J. Thomas, C. Rose, F. Charpillet, "A Multi-HMM Approach to ECG Segmentation," 18th IEEE International Conference on Tools with Artificial Intelligence (IICTAI'06), 2006, pp. 609-616.

[39] D. A. Coast, R. M. Stern, G. G. Cano, S. A. Briller, “An Approach to Cardiac Arrhythmia Analysis Using Hidden Markov Models,” IEEE Transaction on Biomedical Engineering7, No. 9, Sept 1990, pp. 826-836.

[40] Xue Q., Hu Y. H., Tompkins W. J., “Neural-Network-Based Adaptive Matched Filtering for QRS Detection,” IEEE Trans. Biomed. Eng, vol. 39, no. 4, pp. 317-329, 1992.

[41] I. Saini, D. Singh, A. Khosla, “QRS Detection Using K-Nearest Neighbor (KNN) and Evaluation on Standard ECG Databases,” Int J Adv Res, vol. 4, no. 4, pp. 331–344, July. 2013.

[42] M. Šarlija, F. Jurišić, S. Popović, “A Convolutional Neural Network-Based Approach to QRS Detection,” in Proc. ISPA, 2017, pp. 121–125.

[43] W. Zhong, L. Liao, X. Guo, G. Wang, “A Deep Learning Approach for Fetal QRS Complex Detection,” Physiol Meas, vol. 39, no. 4, Apr. 2018.

[44] Xiang Y., Lin Z., and Meng J., “Automatic QRS complex detection using two-level convolutional neural network,” Biomed. Eng. Online, vol. 17, no. 13, 2018.

[45] Sedghamiz H., “Complete implementation of Pan & Tompkins software. Humanist,” The MathWorks, https://www.mathworks.com/matlabcentral/fileexchange/45840-complete-pan-tompkins-implementation-ecg-qrs-detector. 2014.

[46] Shaik B. S., Naganjaneyulu G. V. S. S. K. R., Chandrasheker T., Narasimhadhan A. V., “A Method for QRS Delineation Based on STFT using Adaptive Threshold,” in Proc. IMCIP, pp. 646-653, 2015.

[47] Elgendi M., “Fast QRS detection with an optimized knowledge-based method: evaluation on 11 standard ECG databases,” PLoS ONE, vol. 8, no. 7, 2013.

[48] Bal R., and Kumar A., “Improved Qrs Detector Using Parallel based Hybrid Mamemi Filter,” IJIGSP, vol. 9, no. 3, pp. 55-61, 2017.

[49] Hashim M., Hau Y., and Baktheri R., “Efficient QRS complex detection algorithm implementation on a soc-based embedded system,” J Teknol, vol. 78, no. 7-5, pp. 49-58, 2016.

[50] M. A. Belkadi, A. Daamouche, “Swarm Intelligence Approach to QRS Detection,” IAJIT, vol. 17, no. 4, Jully. 2020.

[51] Mallat SG (1989) “A Theory for Multiresolution Signal Decomposition: The Wavelet Representation”. IEEE Trans. Pattern Anal. Mach. Intell. 11:674-693. https://doi.org/10.1109/34.192463.

[52] M. A. Belkadi. A. Daamouche, “A New Method for Accurate QRS Detection Using Stationary Wavelet Transform,” ICCE-B 2017. In: Proceedings of the IEEE 2017 5th International Conference on Electrical Engineering, 29-31Oct. 2017, Boumerdes, Algeria,14 Dec 2017.

[53] Uk-Jin Yoon, In-Seop Hwang, Yeon-Sik Noh, In-Cheol Chung, Hyung-Ro Yoon, “ Comparison of CWT with DWT for detecting Qrs Complex on Wearable ECG Recorder,” 2010 International Conference on Wavelet Analysis and Pattern Recognition, Jully 2010, pp. 300 - 303.

[54] M. Elgendi, M. Jonkman, F. DeBoer, “FREQUNCY BANDS EFFECTS ON QRS DETECTION,” Conference: BIOSIGNALS 2010 - Proceedings of the Third International Conference on Bio-inspired Systems and Signal Processing, January 2010.

[55] Choi S, Adnane M, Lee G-J, Jang H, Jiang ZW, Park H-K (2010) “Development of ECG beat segmentation method by combining lowpass filter and irregular R-R interval checkup strategy”, Expert. Syst. Appl, vol. 37, no. 7, pp. 5208–5218, July 2010.

[56] Salih SK, Aljunid SA, Yahya A, Ghailan K (2012) A Novel Approach for Detecting QRS Complex of ECG Signal. IJCSI 9(6):205-215.

[57] J. Schmidhuber, “Deep Learning in Neural Networks: An Overview,” Neural Netw., vol. 61, pp. 85–117, Jan. 2015.

[58] Y. Cun, Y. Bengio, G. Hinton, “Deep Learning,” Int J Sci Nat, vol. 521, no. 436, pp. 436–444, May. 2015.

[59] Y. Yu, H. Guan, Z. Ji, “Automated Detection of Urban Road Manhole Covers Using Mobile Laser,” IEEE Trans. Intell. Transp. Syst., vol. 16, no. 6, pp. 3258–3269, Dec. 2015.

[60] Z. Zhang, Qingjie Liu, “Road Extraction by Residual U-Net,” IEEE Geosci. Remote Sens. Lett., vol. 15, no. 5, pp. 749–753, May. 2018.

[61] J. Chung, K. Sohn, “Image-Based Learning to Measure Traffic Density Using a Deep Convolutional Neural Network,” IEEE Trans. Intell. Transp. Syst., vol. 19, no. 5, pp. 1670–1675, May. 2018.

[62] Z. Hong, D. Ming, K. Zhou, Y. Guo, T. Lu, “Road Extraction from a High Spatial Resolution Remote Sensing Image Based on Richer Convolutional Features,” IEEE Access, pp. 46988–47000, Aug. 2018.

[63] Xiao-Lei Zhang, D. Wang, “A Deep Ensemble Learning Method for Monaural Speech Separation,” IEEE/ACM Trans. Audio, Speech, Language Process., vol. 24, no. 5, pp. 967–977, May. 2016.

[64] J. Du, Y. Tu, Li-Rong Dai, Chin-Hui Lee, “A Regression Approach to Single-Channel Speech Separation Via High-Resolution Deep Neural Networks,” IEEE/ACM Trans. Audio, Speech, Language Process., vol. 24, no. 8, pp. 1424–1437, Aug. 2016.

[65] D. Wang, J. Chen, “Supervised Speech Separation on Deep Leaning: An overview,” IEEE/ACM Trans. Audio, Speech, Language Process., vol. 26, no. 10, pp. 1702–1726, May. 2018.

[66] Y. Zhao, Zhong-Qiu Wang, DeLiang Wang, “Two-Stage Deep Leaning for Noisy-Reverberant Speech Enhancement,” IEEE/ACM Trans. Audio, Speech, Language Process., vol. 27, no. 1, pp. 53–62, Jan. 2019.

[67] N. Zheng, Xiao-Lei Zhang, “Phase-Aware Speech Enhancement Based on Deep Neural Networks,” IEEE/ACM Trans. Audio, Speech, Language Process., vol. 27, no. 1, pp. 63–76, Jan. 2019.

[68] F. Li, L. Tran, Kim-Han Thung, S. Ji, D. Shen, J. Li, “A Robust Deep Model for Improved Classification of AD/MCI Patients,” IEEE J. Biomed. Health Inform., vol. 19, no. 5, pp. 1610–1616, Sept. 2015.

[69] F. C. Ghesu, E. Krubasik, B. Georgescu, V. Singh, Y. Zheng, “Marginal Space Deep Learning: Efficient Architecture for Volumetric Image Parsing,” IEEE Trans. Med. Imag., vol. 35, no. 5, pp. 1217–1228, May. 2016.

[70] S. Albarqouni, C. Baur, F. Achilles, V. Belagiannis, S. Demirci, N. Navab, “AggNet: Deep Learning from Crowds for Mitosis Detection in Breast Cancer Histology,” IEEE Trans. Med. Imag., vol. 35, no. 5, pp. 1313–1321, May. 2016.

[71] J. Shi, X. Zheng, Y. Li, Q. Zhang, S. Ying, “Multimodal Neuroimaging Feature Learning With Multimodal Stacked Deep Polynomial Networks for Diagnostic of Alzheimer’s Disease,” IEEE J. Biomed. Health Inform., vol. 22, no. 1, pp. 173–183, Jan. 2018.

[72] M. Mahmud, M. S. Kaiser, A. Hussain, S. Vassanelli, “Applications of Deep Learning and Reinforcement Learning to Biological Data,” IEEE Trans. Neural Netw. Learn. Syst., vol. 29, no. 6, pp. 2063–2079, Jun. 2018.

[73] H. Jiang, H. Ma, W. Qian, M. Gao, Y. Li, “An Automatic Detection System of Lung Nodule Based on Multigroup Patch-Based Deep Learning Network,” IEEE J. Biomed. Health Inform., vol. 22, no. 4, pp. 1610–1616, Jul. 2018.

[74] F. Xing, Y. Xie, H. Su, F. Liu, L. Yang, “Deep Learning in Microscopy Image Analysis: A Survey,” IEEE Trans. Neural Netw. Learn. Syst., vol. 29, no. 10, pp. 4550–4568, Oct. 2018.

[75] H. Abrishami, M. Campbell, C. Han, R. Czosek, X. Zhou, “P-QRS-T localization in ECG using deep learning,” in Proc. IEEE EMBS-BHI, 2018.

[76] A. Borde, G. Kolokolnikov, V. Skurator, “Development of Neural Network-Based Approach for QRS Segmentation,” in Proc. FRUST-Open Innovations Association, 2019.

[77] A. Habib, C. Karmakar, J. Yearwood, “Impact of ECG Dataset Diversity on Generalization of CNN Model for Detecting QRS Complex,” IEEE Access, vol. 7, pp. 93275 – 93285, Jully. 2019.

[78] Cai, W., Hu, D, “Qrs complex detection using novel deep learning neural networks,” IEEE Access. vol. 8, pp. 97082–97089, May 2020.

[79] Yang, H., Huang, M., Cai, Z., Yao, Y., Liu, C., "A faster r cnn-based real-time qrs detector," IEEE. Singapore, Singapore, pp. in: 2019 Computing in Cardiology (CinC), (pp. Page1–4 September 2019 [Computing in Cardiology conference, 2019].

[80] M. A. Belkadi, A. Daamouche, "New QRS Detection Algorithm Using Discrete Wavelet Transform and Statistical Estimation," Not published yet.

[81] M. A. Belkadi. A. Daamouche, "An Improved QRS Detection Method Using Hidden Markov Models," ICCE-B 2017. In: Proceedings of the IEEE 2017 6th International Conference on Systems and Control (ICSC), 7-9 May. 2017, Batna, Algeria.

[82] M. A. Belkadi. A. Daamouche, "Fast Wavelet approach PSO-based QRS Detector," ICNTBA 2019. In: Proceedings of the First International Conference on Networking Telecommunications, Biomedical Engineering and Applications (ICNTBA'19), 4-5 Nov. 2019, Boumerdes, Algeria.

[83] for the Advancement of Medical Instrumentation, A., et al. (1998). Testing and reporting performance results of cardiac rhythm and st segment measurement algorithms. ANSI/AAMI EC38. 1998.